KUOPION YLIOPISTON JULKAISUJA C. LUONNONTIETEET JA YMPÄRISTÖTIETEET 267
KUOPIO UNIVERSITY PUBLICATIONS C. NATURAL AND ENVIRONMENTAL SCIENCES 267

NIKO JUKARAINEN

NMR Metabolomics Techniques and Mathematical Tools as an Aid in Neurological Diagnosis

Doctoral dissertation

To be presented by permission of the Faculty of Natural and Environmental Sciences of the University of Kuopio for public examination in Auditorium L3, Canthia building, University of Kuopio, on Friday 11th December 2009, at 12 noon

Department of Biosciences
University of Kuopio

KUOPION YLIOPISTO

KUOPIO 2009

Distributor: Kuopio University Library
P.O. Box 1627
FI-70211 KUOPIO
FINLAND
Tel. +358 40 355 3430
Fax +358 17 163 410
http://www.uku.fi/kirjasto/julkaisutoiminta/julkmyyn.shtml

Series Editor: Professor Pertti Pasanen, Ph.D.
Department of Environmental Science

Author's address: Department of Biosciences
University of Kuopio
P.O. Box 1627
FI-70211 KUOPIO
FINLAND
Tel. +358 44 516 5148
E-mail: Niko.Jukarainen@uef.fi

Supervisors: Professor Jouko Vepsäläinen, Ph.D.
Department of Biosciences
University of Kuopio

Docent Kari Tuppurainen, Ph.D.
Department of Biosciences
University of Kuopio

Samuli-Petrus Korhonen, Ph.D.
PERCH Solutions Ltd.
Kuopio, Finland

Reviewers: Professor Erkki Kolehmainen, Ph.D.
Laboratory of Organic Chemistry
University of Jyväskylä

Professor John C. Lindon, Ph.D.
Division of Surgery, Oncology,
Reproductive Biology and Anaesthetics
Imperial College, UK

Opponent: Professor Mika Ala-Korpela, Ph.D.
University of Oulu and Biocenter Oulu,
Faculty of Medicine, Institute of Clinical Medicine
Finland

ISBN 978-951-27-1405-6
ISBN 978-951-27-1460-5 (PDF)
ISSN 1235-0486

Kopijyvä
Kuopio 2009
Finland

Jukarainen, Niko. NMR Metabolomics Techniques and Mathematical Tools as an Aid in Neurological Diagnosis. Kuopio University Publications C. Natural and Environmental Sciences 259. 2009. 155 p.
ISBN 978-951-27-1405-6
ISBN 978-951-27-1460-5 (PDF)
ISSN 1235-0486

ABSTRACT

Nuclear magnetic resonance spectroscopy is a valuable tool in modern chemical and biochemical research and numerous applications can be found in both biology and medicine. The greatest use for NMR spectroscopy has however been in the field of chemistry, which has in recent years been extended to the measurement of metabolite concentrations in biofluids. This research topic is called metabolomics, which is defined as the analysis and evaluation of static cellular and biofluid concentrations of endogenous metabolites.

Metabolomics deals with the metabolome that represents the complete set of small-molecule metabolites. Even though metabolomics can be thought of as a relatively young method, it is nevertheless a rapidly growing one that also has the potential to impact our understanding of the molecular mechanism of disease. Furthermore, along with various mathematical tools, it also provides a powerful instrument for the analysis of individual metabolism, as well as for the examination of perturbations in metabolic pathways and networks in human disease. These are the reasons why NMR metabolomics has been an increasingly active research topic for the last 20 years, nowadays attempts are made in gathering unbiased samples of metabolites that could serve as snapshots of physiological and pathological states. The differentiation of healthy individuals and individuals that have or might develop a disease has also become a fundamental goal of research.

To understand brain function and the complexity within, new ideas and approaches are much needed. The knowledge of metabolic signatures for central nervous system (CNS) disorders could result in the identification of disease specific biomarkers and in the ability for disease progression or response to therapy analysis. Moreover, as the signatures are the final product of interactions gene expression, protein expression and the cellular environment, metabolomics provides tools for the process of drug development by providing detailed biochemical knowledge about drug candidates, their mechanism of action and side effects.

There has recently been explosive growth in this research area driven by the potential for earlier disease detection and ultimately for reaching the goal of personalized medicine. Connecting central and peripheral changes in CNS disorders could be the key to defining if and how biochemical changes in plasma are related to changes in the brain. Combining metabolomics with imaging methods and other omics approaches might be powerful ways to achieve these goals.

National Library of Medicine Classification: QU 25, QU 120, WL 141, WL 300, WT 155
Medical Subject Headings: Metabolomics; Metabolome; Magnetic Resonance Spectroscopy; Diagnostic Techniques, Neurological; Central Nervous System Diseases/diagnosis; Neurodegenerative Diseases/diagnosis; Alzheimer Disease/diagnosis; Biological Markers; Mathematical Computing

You are a fading dream, but one that has been touched by reality.
Run, dream. Run on into the daylight. And walk into reality.

ACKNOWLEDGEMENTS

First, I give my thanks to Prof. Jouko Vepsäläinen for his skillful guidance and his invaluable help in making this thesis finally rise from the lyophilized remains of CSF. Thank you.

Additionally, I thank my other supervisors, Dr. Samuli-Petrus Korhonen and Docent Kari Tuppurainen for their valuable guidance and insights in many matters also beyond the field of science. Thank you both, and remember that the post must flow. I also thank Prof. Tuula Pirttilä for her guidance in the neurological aspects of my work and the pre-examiners (Prof. John C. Lindon and Prof. Erkki Kolehmainen) for doing a very thorough job.

Iisalmi, peaceful countryside, November 2009

Niko Jukarainen

ABBREVIATIONS

1D	One dimensional
2D	Two dimensional
3D	Three dimensional
6-OHDA	6-Hydroxydopamine
Aβ	Amyloid-β-protein
AD	Alzheimer's disease
AHB	α–Hydroxybutyrate
AHIV	α–Hydroxyisovalerate
ApoE	Apolipoprotein E
APP	Amyloid precursor protein
ALS	Amyotrophic lateral sclerosis
BHB	β–Hydroxybutyrate
CA1	Cornu ammonis 1
CAC	Citric acid cycle
cAMP	Cyclic adenosine monophosphate
CNS	Central nervous system
COSY	Correlation spectroscopy
COX-2	Cyclo-oxygenase 2
CPMG	Carr-Purcell-Meiboom-Gill
CSF	Cerebrospinal fluid
CV	Cross-validation
DA	Discriminant analysis
DART	Direct analysis in real time
DESI	Desorption electrospray atmospheric ionization
DOPY	Diffusion ordered projection spectroscopy
DOSY	Diffusion ordered spectroscopy
DQF	Double quantum filtered
DSM-IV-TR	Diagnostic and Statistical Manual of Mental Disorders
DSS	2,2-Dimethyl-2-silapentane-5-sulfonate
EDTA	Ethylenediaminetetraacetic acid
EESI	Extractive electrospray ionization
ER	Endoplasmic reticulum
FLIPSY	Flip angle adjustable one-dimensional NOESY
FTD	Frontotemporal dementia
GABA	γ–Aminobutyrate
GFAP	Glial fibrillar acidic protein
HD	Huntington’s disease
HMBC	Heteronuclear multiple bond correlation
HMDB	Human metabolome database
HMQC	Heteronuclear multiple quantum correlation
HO-1	Heme oxygenase-1
HSA	Human serum albumin
HSQC	Heteronuclear single quantum correlation
J-RES	J-resolved spectroscopy
LBD	Lewy body disease
LOO	Leave-one-out
LMO	Leave-many-out
MHz	Megahertz
MAP	Microtubule-associated protein
MAS	Magic angle spinning
MCA	Middle cerebral artery
MCI	Mild cognitive impairment
MDA	Mean decrease accuracy
MDG	Mean decrease gini
MLR	Multiple linear regression
MTL	Medial temporal lobe
MRI	Magnetic resonance imaging

MRS	Magnetic resonance spectroscopy
MS	Multiple sclerosis
MSI	Metabolomics standards initiative
NAA	N-acetylaspartate
NFT	Neurofibrillary tangle
NINCDS-ADRDA	The national institute of neurological and communicative disorders and stroke and the Alzheimer disease and related disorders association
NMR	Nuclear magnetic resonance
NOESY	Nuclear overhauser enhancement spectroscopy
NOESYPRESAT	Nuclear overhauser enhancement spectroscopy with solvent presaturation
OOB	Out-of-bag
OPLS	Orthogonal projections to latent structures
OPLS-DA	Orthogonal projections to latent structures – discriminant analysis
PB	Phosphate buffer
PC	Principal component
PCA	Principal component analysis
PCR	Principal component regression
PD	Parkinson's disease
PDTC	Pyrrolidine dithiocarbamate
PET	Positron emission tomography
PFG	Pulsed field gradient
PHF	Paired helical filament
PKA	Protein kinase A
PKC	Protein kinase C
PLA2	Phospholipase A2
PLS	Partial least squares
PLS-DA	Partial least squares – discriminant analysis
PR	Pattern recognition
PRESS	Predictive residual sum of squares
RF	Random forest
S-DOSY	Statistical diffusion ordered spectroscopy
SAP	Stress-activated protein
SD	Sprague dawley
SF	Straight filament
SHY	Statistical heterospectroscopy
SIMCA	Soft independent modeling of class analogy
SM	Sammon's mapping
SNc	Substantia nigra pars compacta
SOD	Superoxide dismutase
SOM	Self organizing maps
SRMS	Standard metabolic reporting structures
STOCSY	Statistical total correlation spectroscopy
T_1	Longitudinal relaxation
T_2	Transverse relaxation
TARDBP	TAR DNA binding protein
TG	Transgenic
TG_ES	TG end stage
TG_PDTC	TG PDTC treated end stage
TG_PS	TG presymptomatic
TH	Tyrosine hydroxylase
tMCAO	Transient middle cerebral artery occlusion
TOCSY	Total correlation spectroscopy
TSP	3-(Trimethylsilyl)-propionic-2,2,3,3-d4 acid
VAD	Vascular dementia
WT	Wild type

CONTENTS

1. NMR SPECTROSCOPY IN A NUTSHELL

Nuclear magnetic resonance (NMR) spectroscopy is a valuable tool in modern chemical and biochemical research. Numerous applications can be found in both biology and medicine, though the greatest use for NMR spectroscopy has been in the field of chemistry. NMR is frequently used in the quantification of organic compounds as well as structure analysis and interpretation. In this chapter, the basics of NMR spectroscopy are shortly described. The concepts underlying advanced techniques such as spectral editing are discussed under the respective subtopics in chapter 3.

The nuclei of atoms can be described by the nuclear spin quantum number, I. The spin quantum number can have values greater than or equal to zero, and multiples of ½. When I=0, the mass and atomic numbers are both even, and the nuclear spin is not observable with NMR spectroscopy. Fortunately, all major organic chemistry elements have at least one nucleus that does possess an observable nuclear spin. These are the elements that can be of use in NMR spectroscopy. Examples of biologically useful nuclei include ^{1}H, ^{13}C, ^{31}P and ^{19}F. The reason why the nuclear spin is fundamental to the NMR phenomenon is because the spinning nucleus possesses an angular momentum which gives rise to an associated magnetic moment. When placed in an external magnetic field, such as the NMR instrument, the magnetic moments align themselves relative to the field in a discrete number of orientations, because the energy states are quantized. For a spin of magnetic quantum number I, there exist 2I+1 possible spin states, which means that for a spin-½ nucleus (a nucleus with an odd mass number) such as the proton, there exists two possible spin states denoted –½ and +½. Another example, deuterium with I=1, has three spin states, denoted -1, 0, and +1 and so on. The spin-½ nucleus can be thought of having an orientation parallel to the external magnetic field (α–state), or an orientation antiparallel to the magnetic field (β–state). Since the α–state is usually lower in energy, there is a bit more nuclei in that state. The energy difference between the two spin levels is rather small and the population difference between the α– and β–states can be calculated with the Boltzmann distribution; at 500 MHz the difference is 1 versus 0.9999872. The population difference between the states depends on the strength of the external magnetic field and temperature. The drawback is that only the population difference between the α– and β–states can be detected by means of NMR spectroscopy and this is what makes NMR spectroscopy insensitive relative to other techniques such as infrared or ultraviolet spectroscopy.

The magnetic moment of the spin can be stimulated with short duration radiofrequency energy, called a pulse. Because the energy states are quantized, the pulse induces changes in the populations: $\alpha \rightarrow \beta$, and $\beta \rightarrow \alpha$, of which $\alpha \rightarrow \beta$ is the more likely one; this meaning that if the pulse is repeated many times, the spin populations even out and the system is said to saturate. After the pulse is applied, the

emission signal of the energy stored in the nucleus (called the FID, free induction decay) can be detected. As the nuclei emit energy and relax, the population states return to their normal state and can be restimulated. The FID, known as the time-domain, can be converted to the frequency-domain spectrum by a process known as Fourier transformation (FT). The time-domain-format must be converted, because it is much harder to interpret than the frequency-domain where one can explicitly see the signals arising from nuclei. The domains of time and frequency are functions of intensity versus time, and intensity versus frequency, respectively. There is an important relation between the frequency of the NMR signal and the chemical structure of a molecule; this can be used to identify specific signals and can only be done in the frequency domain.

The frequency of the signal (versus a reference signal) is called the chemical shift and it depends on many factors, both internal, and external. The chemical shift gives information of the chemical environment and type of the nucleus. This information is highly affected by electronegativity and the structure of the molecule in question.

The spins of different nuclei interact with each other and this creates a phenomenon called spin-spin-coupling, which can be seen in the NMR spectrum as the splitting of signals. This coupling is not a direct magnetic dipolar interaction, but is transmitted via the electrons and is referred to as the coupling constant. The coupling constant can be used to identify magnetically active neighboring nuclei, and it also carries information about the three dimensional structure of the molecule.

The integral is the calculated area of a signal and if there is no signal overlap, it is also directly proportional to the molar concentration of the nucleus. By using the integral, it is possible to determine quickly for example the amount of protons for all of the signals because the integrals of the signals within one molecule are related. If, for example, an internal concentration standard is used, it is easy to calculate the concentration of the components using the integrals (when the concentration of the standard is known); in addition, only the number of protons in the standard needs to be known. This procedure is well demonstrated by e.g. Maillet *et al.* [1].

By using the information provided by the chemical shifts (expressed in ppm or hertz (Hz)), coupling constant (Hz), and integrals, the signals in the spectrum can be identified (assigned). By assigning all the signals, the chemical structure(s) of the molecule(s) in the sample can be determined. Furthermore, since the integral of the NMR signal is directly proportional to concentration of the component, it is possible to measure e.g. metabolite concentrations by acquiring an NMR spectrum.

One dimensional (1D) NMR is the most common type of NMR spectroscopy. This is because the experiments are fast to perform, and the spectrum is often quite easy to interpret and therefore, the approach to e.g. any structural problem of a molecule will eventually start by acquiring a 1D spectrum. In normal 1D techniques, a very simple scheme for acquiring spectra is used. The basic procedure is demonstrated in Figure 1 where three elements can be seen: i) a delay before the pulse, ii) the pulse, and iii) the acquisition time. The delay before the pulse is the relaxation delay for the nuclei. Relaxation is covered in more detail in chapter 3.2.

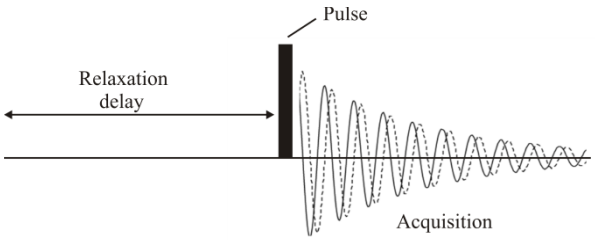

Figure 1. The basic 1D NMR acquisition scheme with including the essential elements: the relaxation (recovery) delay, the pulse, and the data acquisition period.

The most severe problem in 1D NMR is signal overlap. This means that there might be many signals that have a nearly identical chemical shift. These signals are hard to recognize from the spectrum since many signals in one spot tend to form one large signal, often called a multiplet or an unresolved signal. The multiplet however is a totally different concept than an overlapping or unresolved signal since multiplets can usually be seen and identified in the spectra whereas overlapping or unresolved signals might not be distinguished at all. The signal overlap can be reduced by using a higher frequency spectrometer, but often two or three dimensional (2D, 3D) NMR methods are required. 2D NMR techniques are aimed at determining correlations between spins of the same (*homonuclear*, e.g. ^{1}H-^{1}H), or different (*heteronuclear,* X-^{1}H, where X is for example ^{13}C, ^{15}N, or ^{31}P) nuclei. Commonly 2D NMR methods, including their applications, are collected in Table 1.

Table 1. The most commonly used 2D NMR techniques including relevant applications. The X nucleus is a nucleus other than ^{1}H, such as ^{13}C, ^{15}N, ^{19}F or ^{31}P. An inverse technique is one in which the good sensitivity of the ^{1}H nucleus is utilized as an advantage; the X nucleus chemical shift is measured through its connection to the 1H nucleus. Abbreviations: J-RES=J resolved spectroscopy, COSY=correlation spectroscopy, DQF=double quantum filtered, TOCSY=total correlation spectroscopy, HMQC=heteronuclear multiple quantum correlation, HSQC=heteronuclear single quantum correlation, HMBC=heteronuclear multiple bond correlation.

Technique	Principal application	Type
J-RES	Separation of homonuclear or heteronuclear couplings from chemical shifts. Used to determine the multiplicity of the NMR band or to provide direct measurement of coupling constants.	^{1}H-^{1}H/^{1}H-X
COSY	Correlating coupled homonuclear spins. Typically used for correlating protons coupled over 2 or 3 bonds. The basic COSY experiment.	^{1}H-^{1}H
DQF-COSY	Correlating coupled homonuclear spins. Typically used for correlating protons coupled over 2 or 3 bonds. Offers higher spectral resolution than the basic COSY experiment and also removes singlets from the spectra.	^{1}H-^{1}H
TOCSY	Correlating coupled homonuclear spins and those that reside within the same spin system. Powerful technique for analyzing complex proton spectra. A selective TOCSY is also available for producing 1D subspectra for discrete spin-systems within the molecule, potentially revealing multiplet structures that were otherwise overlapped or buried.	^{1}H-^{1}H
HMQC	Correlating coupled heteronuclear spins across a single bond and hence identifying directly connected nuclei. Employs detection of high sensitivity nuclei e.g. ^{1}H, ^{19}F (an "inverse technique"). Well suited for routine structural characterization.	^{1}H-X
HSQC	Correlating coupled heteronuclear spins across a single bond and hence identifying directly connected nuclei. Employs detection of high sensitivity nuclei e.g. ^{1}H, ^{19}F (an inverse technique). Provides improved resolution over HMQC, but is more sensitive to experimental imperfections.	^{1}H-X
HMBC	Correlating coupled heteronuclear spins across multiple bonds. Employs detection of high sensitivity nuclei e.g. ^{1}H, ^{19}F (inverse technique). Powerful tool for linking together structural fragments.	^{1}H-X

Regardless of dimensions, proton NMR spectroscopy is very popular because of the very favorable properties of the nucleus (see below); additionally there are protons practically in every organic molecule. Favorable properties in terms of NMR spectroscopy means that the natural abundance is high (99.98% for ^{1}H), and the sensitivity of the nuclei is relatively good. Because the natural abundance and relative sensitivity (all other nuclei are usually compared to ^{1}H, hence the word relative) are good, ^{1}H spectra are fast to acquire and high concentration samples are not needed. The chemical shifts of protons are usually in the range of 0-10 ppm. ^{13}C is another commonly used nucleus even though it has a poor relative sensitivity (0.016 compared to the proton). ^{13}C NMR is perhaps the most utilized heteronuclear NMR technique used for organic studies, and the second most utilized (^{31}P the most utilized) technique in biochemical and metabolite studies. The low natural abundance introduces an advantage

in interpreting ^{13}C NMR spectra; ^{13}C-^{13}C coupling is not normally visible in the spectrum which makes the chemical shift more readily observable. ^{13}C-enrichment can be used in cases when more sensitivity is required. Carbon chemical shifts are spread on a much wider ppm range (-20 to 220 ppm).

Biologically considered, there are also other useful nuclei. ^{31}P and ^{15}N are useful, but they have some drawbacks, which is why they are not used as often as ^{1}H or ^{13}C. ^{31}P has an excellent natural abundance (100%), but its relative sensitivity is only 0.066 due to its low gyromagnetic ratio. These parameters make the ^{31}P a quite good nucleus, easy to measure, but the experiment times are quite long because of the poor sensitivity. The ^{31}P chemical shifts are usually between -50 to 250 ppm, and even though biological phosphates have a smaller shift range, the total shift range is as large as -1000 to 1000 ppm. Also, the oxidation state of phosphorus can be determined from its NMR spectrum (P(III) $\rightarrow$ shift $\geq$ 100 ppm, P(V) $\rightarrow$ shift $\leq$ 700 ppm). ^{15}N is a much more problematic nucleus since its natural abundance is only 0.365%. In addition, the ^{15}N nucleus only has a sensitivity of 0.001 compared to the proton (again due to its very low gyromagnetic ratio) and a negative nuclear overhauser effect (NOE). The chemical shifts of ^{15}N lie between -50 and 400 ppm. Because of the nucleus's extremely poor properties, ^{15}N labeling (or a ^{1}H-^{15}N inverse experiment, see Table 1) is usually required if a good spectrum is desired.

2. THE AIM OF THIS STUDY

The aim of this study was to a) build up and assess new NMR spectroscopic methods for use in NMR metabolomics, and b) to test the performance of various mathematical multivariate methods in the context of NMR metabolomics.

The NMR methods will tested and used for the purpose of acquiring more reliable quantification results, which can then be used in further analyses such as the exploring the neurological relevance of the concentration changes of various metabolites in the brain. A new quantification method based on *a priori* constraint information will be developed and its performance evaluated in the context of both animal and human models featuring various neurological disorders. The performance of commonly used NMR metabolomics tools will also be studied and commented. The multivariate methods that will be assessed are ones that are currently commonly used in NMR metabolomics (see chapter 3.3). Although it is commonplace to use multivariate methods for e.g. classification purposes, there currently exists no consensus in the NMR community on which method is the most useful one for the different types of data. Therefore these methods also deserve some type of review.

This thesis is presented as a monograph and as such features both published articles and manuscripts. The first manuscript outlines the use of various parameters in T_2-editing as a spectral editing method for NMR metabolomics (Manuscript I: chapter 3.2.6). The second article, recently published in *Metabolomics*, presenting the constrained total-line-shape (CTLS) NMR quantification method, can be found in chapter 3.2.7 as an adapted version (Manuscript II). The applications of the CTLS-method for quantification of brain metabolites used in subsequent classification and characterization of the patients are outlined in the manuscripts based on both human (Manuscript III: chapter 4.3.2) and animal models (Manuscript IV: chapter 4.3.3). The multivariate methods have been assessed to a great extent for the human CSF data in manuscript III.

3. NMR METABOLOMICS

The measurement of metabolite concentrations in biofluids is not a new concept. The current principles, strongly influenced by the pioneering group led by Prof. Jeremy Nicholson and Prof. John C. Lindon (both from Imperial College, London), now define two words for this type of research: 1) metabonomics, which is defined as the "*quantitative measurement of the time-related multiparametric metabolic response of living systems to pathophysiological stimuli or genetic modification*" [2, 3] and, 2) metabolomics, which is defined as the analysis and evaluation of *static* cellular and biofluid concentrations of endogenous metabolites [2]. Metabolomics naturally deals with the metabolome that represents the complete set of small-molecule metabolites. These include hormones and other signalling molecules, metabolic intermediates, and secondary metabolites. Thus metabolomics, or metabolic profiling, can instantly give a snapshot to the in depth physiology of a sample under scrutiny. NMR metabolomics has been an increasingly active research topic for the last 20 years, nowadays attempts are made in gathering unbiased samples of metabolites that could serve as snapshots of physiological and pathological states. A fundamental goal has become the differentiation of healthy individuals and individuals that have or might develop a disease [3].

Some form of spectroscopy is a common way of acquiring the metabolite concentration wanted. It does not really matter that much which spectroscopic method is used, as long as the datasets are rich in molecular information, but NMR spectroscopy does have several advantages over other methods. The main reason being that this method allows the harvesting of all small molecule metabolite concentrations simultaneously, without complex sample treatment and instrumental calibration [4]. Additionally, NMR spectroscopy is the only detection technique which does not rely on separation of the analytes, and the sample can thus be recovered for further analyses. Furthermore, NMR is the only method currently available for studying intact tissue samples [2]. The other common metabolite detection method, mass spectrometry (MS), is however more sensitive; detection limits in NMR and MS are in the ≥1 μmol/L and <1 pmol/L range, respectively [5]. Many metabolomics studies do employ some type of MS-coupled detection method and the differences of these methods are summarized and compared to NMR spectroscopy (see Table 2). The MS-coupled methods feature an earlier separation of analytes typically by gas chromatography (GC) or liquid chromatography (LC), the latter currently being the most important form of application because of its sensitivity and rich information content [6]. Recently, other MS methods have also been developed, including extractive electrospray ionization (EESI)-MS [7], desorption electrospray atmospheric ionization (DESI)-MS [8] and direct analysis in real time (DART)-MS [9]. Advantages of these novel methods feature very little or no sample preparation or extraction [10].

Table 2. A comparison of different techniques currently commonly used for metabolite concentration measurements, including their advantages and disadvantages.

Technology	Advantages	Disadvantages
NMR spectroscopy	Quantitative Non-destructive Fast (2-3 min/sample) No derivatization needed No separation needed Detects a large scale of organic compounds Allows ID of new chemicals Robust, mature technology Can be used for metabolite imaging (MRS or MRSI) Large amounts of software and databases for metabolite ID Compatible with liquids and solids	Not very sensitive Expensive instrumentation Large instrument footprint Cannot detect or identify salts and inorganic ions Cannot detect non-protonated compounds Requires larger (0.5 ml) samples although microprobes can handle as little as 10 µl
GC-MS spectroscopy	Robust, mature technology Relatively inexpensive Quantitative (with calibration) Modest sample size needed Good sensitivity Large amounts of software and databases for metabolite ID Detects most organic and some inorganic molecules Excellent separation reproducibility	Sample not recoverable Requires sample derivatization Requires separation Slow (20-30 min/sample) Cannot be used in imaging New compound ID difficult Only applicable for small molecules that are easily vaporized
LC-MS spectroscopy	Superb sensitivity Very flexible technology Detects most organic and some inorganic molecules Minimal sample size requirement Can be used in metabolite imaging (MALDI) Requires no separation (direct injection) Has potential for detecting the largest portion of the metabolome	Sample not recoverable Not very quantitative Expensive instrumentation Slow (20-30 min/sample) Poor separation resolution and reproducibility (vs. GC) Less robust instrumentation than NMR or GC-MS Limited amount of software and databases for metabolite ID New compound ID difficult

An important aspect to note is that while it has been argued that the biggest challenge facing the scientist in NMR based studies is not the analysis itself, which has been shown to be reproducible and robust, but the reduction of the biological variation of the samples themselves [11]. Even though differences in "spectrometer output", based on deviations in solvent suppression or internal spectrometer variations, have been reported in the literature [12, 13], these differences are commonly minor when compared to those caused by e.g. toxicological effects [14-17]. The largest amount of variability is naturally expected, and indeed detected, in human studies. Studies involving animals, such as rodents, enable experiment protocols to be more tightly controlled because factors such as diet, environment, strain and gender can be monitored and affected, allowing the establishment of "normal" variation

[11]. Studies involving humans are commonly complicated by the lack of control over diet, age, lifestyle, and the time of sampling [18-22]. However, some studies on the same subjects have shown that despite tight dietary and lifestyle control, differences in at least ^{1}H NMR derived urinary and plasma profiles can arise [21]. Further information on disease states, perhaps multiple diseases, information on administered medication, and pharmacological effects of medication can complicate the data. Moreover, even the effect of aging is very important and should not be ignored. Because of these numerous sources of variation, determining and minimizing the normal variation is crucial for every study, irrespective of the analytical technique subsequently used for analysis [11].

Key applications of metabolomics include **toxicology and toxicity assessment** (e.g. the detection of changes caused by the toxicity of a chemical), **functional genomics** (e.g. predicting the function of unknown genes by comparison with the metabolic perturbations caused by deletion or insertion of known genes), **nutrigenomics** (e.g. determine a biological endpoint of the metabolism of an individual), **metabolic fingerprint creation** and various types of **disease diagnostics** (e.g. early stage detection of neurological disorders). The relevant applications will be covered in more detail in later chapters.

Some shifting from biofluid NMR toward *in vivo* methods has been observed in cases when dealing with more invasive biofluid sampling, such as acquiring cerebrospinal fluid (CSF). *In vivo* studies though, while noninvasive, are not as sensitive as biofluid based NMR spectroscopy and therefore fewer metabolites are detected and the spectral resolution is compromised. Intact tissues however, are a different matter as they can be analyzed by the rapidly developing high-resolution ^{1}H magic angle spinning (MAS) NMR spectroscopy. With MAS NMR, the analysis of small pieces of intact tissues has become feasible. MAS NMR involves the rapid spinning (c.f. to no spinning in normal biofluid NMR) of the sample (typically at ~4-6 Hz) at an angle of 54.7° relative to the applied magnetic field, which reduces the loss of information caused be line broadening effects seen in nonliquid samples such as tissues. Sample preparation, although manual, is also straightforward. The basic NMR spectroscopy experiment on a tissue sample is the same as in solution state NMR and all common pulse techniques can be employed in order to study metabolic changes and to perform molecular structure analyses [23].

3.1 From NMR Spectra to concentrations

An NMR spectrum in itself does not reveal all the information necessary for analytical purposes, several identifiable resonances are likely visible, but for a more accurate analysis, integration or quantification is needed. Simple integration of the signals is not usually sufficient since, especially in 1D NMR spectra, many of the hundreds of signals in the spectrum are overlapped. The selection of the biological medium used for the analysis makes a profound difference in signal analysis and therefore the most common mediums will be shortly discussed below. Some mediums are more complex than others; whereas some contain e.g. a larger concentration of protein which naturally affects the analysis of metabolites. For an example of biofluid complexity, see Figure 2.

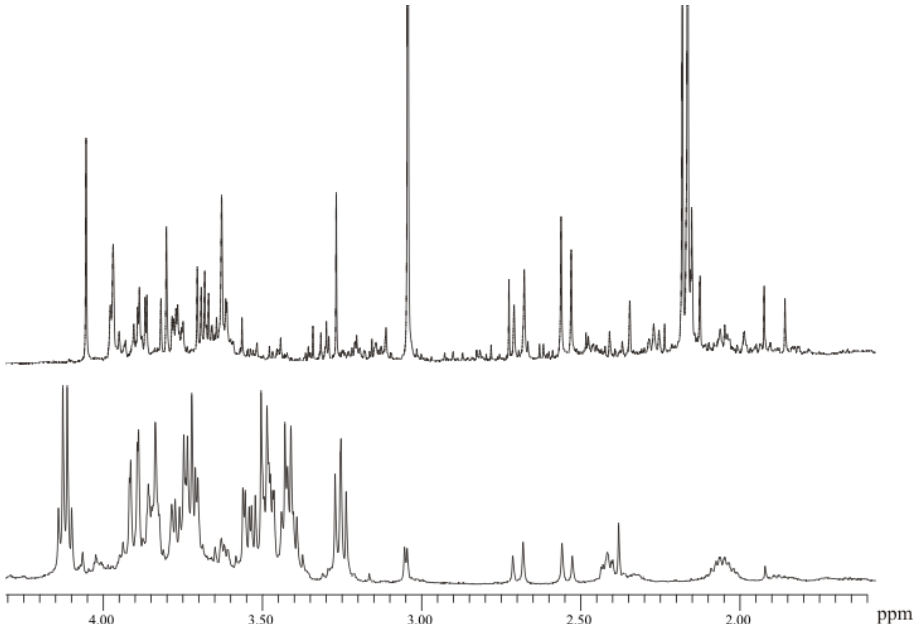

Figure 2. A representation of biofluid NMR spectra complexity. Above, part of the aliphatic region of a 500 MHz ^{1}H spectrum of human urine and, below, the same region from a 500 MHz ^{1}H spectra of human cerebrospinal fluid.

Quantification of metabolites can be done in several ways. The traditional approach is to integrate defined spectral regions or "bins" to reduce a complex spectrum of single peak intensities to a more limited number of spectral variables commonly referred to as bins or "buckets". This method in itself is simple and can also be automated [24] but has its own limitations such as the loss of information and the occurrence of artifacts caused by peaks shifts [25]. Many biologically important metabolites such as citrate, taurine, and glucose, possess peaks whose chemical shifts vary in an uncontrolled manner between samples [26, 27]. This is a result of variation in pH and metal ion concentration and gives rise to different levels of ionization or conjugation in the target molecules. More "modern" methods alleviating or simplifying quantification include methods based on "intelligent bucketing" [25, 28], artificial neural networks [29], total-line-shape fitting and deconvolution [26], and curve-fitting [27, 30]. A recent study [31] also reports that the combination of ethylenediaminetetraacetic acid (EDTA) and an appropriate buffer effectively minimizes both pH dependent frequency shifts and ionic strength dependent variations in urine NMR spectra. Furthermore, practical use can likely be found for the algorithms for automated chemical shift calibration presented in another study [32].

Prior to quantification, the NMR spectrum in itself can be simplified by applying different types of spectral editing methods. These methods are discussed in more detail in chapter 3.2. All of these methods do have at least one aim in common: more reliable quantification of overlapping signals in 1D NMR spectra. Once the desired resonances of metabolites have been selected, assigned, and quantified, the acquired concentrations can be used for further analyses.

3.1.1 Blood plasma and serum

Blood plasma and serum are common biofluids in NMR metabolomics for various reasons. Serum is preferred over plasma for most experiments since blood clotting corrupts the analysis of small molecule composition [33]. Blood samples are relatively easy to obtain and most of the relevant NMR detectable metabolites have been assigned in literature and furthermore, NMR chemical shift information for a large number of metabolites present in different biological mediums are freely available on the internet (The Human Metabolome Database) [34-36]. Blood plasma and serum contain both low and high molecular weight compounds that feature a wide range of signal line widths. Especially the broad bands from protein and lipoprotein signals contribute strongly to the ^{1}H NMR spectra, with sharp peaks from small molecules superimposed on them. The broad resonances can be suppressed by using various methods of spectral editing (see chapter 3.2 for details) and the large NMR signal arising from water, present in all biofluids, is easily eliminated by the use of appropriate standard NMR solvent

suppression methods [23]. The standard chemical shift reference used for biofluids is 3-(trimethylsilyl)-propionic-2,2,3,3-d4 acid (TSP), but due to its affinity to proteins which likely results in quantification errors, it is not recommended as a quantification reference in blood plasma and serum because of the high (~5 %) protein content of the mediums [37]. As an alternative, 2,2-dimethyl-2-silapentane-5-sulfonate (DSS) is commonly used [23, 38]. Some methods for plasma deproteinization as a solution to high protein concentration also exist [39]. The study by Daykin *et al.* presents results based on the fact that since several methods (e.g. ultrafiltration and acetonitrile precipitation) are available, choosing the correct one for use is an essential part of the NMR study of metabolites in human blood plasma (e.g. the filtration of proteins will also result in the loss of protein bound metabolites).

Blood based samples are commonly used for clinical diagnostics because the protein composition bears a wealth about the health of an organism. Due to the previous, blood plasma and serum have been extensively used in NMR metabolomics studies such as the fat oxidation capacity of blood [40], pancreatic cancer studies [41], hepatoxicity [42], dietary studies [43], hypertension [44], and coronary heart disease [45]. Many applications also currently include the analysis of blood lipid content [3, 46]. For the purposes of future disease diagnostics and large patient populations, several models involving high sample throughput and analysis automation have also been in development [47, 48].

3.1.2 Urine

Urine is another common biofluid in metabolomics, mainly due to the fact that sample collection is even more noninvasive than when dealing with blood. This creates advantages especially in toxicology or drug follow-up studies where several samples (e.g. pre dose, after dose) are needed, hence effects prior to and post dosing can be monitored effectively. Urine samples can also be pooled, thus averaging variability (exercise, diurnal variation, etc), which is important since variability is a problem in some sample cases [11]. Urine contains more metabolites than blood and CSF, which in turn creates more overlapping signals in an NMR spectrum, and while urine is one of the simplest fluids in physicochemical terms, the need to maintain homeostasis results in it being one of the most complex in composition [49].

Many urine studies of toxicology deal with animal models the results of which can however be quite easily related to human metabolism. Key applications in urine NMR metabolomics include the profiling of specific metabolic maps in various diseases [50, 51], toxicology studies in animal models [16, 52-55], drug treatment observation [56-59] and a tool in transplantation success survey [60].

3.1.3 Cerebrospinal fluid

CSF indirectly reflects the biochemical processes occurring in the brain. Therefore its composition can be anticipated to provide information about states of normal or pathological metabolism of the brain. The biochemical composition of CSF resembles that of ultrafiltered blood plasma, but it additionally contains metabolites which are secreted by the central nervous system (CNS) [1, 35]. Although CSF samples are more difficult to obtain than blood or urine samples, for an NMR analysis, CSF possesses clear advantages due to the relatively low protein and lipid content and the low viscosity of the medium. The low protein content also makes it possible to use TSP as an internal standard. Additionally, signal overlap in CSF is not as serious as in urine or whole blood, because of the fewer metabolites present [35].

Several NMR studies on CSF have been reported [1, 26, 61-63] and nowadays the cerebrospinal fluid metabolome is available for free access on the internet [64]. Because of the invasive nature of the sampling the NMR analysis of CSF tends to lean toward *in vivo* methods. This is due to medical, technical, and ethical constraints and the lack of specific information on metabolic perturbations which are truly characteristic of CNS disorders [65-68].

3.2 Methods of spectral simplification

Several methods for spectral editing are readily available, the most prominent ones being relaxation (T1, T1ρ, and T2) and diffusion editing. The other topics, curve fitting and deconvolution, are not strictly spectral editing methods. Instead, these techniques aim to simplify NMR spectra quantification by utilizing the underlying quantum mechanics and alleviating the problems of signal overlap and frequency shift. The most commonly used methods, including their advantages and disadvantages, have been summarized in Table 3.

Table 3. A summary of the advantages and disadvantages of commonly used spectral measurement and editing methods in NMR metabolomics studies.

Method	Usage	Advantages	Disadvantages
Presaturation and NOESY (NOESYPRESAT)	Detects signals from both small- and relatively large-molecular weight metabolites; this is also the current 1D sequence of choice [23][$]	Highly quantitative and good for high-throughput screening	Spectra are generally complex because of the presence of both low- and high-concentration molecular signals and extensive J coupling
Flip angle adjustable one-dimensional NOESY (FLIPSY) [69]	An interesting option for replacement of NOESYPRESAT as the 1D sequence of choice for metabolomics	Same as above, except for a better signal to noise ratio	Same as above
Relaxation editing (T_2)	Provides signals from small molecules by suppressing NMR signals from large molecules	Spectra are easy to interpret due to the simplification achieved and are good for high-throughput screening applications using e.g. serum or blood plasma samples	Does not show appreciable simplification for biofluids such as urine in which the majority of the metabolites are small molecules; is also less quantitative than normal 1D sequences
Diffusion editing	Provides information on relatively large molecules such as lipids	Simple, good for high-throughput screening of large molecules in serum and blood plasma samples	Not useful for samples such as urine where there are no appreciable differences in diffusion coefficients; is also less quantitative than normal 1D sequences

[$]NOESYPRESAT is the method of choice instead of a "normal" 1D sequence because NOESY spectra feature more efficient water suppression especially in the peak wings.

3.2.1 Relaxation editing

To understand relaxation, we must first understand, what happens when a radiofrequency pulse is applied to the sample. When a sample is placed in the NMR instrument, it experiences an external magnetic field (B_0) aligned on the positive z-axis and the nucleus spins around its own axis. In the presence of the magnetic field, this axis of rotation will precess around the magnetic field (Figure 3). This precession occurs at a certain frequency, which is called the Larmor-frequency, specific for each nucleus. When applied, the radiofrequency pulse creates an external magnetic field (B_1) which lies in the x-y plane perpendicular to the internal B_0 field along which the net magnetization is aligned.

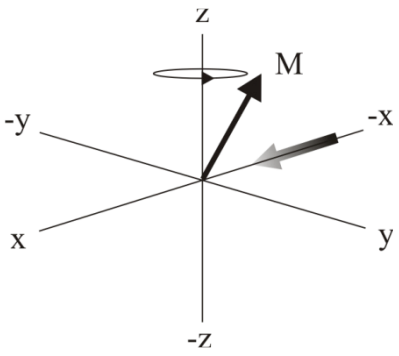

Figure 3. The magnetic moment vector (M) precessing around the z-axis.

Before the pulse is applied, the nuclear spins are in a relaxed state, and the total magnetic moment is on the z-axis (Figure 4). In the following examples, the radiofrequency pulse is applied from the negative x direction. This pulse perturbs the nuclear spins from their relaxed state and the magnetization vector is driven on the y-axis (Figure 4). The pulse is said to be a $\pi/2$ pulse (also called as a 90° pulse) if the magnetization is driven all the way to the xy-plane. This is favorable because the receiver is on the xy-plane, and by driving the vector 90° from the z-axis to the y-axis, the maximum intensity of the signal can be observed. If a longer pulse is applied, the magnetization vector moves even further, i.e. a π (180°) pulse would invert the magnetization to the −z-position, and a 2π (360°) pulse would turn the magnetization back to where it was at the beginning.

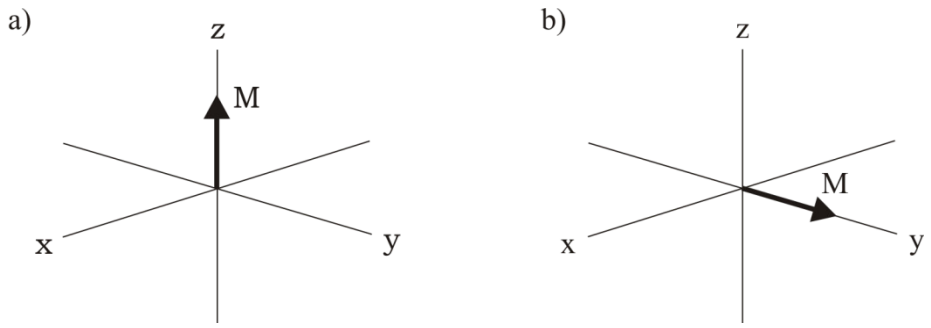

Figure 4. a) The total magnetic moment of the nuclear spins in its relaxed state on the z-axis, b) the magnetization vector driven to the y-axis by a $\pi/2$-pulse.

To aid visualization of the occurring NMR processes during the experiment, some conceptual changes are employed. After the pulse has been applied, the oscillating B_1 field is considered to be composed of two counter-rotating vectors in the x-y plane; the resultant of which corresponds exactly to the oscillating field (Figure 5). Things can be simplified considerably by eliminating one of these vectors and simultaneously freezing the motion of the other by picturing events in a *rotating frame* of reference (Figure 6). This way, the set of x, y, and z co-ordinates are viewed as rotating along the nuclear precession, in the same sense and at the same rate. Because the frequency of oscillation of the rf field exactly matches that of the nuclear precession, the rotation of one of the rf vectors is now static in the rotating frame whereas the other is moving at twice the frequency in the opposite direction. This latter vector precesses at such a high frequency, that it does not interact with the magnetic moment of the nucleus, and can therefore be ignored. At the same time, the precessional motion of the spins has been frozen because these too are moving with the same angular velocity as the rf vector and hence the co-ordinate frame. Also, since this precessional motion was induced by the B_0 field, it also is no longer present in the rotating frame representation. This simplification aids in understanding the upcoming notions about the NMR vector model.

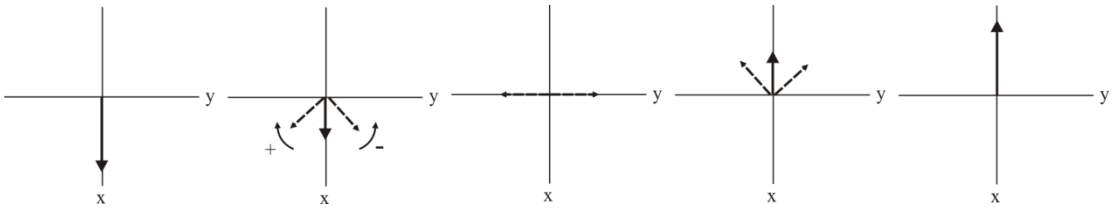

Figure 5. The rf pulse provides an oscillating magnetic field along one axis (here the x-axis) which is equivalent to two counter-rotating vectors in the transverse plane.

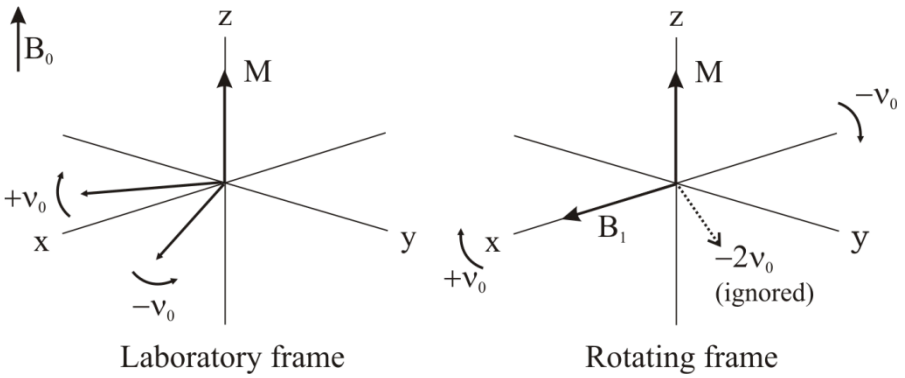

Figure 6. The laboratory and rotating frame representations, where M is the total magnetic moment vector, B_0 is the external magnetic field produced by the NMR instrument, and B_1 is the magnetic field provided by the rf pul-se. The difference is that in the laboratory frame the co-ordinate system is viewed as being static, whereas in the rotating frame it rotates at a rate equal to the Larmor frequency of the nucleus in question (ν_0). In this representation the motion of one component of the applied rf is frozen whereas the other is far from the resonance condition and may be ignored. This provides a simplified model for NMR experiments.

When the pulse has been applied, there exist two types of relaxation, defined as the loss of magnetization. The T_1-relaxation: also called longitudinal relaxation or spin-lattice relaxation (enthalpic relaxation), and the T_2-relaxation: also called transverse relaxation or spin-spin relaxation (entropic relaxation). The T_1-relaxation time is a constant that represents the "lifetime" of the first order rate process that returns the magnetization to the +z-axis. It is thus the time it takes for the signal to recover 1-(1/e) of its initial value after being flipped into the magnetic transverse plane (xy-plane). It therefore takes 5 x T_1 for 99.33% of the magnetization to relax back to the +z-axis (Figure 7). The mathematics behind T_1-relaxation is the Bloch theory of NMR that assumes that the recovery of the +z-magnetization, M_z, follows exponential behavior, described by the following equation:

$$\frac{dM_Z}{dt} = \frac{(M_0 - M_Z)}{T_1}$$

where M_0 is the magnetization at thermal equilibrium, and T_1 is the (first order) time constant for this process. Starting from the position of no net z-magnetization (Figure 4) the longitudinal magnetization as shown in the following at time t will be:

$$M_Z = M_0(1 - e^{-t/T_1})$$

and so the rate at which magnetization recovers is represented by the *rate constant* $1/T_1$ (s^{-1}).

The difference between the two relaxation methods is that T_1-relaxation is the process of losing energy to the surrounding nuclei and the magnetization returning to the z-axis (Figure 7, where it was before

the pulse); while T_2-relaxation occurs when spins in the high and low energy state exchange energy but do not loose energy to the surrounding nuclei. The T_2-relaxation time is the time it takes for the transverse signal to reach 1/e of its initial value after flipping into the xy-plane (Figure 7). If the nuclei studied possess different properties, they can be differentiated by their T_2-relaxation time. This is used for advantage i.e. in some 2D NMR experiments, or relaxation edited experiments such as protein-ligand interactions.

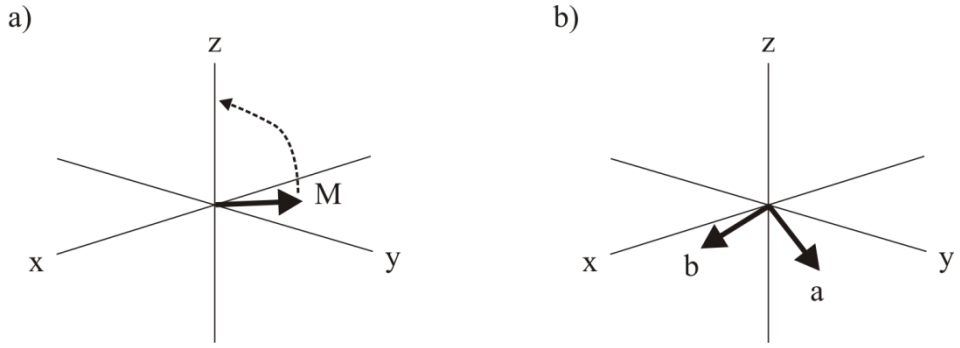

Figure 7. a) T_1-relaxation. The magnetization vector is returning back to the z-axis, b) T_2-relaxation. The magnetization vectors of two components (a and b) precessing in the xy-plane.

When the pulse is applied, it takes some time for the relaxation to occur. It is not very useful to apply a new pulse before the relaxation has occurred, because that will reduce the signal intensities and eventually lead to saturation. The relaxation time is very different depending on the chemical nature of the nuclei, molecular size, mobility, and structure. Basically proton relaxation times are usually between 1-5 seconds, while in some very simple structures they might be as long as 60 seconds. Macromolecules on the other hand, have very short relaxation times for protons. Quaternary and carbonyl carbons usually have very long (ca 60-90 seconds) relaxation rates, while "normal" carbon atoms with a proton have relaxation rates between 2-20 seconds. A unusual case would be very long aliphatic chain structures (e.g. fatty acids) in which the carbons in the middle of the chain have very short relaxation times, while the carbons at the end of the chain have very long relaxation times. A special case with an exceptionally long relaxation time would be a small and symmetric molecule such as H_2O or chloroform.

Knowledge of the relaxation times of biologically relevant nuclei is essential for carrying out successful *in vivo* and solution state NMR spectroscopy. The T_1 and T_2-values assist in selecting appropriate pulse parameters for basic measurements, optimizing signal to noise ratio, and in particular, allow the use of spectral editing techniques. T_1 and T_2 can also provide information about molecular mobility and some hints about structure. T_2 measurements by using different intervals between 180° pulses can

provide information about diffusion rates and pulse sequences that are used for T_1 and T_2 measurements can also provide a method of simplifying spectra and enhancing resolution.

The T_1-relaxation time is easy to measure for any sample. It is important to note that for a spin to relax thoroughly, it is necessary to wait a period of at least 5 x T_1 and thus it might be necessary to wait for many minutes. This is especially important if quantitative (accurate signal-area values) results are desired. There is however a way to lower the time required for relaxation by applying a shorter pulse, which does not drive the magnetization vector all the way to the y-axis. This naturally makes relaxation much quicker, but signal intensities are much smaller. However, usually a good compromise between these two aspects can be found.

The most commonly applied method for T_1-relaxation measurements is the use of the inversion recovery sequence. Basically the only thing that needs to be done is to perturb a spin system from equilibrium, and then devise some means of following its recovery as a function of time. The pulse sequence for the inversion recovery experiment is shown in Figure 8. The 180° π pulse first inverts the magnetization to −z-position after which there is a recovery delay (τ). The delay is followed by a normal π/2-pulse, which moves the magnetization vector 90° from where it was after the τ–delay. In the beginning of the experiment, the signals will start out inverted because of a short τ–delay and as the recovery time is increased, the signals will recover their equilibrium magnetization and a typical "positive" spectrum is obtained. The point when a given signal has zero intensity in this experiment is termed τ_{NULL}. The T_1-relaxation can now be calculated as it is approximately $1.44*\tau_{NULL}$. For more details, see e.g. [70].

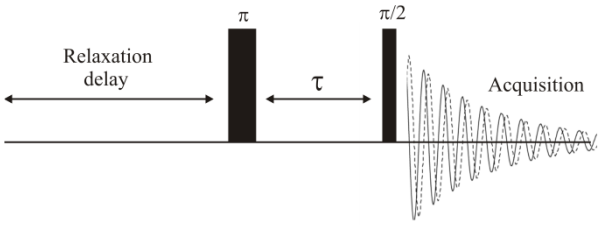

Figure 8. The inversion recovery experiment. This sequence consists of a relaxation delay followed by a π-pulse (180°). τ is the delay after the long pulse, followed by the normal π/2-pulse and acquisition.

The measurement of T_2 times features a spin-echo sequence or some variation of it. In a simple spin-echo sequence a 90° π/2-pulse first tilts the magnetization to the xy-plane and then the magnetic vec-

tors fan out during the dephasing period (τ) due to T_2 relaxation and magnetic field inhomogeneity (Figure 7). A π pulse is then applied and this inverts the magnetization on the xy-plane and after time τ the formation of an echo can be observed (Figure 9). If molecular diffusion is negligible, it is only necessary to measure the echo amplitude for several values of τ and to use a single exponential fit to obtain the T_2 time. The T_2 time can also be measured from the half-width of the peak of the molecule in question but this method is prone to errors because of magnetic field inhomogeneties resulting in wider NMR signals.

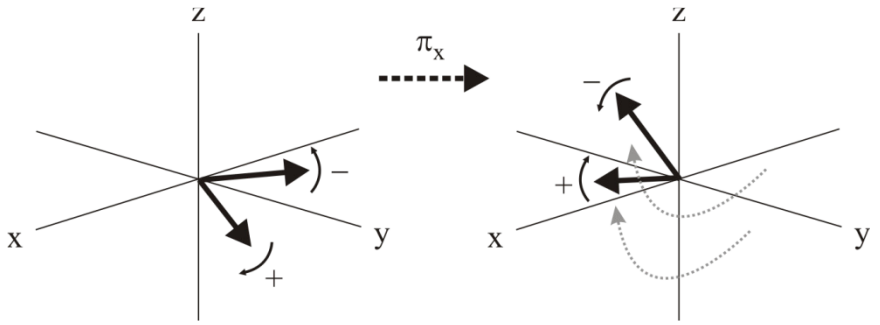

Figure 9. The magnetization inversion in the xy-plane as a result of the 180° pulse.

Measuring T_2 times is not however the most useful application of T_2 relaxation based sequences. The most useful ones deal with spectral editing and for this purpose (and to reduce the effect of molecular diffusion) a modification of the spin-echo sequence has been introduced which involves replacing the single 180° π pulse by a train of 180° pulses at intervals of 2τ [71]. There were difficulties related in obtaining precise pulse lengths for the inversion however, and an adaptation in the form of another modified pulse sequence was created four years after the first modification was presented. This newer sequence is commonly known as the Carr-Purcell-Meiboom-Gill (CPMG) sequence [72]. In this sequence there is a 90° phase shift between the initial 90° and subsequent 180° pulses (see Figure 10). Thus, for the 90° pulse along the x-axis, subsequent 180° pulses are applied on the y-axis. This has two important effects: i) the echoes all form along the same direction (y-axis) and, ii) any errors in the accuracy of the 180° pulses tend to cancel out.

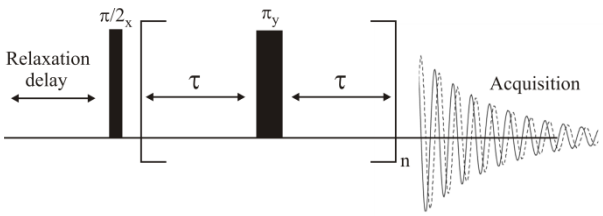

Figure 10. The CPMG pulse sequence.

The abovementioned CPMG sequence is nowadays routinely used in simplifying ^{1}H NMR spectra in cases where the broad macromolecular resonances overlap the sharper and smaller signals of molecularly smaller components such as metabolites [73]. This can be done because of the drastically different T_2 times of the two molecule sets; a protein molecule is much larger and therefore has a much shorter T_2 time than a small metabolite. When T_2 editing is applied in e.g. a ^{1}H NMR spectrum of blood, the metabolite signals remain visible in the spectrum whereas the protein signals disappear (see Figure 11). The method has been successfully used in many biofluids and tissues such as blood plasma [74] and liver tissue [73], and while some other approaches, such as different types of mathematical transformation of the free induction decay have been assessed [75], T_2-editing can be defined as the current method of choice in NMR metabolomics [76].

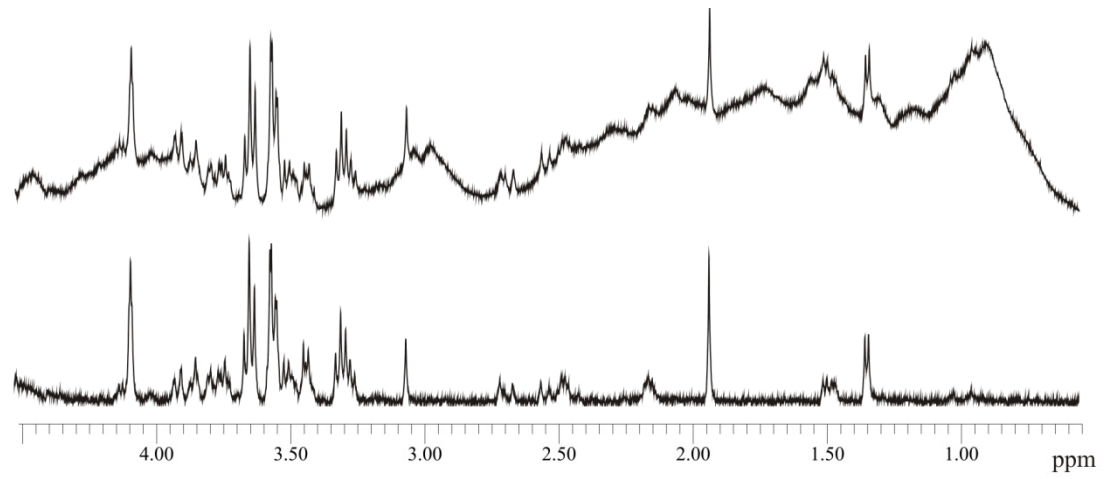

Figure 11. An example of the effect of T2-editing on a 1H NMR spectrum of a synthetic mixture of common metabolites and a human serum albumin concentration of 5%. The above spectrum features the non-edited spectrum in which the broad protein resonances can clearly be seen while the spectrum below shows the effect of a 320 ms T2 filter on the same spectrum: the broad protein resonances have completely vanished revealing the underlying metabolite signals.

3.2.2 Diffusion editing

Diffusion editing aims to simplify over crowded 1D NMR spectra by utilizing the differences in molecular diffusion coefficients either alone or by using a combination of diffusion and relaxation parameters. Therefore, diffusion editing methods are commonly used for the same type of purpose than relaxation editing method. These experiments are usually based on two standard types of pulse sequences, the spin echo diffusion sequence [77] and the stimulated echo sequence [78]; both of these are based on pulsed field gradients (PFGs). All other published sequences can be understood as modifications of these two sequences. For more details on the diffusion sequences, se e.g. [70].

In complex biofluids the combination of both diffusion and relaxation editing brings about considerable spectral simplification leading to an easier resonance assignment and quantification process. Both methods can additionally be combined with 2D NMR experiments. It is generally known that the separation of slowly diffusing species (generally large macromolecules) can be separated from fast diffusing ones (small metabolites) by diffusion editing [76]. The diffusion properties are most commonly used to select macromolecular signals [23]. However, by combining diffusion and relaxation editing simultaneously, one can for example remove the peaks of the smallest, fastest diffusing components (e.g. solvents such as H_2O) and at the same time remove peaks from the fastest relaxing macromolecular components, thus resulting in a spectrum displaying small metabolites and lipids. A schematic representation of this experiment is shown in Figure 12.

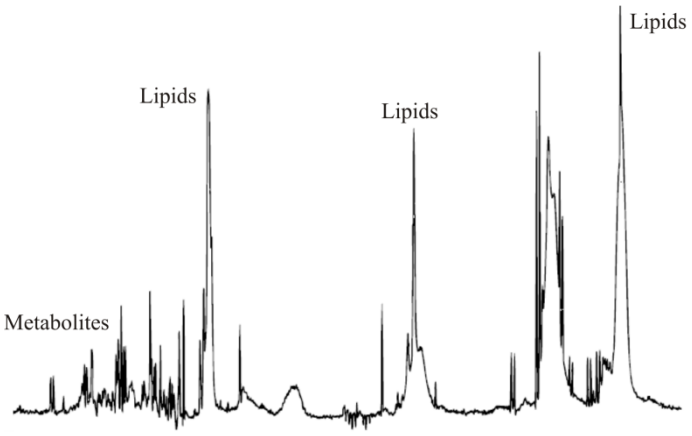

Figure 12. A schematic representation of the resulting spectrum when simultaneous diffusion and relaxation editing is applied. Some metabolite and lipid signals have been highlighted.

Diffusion edited experiments have been applied to studies dealing with protein ligand binding [79, 80]. Also protein properties and concentrations can be measured by removing the small metabolite signals [81]. Protein-ligand binding studies are nowadays the most common use for diffusion editing and various modifications for different types of pulse sequences, including 2D NMR sequences, have been presented [82, 83]. Diffusion edited NMR spectra are also commonly used to create baseline data as a starting point for more sophisticated methods [84].

3.2.3 Curve fitting

Curve fitting methods are totally different in regards to the previous methods presented. Curve fitting aims to remove peak alignment problems resulting from pH and ionic strength differences in the NMR samples therefore providing more reliable data for further analyses and classification of the samples. This type of data will also help in the automation of NMR spectra processing and quantification, resulting in reduced experiment times in large studies. For the above reasons, many sophisticated curve fitting schemes already exist [85], but these often require some sort of supervision to be effective [27]. The previously mentioned "intelligent binning" algorithms could theoretically also be used for the same purpose, but regardless of how the bins are defined, the edges of many bins must extend well beyond the substantive widths of the associated NMR signals. Such wide bins contain a considerable portion of baseline and are more likely to engulf interfering peaks, which may not be present in all samples, therefore making calibration across data sets difficult. Additionally, since there is no information available on the percent of the noise intensity for a specific bin, there is no way of knowing what has been integrated, unless each spectrum is inspected manually [27].

Many modern methods used for quantification share much in common with those used for peak alignment and are mainly distinguished by the sought end point. Peak alignment is often seen as a preprocessing step in multivariate analysis (see chapter 3.3 for details on multivariate methods). Curve fitting precursor methods include e.g. a partial linear fit [86] which requires a lot of manual intervention, peak alignment based on genetic algorithms [87], an improved version of the previous by using a beam search algorithm instead of a genetic one [88], resulting in an increase in computation time, and an algorithm based on the shifting and matching of peak positions by using graph theory [89]. What complicates matters however is the fact that even though peak alignment methods can make the analysis of NMR spectra more automatic, it has been shown that variations in peak positions can be linked to biological of physicochemical phenomena and can provide useful information [90, 91]. The question then arises, would it be possible to automate processing and still retain the important information? Solutions have been suggested in the form of the automatic alignment of spectral peak-regions [92], by the use of a *targeted profiling* method approach based on pre-fitted model signals of components [93], an extended version of the previous known as the *targeted profiling of unknowns* dealing mainly with low intensity signals [94], peak alignment using reduced set mapping [95], and a method for stepwise selection of peaks in NMR spectra from multiple groups [96]. These methods have indeed been partially successful.

As another type of solution, an algorithm featuring an NMR signal "probe" has been introduced by *Crockford et al.* [27]. This method uses a known type of reference signal observed in a pure compound spectrum. This probe is then chosen to occupy the narrowest suitable chemical shift range over which its distinctive shape is well represented. A search range is then defined which is swept by the probe seeking a signal match. Prior knowledge of compounds is important here since it can be used to create a choice of suitable probes and chemical shift ranges for the metabolites that need to be detected from the multicomponent spectra. This approach has been promising but it does still require regions in the multicomponent spectra where the probes can match the pure compounds. Additionally, it has been suggested that curve fitting methods may introduce bias to the data [97]. For more details on bias, see chapter 3.3.2.

3.2.4 Deconvolution

Since the area determination for overlapping NMR signals by traditional means (bucketing, integrating) is problematic and produces inaccurate results, methods using a totally different approach have been created. These methods use deconvolution, or total-line-shape (TLS) fitting of the spectral signals. Deconvolution is based on peak fitting onto the observed spectrum by using a least-squares based method. The fitting requires some peak parameters (signal frequency and height, line width and line shape), that can be acquired by using prior knowledge, a spectral parameter library, calculations or estimates, or by performing peak picking. Deconvolution algorithms however will commonly find the local minimum only so in this case prior knowledge is essential in performing a good initial guess thus facilitating the finding of the global minimum.

Many methods commonly in use only make use of a database to acquire the initial values needed. This database contains model spectra of pure individual components recorded with certain parameters in e.g. a certain pH and the mixture spectrum is created as a linear sum from the model spectra. Programs such as LCModel [98-100], Bruker AMIX [101], and the Chenomx NMR Suite [93, 94, 102, 103] have been developed for this purpose. Model based approaches however require a huge database since spectral conditions can vary a lot and each condition demands its own entry. Another problem with these approaches is that commonly no variation in peak frequencies is allowed. Since the frequencies of NMR signals depend on e.g. pH and ionic strength, this can lead to uncertainties of signal positions and therefore generate quantification errors. Other applications attempting to overcome the abovementioned problems have been reported; a method based on weighted least-squared fitting [104], and a further one based on linear least-squares fitting by using singular value decomposition [105]. Another recently introduced method [106] used total-correlation spectroscopy combined with covariance NMR

to deconvolute the mixture spectra into its components, thus allowing the quantification of overlapping signals.

Deconvolution can also be done by simply adding the wanted signals to the spectrum and fitting the parameters for each signal. A basic deconvolution is available in many software packages, but programs fitting hundreds or thousands of signals simultaneously and combining the ever useful prior knowledge with a spectral database are rare. So far, only one software package, the PERCH NMR Software [107], is available. More specifically, the TLS program included, contains advanced deconvolution protocols based on a Gauss-Newton type iterative algorithm [108]. Prior knowledge can be used to create constraints derived from spectral structures and this data, e.g. chemical shift information, coupling constants and multiplet structures, can then be combined to act as a guideline in the TLS fitting. It has previously been demonstrated that constraints describing spectral structures improve the statistics of concentrations obtained by TLS analysis [109]. It should however be noted that overlap or closeness of very large signals leads to problems in estimation of the signal areas [110].

An extension of the "normal" TLS fitting, constrained total-line-shape (CTLS) fitting, applying the abovementioned constraints has been recently presented and applied for studies of CSF metabolomics and neurological disorders [26]. In the case of CTLS, prior knowledge was used to create spectral structures that could be incorporated into the fitting algorithm. The multiplet structures (the relative positions and intensities of the signals), can be obtained by measuring a single component spectrum and performing the TLS fitting on pure component multiplets, much like described elsewhere [27, 93]. However, in CTLS fitting the structures are defined for the program as line positions and intensities or constraints instead of prefit lineshape curves. These spectral parameters are then iterated, enabling the CTLS algorithm to automatically adapt to small changes in line positions and intensities and, furthermore, to baseline differences as well. This approach also suits signals which do not obey any strict rules arising from the spinsystem. As another example, lipoprotein sub-fraction signals can be treated in this way [111]. For a more detailed description of the CTLS protocol the reader is suggested to see the reference in which it was first reported [26].

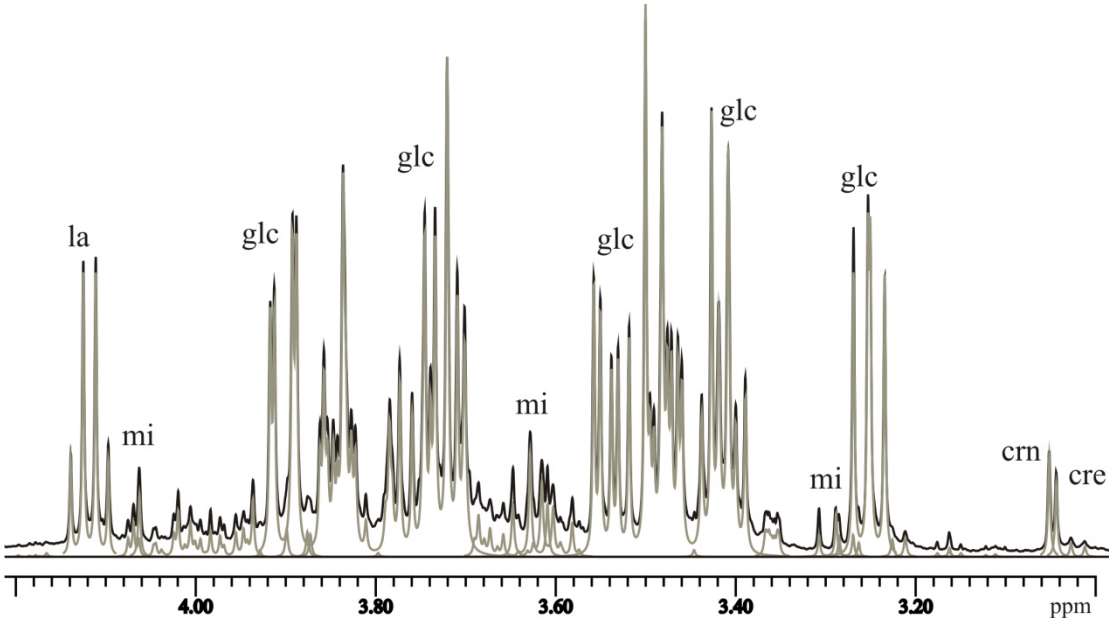

Figure 13. An example of CTLS fitting performed on human CSF (^{1}H 500 MHz). A few metabolites have been assigned and are presented as spectral multiplet structures instead of single peaks: la=lactate, mi=myo-inositol, glc=glucose, cre=creatine, crn=creatinine.

3.2.5 Other applicable methods

Some other novel methods for the purpose of "spectral simplification" have also been created. Although the previous methods have dealt mainly with 1D NMR spectroscopy, a few 2D NMR related methods should be mentioned here. Basic 2D NMR experiments are often too time-consuming to be included in a metabolomics protocol and therefore experiments based on simplifying or extracting the most information possible from 1D NMR data are preferred.

Statistical Total Correlation Spectroscopy

One of these methods features the identification of multiple NMR peaks from the same molecule within a complex mixture. This method is based on the concept of Statistical Total Correlation Spectroscopy (STOCSY) which has been demonstrated by *Cloarec et al.* [90]. STOCSY encompasses the computation of correlation statistics between the intensities of all points in a set of complex mixture spectra, thus generating connectivities between signals from molecules that vary in concentration between samples. Moreover, this method is not limited to the usual connections (e.g. coupling information) that are deducible from more standard 2D NMR experiments. The additional information is available by examining lower correlation coefficients or even negative correlations, since this leads to the connection between two or more molecular species involved in the same biochemical process. The STOCSY method can also be combined with chemometric methods if the classification of samples groups is de-

sired (see chapter 3.3), thus providing a new framework for the analysis of metabolomic data. STOCSY has been applied e.g. in cases of population based identification of drug metabolites in human urine samples [112], for generation of biochemical pathway information [113], and for the identification of drug metabolite peaks in biofluids and for deconvolution of drug and endogenous metabolite signals [114].

The STOCSY approach has also been extended from a homonuclear context to heteronuclear, referred to as Statistical Heterospectroscopy (SHY). The SHY method has been applied to the coanalysis of both NMR and MS in metabonomic toxicity studies [56, 115]. Other similar methods developed include a statistical diffusion ordered spectroscopy (S-DOSY), which combines diffusion ordered spectroscopy (DOSY) and STOCSY for the analysis of biofluids to give enhanced information about the diffusion properties of biomolecules. Additionally, a visualization tool called diffusion-ordered projection spectroscopy (DOPY) has been developed, in which the apparent diffusion coefficients from diffusion ordered spectra are projected onto a 1D NMR spectrum [83].

Other possibilities

Some advantages to metabolomics have also been found in the form of 2D J-RES spectroscopy. This being a method that can provide a proton-decoupled projection of a 1D NMR spectrum, thus simplifying the crowded spectral regions (see Table 1). These projected spectra can then be used in further analyses as well as supporting information and thus, the relative changes in metabolite concentrations can be obtained. A serious drawback of the J-RES method is the lack of quantifiable signals due to the spin-echo sequence involved [70]. Even though the experiment times are increased threefold, the benefits of this method may in some cases outweigh the disadvantages and therefore, although the signal-to-noise ratio is not as good as in normal 1D spectra, this method could even be considered for routine analysis [116].

In addition to the above, methods based on interpreting the FID resulting from NMR experiments have also been devised. The FID is essentially a sum of exponentially damped sinusoidal components, and this model has proven to be adequate in a number of applications, including the analysis of solution state metabolomics. It is mathematically challenging to identify all the components in a biological matrix of metabolomic data and naturally one would ideally like a method which is fully automated but still capable of resolving as many resonances as possible in a complex biological sample. An algorithm for the purpose of joint estimation of the number of components and their parameters within a Bayesian framework for a NMR spectrum has recently been presented [117]. This algorithm has been successfully applied to the processing of both simulated and real data. Additionally, by analyzing the FID in the time domain, the approach has provided improved resolution in the time domain of complex

mixtures such as blood plasma. Most of the data processing steps used in NMR spectroscopy of mixtures such as peak removal and baseline and phase correction can also be automated. This approach could therefore greatly facilitate the quantitative use of NMR as well as comparative studies and pattern recognition based techniques such as those used in metabolomics.

Chemical shift calibration methods have also been assessed to be used as a tool for automatic calibration in situation when normal internal standards cannot be used due to e.g. high concentrations of protein [32]. The procedure presented by Pearce *et al.* is based on locating and calibrating ^{1}H NMR spectra to the α−glucose anomeric doublet. It is also clearly stated that this kind of automation is important especially in large-scale metabolomics studies where hundreds or even thousands of spectra may be analyzed in high-resolution by pattern recognition analysis.

3.2.6 Assessment on the effect of various parameters on T_2-edited spectra

(This chapter is loosely based on **Jukarainen, N. M.**, On the effect of acquisition parameters, protein concentration and spectral processing on T2-edited metabolite concentrations. Manuscript, **2009**.)

Background

Previous research on T_2-editing has demonstrated, that the use of T_2-editing results in systematic errors of 5-25 % in peak amplitudes [118]. It is also known that T_2-editing is complicated by J-coupling evolution, diffusion and selective signal loss due to different T_2 relaxation times [119] and that the varying protein concentration of samples might pose issues in quantification reliability [26]. Furthermore, it has been reported that baseline distortion and differential metabolite intensities possibly result in additional quantification errors [120]. Some work in determining optimum parameters in T_2 experiments has been done [103], and more specifically, the effects of the relaxation delay in the CPMG sequence have been explored [74]. It is generally suggested that a recycle delay should ideally be five time the longest longitudinal (T_1) relaxation time of a particular metabolite in the sample [121]. Interestingly, more recent study has shown that by a proper selection of correction parameters, long relaxation times are not needed and relatively good quantitativity can nevertheless be achieved [122]. The above naturally applies when absolute quantitative results are desired which is not always the case in metabolomic studies. It is more important to obtain comparable results, which can most definitely be achieved by using T_2-editing, as long the same acquisition parameters are used for each sample.

To assess the validity of the above, a set of spectra containing various concentrations of human serum albumin (HSA) and common metabolites was created. Because an excellent protocol for performing NMR measurements in metabolomics studies already exists [23], this protocol and the parameters suggested therein, was used as a basis for this study. It was then explored what would happen if one de-

cided to deviate from these parameters and, additionally, the effect of the total protein concentration in the samples and its effect on the resulting metabolite concentrations was investigated. Furthermore, it was examined whether a different type of processing of the free induction decay (FID) would change the results. It should be emphasized that this study is clearly most relevant in the case of blood plasma since the protein concentration in plasma is as high as ~5% which, when compared e.g. with CSF, is a tenfold concentration and is therefore more likely to affect the analyses performed.

Methods

Two sample sets containing HSA in concentrations of 0.01 %, 0.05 %, 0.5 %, 2 % and 5 % were created. The normal HSA concentrations in cerebrospinal fluid and blood are 0.5 % and 5.0 %, respectively, and therefore the concentrations in the samples were selected to include these concentrations. The metabolites selected for these experiments were ones that are commonly found in various biological fluids; histidine, phenylalanine, myo-inositol, creatine, glucose, citrate, acetate, lactate, alanine and isoleucine. The metabolites and HSA were dissolved in a deuterated phosphate buffer pH 7 with a potassium concentration of 4 mM. Metabolite concentrations in the samples were used in accordance to literature values [36]. Each sample contained the same metabolite concentrations, but a different HSA concentration.

The pulse program used for these experiments was the standard CPMG sequence since no solvent suppression was required. The T_2-editing time was varied by the number of loops in the pulse sequence, more specifically; values were selected because they fit the range of values used in previous research [23, 73, 74, 123]. Values ranging from 50 to 400 loops were used, resulting in a total echo time of 40-480 ms. The other relevant parameters used were: relaxation delay 4 s, acquisition time 6 s, number of scans 64, τ delay 400 μs. These parameter values were chosen because they are part of an existing protocol for biofluid metabolomics [23]. All spectra were measured by using a Bruker AVANCE DRX 500 instrument operating at 500.13 MHz equipped with a 5.0 mm inverse triple resonance probe. TSP was used only as a chemical shift reference and not as a quantification reference since it known to bind with proteins [37]. Instead, 1,2,4-triazol was used as a quantification reference.

All spectral model creation and quantification was performed by using PERCH NMR Software version 2008.1 (PERCH Solutions Ltd., Kuopio, Finland). Spectral processing was performed i) by zero filling and applying a line broadening of 0.5 Hz and ii) by using a trapezoid type function where no zero filling was performed and only the end of the FID was cut off. The two types of processing were used to determine if spectral processing affect the quantification results. For each NMR signal, the frequency, line width and intensity were optimized during the fitting. Only one clearly resolved NMR signal was

selected for quantification for each metabolite. Quantification results were first proportioned to the non T_2-edited values and then visualized relative to glucose (Figure 14).

Results

It must be noted that these results obtained are indeed interesting, especially the oscillation of myo-inositol (see below), but at this point still preliminary. Therefore more research is required before the publication of all results related to this project. Since the concentrations acquired from the two sets of spectra measured were nearly identical, the measurements themselves were deemed accurate enough for these preliminary results.

The results are presented in Figures 14 and 15. Figure 14 (a-d) shows metabolite concentrations of all metabolites, visualized relative to glucose, in four different HSA concentrations. Figure 14 (e) shows metabolite concentrations when a 480 ms T_2-filter was applied, visualized as a function of protein concentration. The myo-inositol concentration fluctuations relative to glucose, during various T_2-filter times, are shown in Figure 14 (f). A representation of baseline distortions created by the T_2-editing pulse sequence is presented as a stack plot in Figure 15. The results for trapezoid processed spectra were not significantly different and are therefore not shown.

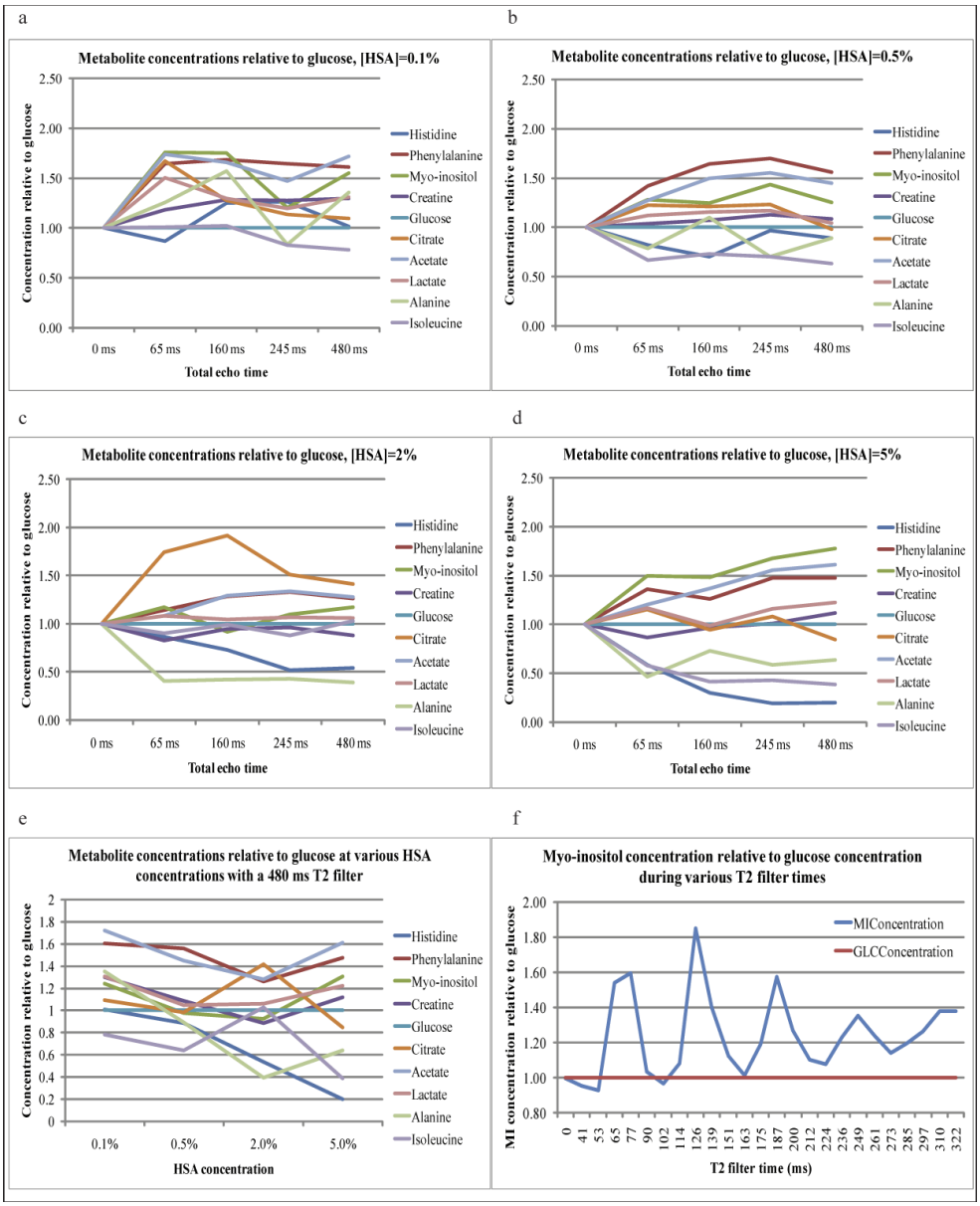

Figure 14. a-d) The apparent metabolite concentrations of common metabolites in various protein concentrations. The y-axis shows the relative deviation from the correct one, when they are related to that of glucose. For example, a value of 0.5 means that the T_2-edited concentration is 50% of the correct one. The x-axis shows the total T_2 echo time in ms (x-axis). e) The relative metabolite concentrations of the quantified metabolites, when using a total T_2 echo time of 480 ms. f) Myo-inositol concentration relative to glucose during various T_2-editing times.

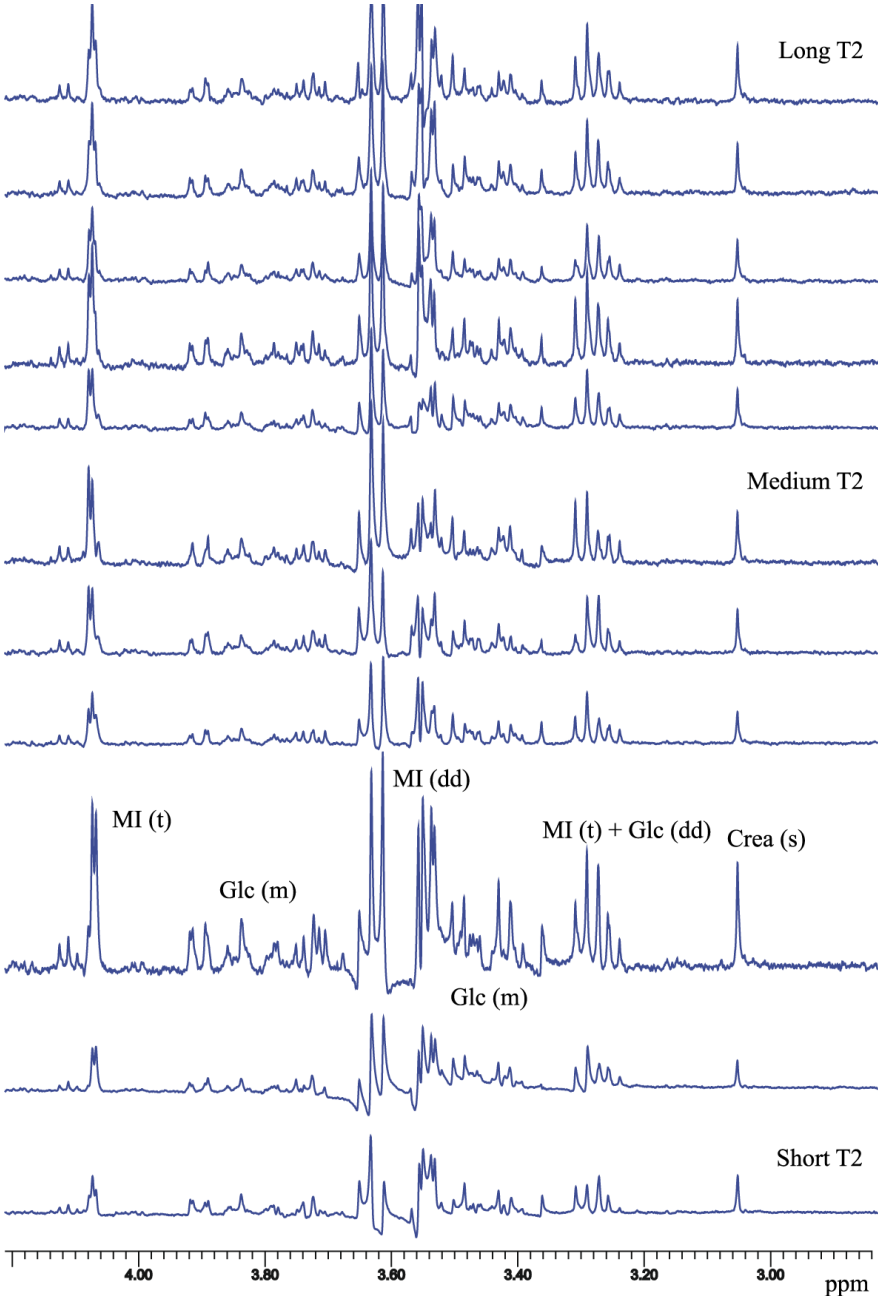

Figure 15. A stackplot of the spectra used in this study. Baseline distortions induced by T_2-editing are clearly visible. MI=myo-inositol, Glc=glucose, Crea=creatine.

Discussion

The results show that there is a lot of variation in the metabolite concentrations. More specifically, if short T_2 filter times are used, the errors in the concentrations are more intense. On the other hand, concentrations are relatively stable when using T_2 filter times that are longer than 245 ms. Thus it would seem to be best to stick with the longer T_2 filter times that are most commonly used in metabolomics

studies. The results also revealed that the differences in spectral processing do not significantly affect the quantification results if the line width and shape is fit individually for each signal.

It can also be seen that the HSA concentration in the samples is relevant when performing T_2-editing. Very low (0.1-0.5 %) and high (5.0 %) HSA concentrations result in larger errors than a medium (2.0 %) concentration of protein. This might be a problem if results between different biological mediums are compared; the protein content in urine for example is much lower than that of blood plasma. However, as stated earlier, these results are still preliminary, and furthermore, an explanation to the oscillation of myo-inositol has not yet been found, care should be taken when interpreting the results at this point. More research on the subject is still clearly needed.

The results obtained in this study suggest that while T_2-editing can be used as a means of detecting small components when creating a metabolomic model, it should not be the first option when absolute quantitative results are desired. However, as earlier stated, and proved in countless metabolomic studies, absolute quantification is rarely required.

As an additional note, a recent publication quite thoroughly assesses the effect of T_1 and T_2 relaxation effects on quantitative NMR [122]. This publication also proposes that with the use of correction factors, T_2 editing can be performed by using significantly shorter relaxation delays and, furthermore, absolute concentrations can also be acquired.

Conclusions

It can be seen that the T_2-edited metabolite concentrations vary significantly from the correct ones. The amount of deviation depends on the length of the T_2 filter time and the amount of protein in the sample. The good news is that protein signals are effectively removed from the 1D spectrum and, the T_2-edited concentrations (relative to glucose) are fairly constant when typical total echo times of 250-500 ms are used. The darker side is that the T_2-edited concentrations may vary up to ± 150 % from the real ones and, moreover, they depend strongly on the protein concentration, which is not necessarily known and may vary significantly in biofluids. One should therefore take care to stick to proven protocols, not desire absolute quantification and, not compare results acquired from different types of biofluids by using the same parameters.

3.2.7 A practical approach toward improved deconvolution

(This chapter is loosely based on **Jukarainen, N. M.**, Korhonen, S. P., Laakso, M. P., Korolainen, M. A., Niemitz, M., Soininen, P. P., Tuppurainen, K., Vepsalainen, J., Pirttila, T., Laatikainen, R. Quanti-

fication of H-1 NMR spectra of human cerebrospinal fluid: a protocol based on constrained total-line-shape analysis. Metabolomics, 2008. 4(2): p. 150-160.)

Background

CSF is a good choice for a medium when dealing with the biochemical processes occurring in the brain. The composition can be anticipated to provide information about states of normal or pathological metabolism of the brain. Even though CSF samples are more difficult to obtain than blood samples, when considering an NMR analysis, CSF has its advantages because of the relatively low protein and lipid content, the low viscosity of the medium, and less severe signal [35]. It is therefore not surprising that several NMR studies on CSF have been reported [4, 62, 124, 125] and that some changes in NMR observable metabolites in the brain associated with AD have been reported [65]. These include an increase in the myo-inositol concentration and its ratio to creatinine, as well as a decrease in N-acetyl-aspartate and its ratio to creatinine and myo-inositol.

A major problem in a human metabolomic model seems to be the physiological variation, attributable to several intrinsic and extrinsic factors such as genetics, ageing, gender, dietary variation, smoking, stress and physical exercise [126]. The existing NMR analytical protocols do not fully utilize the spectral information. In principle, the information content of biofluid ^{1}H NMR spectra is high, but the transformation of this information into concentrations of individual metabolites, essential to many applications, is not straightforward. Each metabolite may contribute up to tens of individual signals in the spectrum and the signals may seriously overlap with each other. Several approaches for solving problems such as signal shifts and peak overlap and other problems have so far been presented (see chapter 2). Shortly, these strategies include a 'curve-fitting method' based on pre-fitted model signals of components [27, 93], the automatic alignment of spectral peak-regions [92], spectral editing via relaxation and diffusion [73], peak alignment using reduced set mapping [89, 95], and a method for stepwise selection of peaks in NMR spectra from multiple groups [96]. Several methods and the validity of the results of various methods have also been assessed [127].

The objective of this study was to build up and assess approaches for using quantitative ^{1}H NMR analysis of CSF and to evaluate their applicability for metabolic profiling of neurological patients. A TLS fitting based method [109] extended with constraints, hereafter referred to as CTLS, was used to alleviate the aforesaid problems.

Methods

CSF samples of neurological controls

The control group of 45 patients aged 45 – 82 consisted of individuals examined for various neuropsychiatric symptoms, such as depression or headache, but who did not have cognitive decline or a chronic neurological disease. These patients were further divided into two groups: patients with an AD marker profile (low β-amyloid$_{42}$ and/or high tau protein) present in CSF (control class abbreviation: C_ADP) and patients that do not have an AD marker profile in CSF (control class abbreviation: C_NRM). The C_ADP group consisted of 10 patients of whom 7 were female (females aged 57-79 years; males aged 57-66 years), the C_NRM group consisted of 34 patients of whom 19 were female (females aged 52-81 years; males aged 45-78 years). No other confounding disease states were associated with these patients. Lumbar CSF samples were obtained using a standardized protocol. All samples were placed in a cold gel pack immediately after sample acquirement and frozen within 2 hours. The study was approved by the local ethics committee of the University of Kuopio and Kuopio University Hospital, and informed consent for participation in the study was obtained from all subjects.

Sample preparation

The samples were prepared according to the protocol described by Maillet [1]. First, 1800 µl of each sample was subjected to an identical lyophilization protocol for 40 hours. The freeze-dried samples were then stored at -20° C in sealed vials until analysis. Prior to the NMR measurements, the samples were reconstituted in 600 µl of D_2O (99.98%-D, Merck) and 450 µl of this liquid was transferred to a separate vial followed by addition of 50 µl of 21.5 mM TSP-d4 in D_2O to be used as an internal standard of known concentration. The pH of the samples was not adjusted, being typically around 7.00±0.05. This pH can be defined as pH*, which is the reading of the pH meter as measured with a standard pH electrode. The pD value is ca. 0.4 units higher than pH*.

NMR Spectroscopy

The metabolic profiling was based on a standard 1D ^{1}H NMR spectrum. All spectra were measured by using a Bruker AVANCE DRX 500 instrument operating at 500.13 MHz (Bruker-Biospin GmbH, Karlsruhe, Germany), equipped with a quadronuclear probe. The Bruker XWIN-NMR software version 3.5pl5 running on a standard PC was used for acquisition of all spectra. The relevant parameters used in the 1D experiments, were calibrated and used as follows: recycling delay 45 s, acquisition time 6.5 s, number of scans 128, and a sweep width of 9.5 ppm. A calibrated 90° pulse was used for all spectra and all acquisitions were performed on non-spinning samples. To assess the use of relaxation editing in spectral simplification, T_2 edited 1D NMR spectra were measured. For the three spectra (not edited, minimally and heavily edited) measured, a standard 1D CPMG pulse sequence with a 40 ms or

320 ms (for minimally edited and fully edited, respectively) T_2-filter using a fixed echo delay of 400 μs that eliminates diffusion and J-modulation effects was used.

Identification of metabolites

The assignments of the spectral signals were done according to available chemical shift and coupling constant information in the literature [1, 34, 128, 129]. Some metabolites and signals were verified by using 2D NMR spectroscopy and by performing 1D spiking experiments.

Metabolic concentration analysis and classification

Metabolite concentrations and ratio relations were analyzed in the hopes of finding patterns within the control patient group. Concentrations were assessed by using one way ANOVA as implemented in SPSS v14.0. Separation of the two patient classes was explored by using the Self-Organizing Map algorithm (SOM) [130] which uses competitive learning to create a two-dimensional map of the original data in such a manner that it conserves the maximum amount of the structure present in the original data. The actual analysis was performed by using the SOM_PACK software, version 3.1, freely available in the internet.

Quantification analysis

All spectral processing prior to the model creation was done using the PERCH NMR Software version 2005/1 (PERCH Solutions Ltd., Kuopio, Finland). The total-line-shape (TLS) fitting tool of PERCH NMR Software version 2007.2 was used in the quantification analyses. The local baseline option was added to the software during these analyses.

Magnesium and calcium concentrations

Ca^{2+} and Mg^{2+} concentrations were measured by a Perkin Elmer PE 460 AAS and a Perkin Elmer PE 5100 AAS instrument, respectively, using a multi-element hollow cathode lamp and an air-acetylene flame.

Results and discussion

Quantification: CTLS fitting

The positions of the signal frequencies of some metabolites (e.g. citrate and glutamine γ–CH_2) vary significantly (up to 10 Hz) from one spectrum to another, likely reflecting variations in ionic strength and Ca^{2+} and Mg^{2+} concentrations. This means that the traditional methods based on integrals (buckets) would not perform well and, therefore, the analysis was performed using the CTLS method.

As shown in the following Equation, the ^{1}H NMR spectrum I(v) is sum of the numerous individual lines $L_n(v)$

$$I(v) = \sum L_n(v)$$

A single compound may produce tens or more lines that may overlap with lines of other metabolites. The concentration of the compound is fairly strictly proportional to the area of the lines arising from the compound. TLS fitting, or deconvolution, is an efficient way and in fact the only way when dealing with 1D NMR spectra, to integrate the area of overlapping multiplets of different protons. However, overlap or closeness of very large signals, leads to problems in estimation of the line areas [110]. In this work, a CTLS fitting strategy, utilizing constraints derived from spectral structures, was applied. As previously shown [109], constraints describing spectral structures improve the statistics of concentrations obtained by TLS analysis. In this work, 20 constraints were written to define doublets, triplets, quartets and quintets of the most intensive signals arising from the major metabolites. This helps in quantification of the smaller signals that are close to major components, such as glucose and lactate (see below), and also reduces the number of parameters to be fitted. For example, a triplet can be described by 4 parameters (position, intensity, line-width and splitting) instead of the 9 parameters needed for three separate lines. Because the number of the parameters is presently limited to 1000, the spectrum must usually be fitted in parts. Some parameters are also needed to describe the line-shape and the baseline.

The TLS fitting is a nonlinear problem that can be solved only iteratively. A special problem is formed by the baseline arising from instrumental artifacts and broad signals of macromolecules. Another problem, related to weak signals close to strong signals, is that the real line-shape cannot be completely described by the theoretical Lorenzian line-shape. This has been discussed in detail in another publication [110].

The concentration of a metabolite is proportional to the area of the sum of the signals arising from it. The standard deviation of the area, and thus that of concentration, can be computed from the normal equation (variance-covariance) matrix formed in the iterative protocol, which has been described before [109]. The protocol also gives estimates of standard deviations of the populations and it is notable that the standard deviations must be computed taking the correlations of the individual signal parameters into account.

The estimate of standard deviation (s) for single line and multiplet area are obtained from the equation

$$s(n) = rrms * \sqrt{A_{nn} I^2 + A_{kk} W^2 + 2 A_{nk} W}$$

where I_n = the intensity of the line, W_n = the half-height width of the line, normalized so that the area = $I*W$, A_{kk}, A_{nn} and A_{nk} are elements of the inverse matrix of correlation-covariance matrix D, corresponding to I and W. The matrix D element D_{nk} can be approximated by the the equation

$$D_{nk} = \sum_{i}^{I} \frac{\partial I_i(v)}{\partial I_n} * \frac{\partial I_i(v)}{\partial W_k}$$

where the derivatives $\partial I_i(v)/\partial I_n$ and $\partial I_i(v)/\partial W_k$ are computed for the iterative algorithm. *Rrms* is the residual root mean square.

For the standard deviation estimate of a sum of areas also the correlations of the contributing lines need to be taken into account:

$$s(sum) = rrms * \sqrt{\sum_{n}^{N} s^2(n) + 2\sum_{n}^{N}\sum_{m}^{M}(A_{kl}I_nI_m + A_{ij}W_nW_m + A_{li}I_mW_n + A_{kj}I_nW_m)}$$

where n and m refer to the lines belonging to the structure, k, l, i, j are the indices relating the line-widths and intensities, respectively, to the A matrix. The second sum term is normally negative, which means that $s^2(sum) < \Sigma s^2(n)$, which would be the standard deviation of the sum of independent terms. This also means that the integration based on deconvolution, while ignoring the correlations and spectral structures, may give poor statistics for the quantified area. To illustrate the effects of the constraints and the correlations equations we took an example. For example, if the doublet at 2.44 ppm (marked by an arrow in Figure 17) is devonvoluted asuming two independent lines, their total area is 0.400 ± 0.077 (area ± rms, as reported by TLS). If the standard deviation was calculated by assuming $s^2(sum) = \Sigma s^2(n)$, the result would be 0.088, reflecting the effect of the correlations to the error parameters. If however the lines are defined to form a 1:1 doublet, the total area is 0.408 ± 0.028. Similar effects are obtained for many other lines, some of which are marked by arrows in Figure 17.

Error statistics produced by the CTLS algorithm for a typical CSF case are shown in Table 4. Although the estimated standard deviations based on the variance-covariance matrix are usually systematically slightly too small, they can be assumed to give a fair picture about the relative reliability of the compound populations, if the fitting is done with a similar protocol for each case. Expectedly, the accuracy of major components is better than that of minor ones. This may also depend more on the protocol, especially on the number of baseline terms and how the spectrum is divided into fitting segments.

Table 4. Error statistics for a typical case for all the metabolites quantified. Table columns as follows: area=population of the metabolite, Std.Dev.=standard deviation of the area, REL%=the relative percentage of the metabolite in comparison to the total spectral intensity, Std.Dev.%=the standard deviation for the REL% value. Labels for metabolites: X=unknown metabolite, AREA=populations for several overlapping components. For additional details, see footnote.

Metabolite	Area	Std.Dev.	REL%	Std.Dev%
Tyrosine	0.708	0.070	0.091	0.009
Histidine	0.161	0.009	0.021	0.001
Phenylalanine	1.027	0.016	0.132	0.002
Tryptophan*	0.608	0.010	0.078	0.001
Formate	0.278	0.006	0.036	0.001
X1[a]	0.071	0.003	0.009	0.000
X2[b]	0.070	0.003	0.009	0.000
Lactate	30.953	0.094	3.974	0.012
Myo-inositol	12.652	0.062	1.624	0.008
AREA1[c]	20.382	0.096	2.616	0.012
Glucose	376.961	0.153	48.390	0.019
AREA2[d]	23.414	0.065	3.006	0.008
AREA3[e]	4.767	0.211	0.612	0.027
X3[f]	1.202	0.072	0.154	0.009
Creatinine	4.349	0.052	0.558	0.006
Creatine	3.002	0.050	0.385	0.006
Citrate	13.244	0.048	1.700	0.006
Glutamine	15.564	0.054	1.998	0.007
AREA4[g]	4.805	0.016	0.617	0.002
X4[h]	0.215	0.015	0.027	0.002
Acetate	11.299	0.069	1.450	0.009
AREA5[i]	3.142	0.038	0.403	0.005
AREA6[j]	1.412	0.087	0.181	0.011
β–hydroxybutyrate	0.678	0.115	0.087	0.015
X5[k]	0.362	0.084	0.046	0.011
X6[l]	0.854	0.070	0.110	0.009
X7[m]	1.032	0.072	0.133	0.009
α–hydroxybutyrate	1.587	0.068	0.204	0.009
α–hydroxyisovalerate	0.546	0.069	0.070	0.009
AREA7[n]	3.728	0.084	0.479	0.011
Pyruvate	2.766	0.031	0.355	0.004

*Tryptophan + other metabolites underlying its aromatic signal, [a]Unknown aromatic signal, [b]Unknown aromatic signal, [c]Several overlapping amino acids, [d]Metabolites in the 3.70-3.56 ppm range, not including myo-inositol, [e]A hump of signals (3.37-3.34 ppm), [f]A triplet + underlying signals at 3.16 ppm, [g]Several overlapping metabolites in the range of 2.37-2.24 ppm, [h]Unknown signal at 2.13 ppm, [i]The spectral region 1.56-1.40 ppm, [j]The spectral region 1.32-126 ppm, [k]Unknown doublet at 1.13 ppm, [l]Unknown doublet at 1.07 ppm, [m]Unknown doublet at 1.03 ppm, [n]The spectral region 1.02-0.93 ppm

Prior knowledge

In the CTLS approach, practically any prior knowledge about spectral structures can be easily incorporated into the fitting algorithm. The multiplet structure (the relative positions and intensities of

the lines), can be obtained by measuring a component spectrum and performing the TLS fitting on pure component multiplets, much like described elsewhere [27, 93]. However, in CTLS fitting the structures are defined for the program as line positions and intensities or constraints instead of prefit lineshape curves. These spectral parameters are then iterated, enabling the CTLS algorithm to automatically adapt to small changes in line positions and intensities. This approach also suits signals which do not obey any strict rules arising from the spinsystem. As an example, lipoprotein sub-fraction signals can be treated in this way [111].

There are two ways to create the multiplet structures for a well defined spinsystem. Firstly, one can make a TLS fitting for the spectrum of a pure compound in conditions that are close to the system to be studied. The structure in certain conditions like CSF, can be obtained by making a perfect TLS fitting for one good quality spectrum, in which the signals of the components can also be enhanced by spiking. Secondly, one can apply the principle of the "adaptive spectrum library" [131] by making a quantum mechanical TLS analysis of the component spectrum [132] thus obtaining the chemical shifts and coupling constants of the spinsystem. This information can then be used to simulate the multiplet structures at any field strength and also with different chemical shifts, on the condition that the couplings constants can be assumed unchanged. When the spectrum has no strong second order effects, the multiplet structures are not sensitive to small variations in chemical shifts and the quantum mechanical approach allows complete presentation of the multiplet structures, free of spectral artefacts that vary from spectrum to another. There are also two ways to define the structure for the fitting. One can create a "structure", defined by a list of spectral lines with characteristic relative positions, intensities and linewidths. This structure is then exactly preserved during the iteration, while the intensity and position of the multiplet and the lineshape parameters are optimized. This mimizes the number of the parameters to be optimized. The second way is to use "soft constraints", meaning linear equations for peak positions, intensities and linewidths. The amount of allowed deviation from the given structure is defined by the weight of the constraint, which is taken into account within the least square principle. Soft constraints are useful for signals for which no strict quantum mechanical rules are available, or if coupling constants vary from case to case. These constraints can be built up automatically.

The constraints used in our human CSF protocol have been listed in Table 5 along with metabolite and constraint type information. Metabolites not identified in Table 5 were defined as multiplets having no constraints between spectral lines. These are also examples of constraints that can be easily applied. Most of the structures are simple 1:1, 1:2:1 and 1:3:3:1 multiplets, and although in some of these the intensity ratio is not exactly 1:1, a more accurate definition of the intensity ratio (which could be easily

done) does not improve statistics. The strongly coupled signals for citrate can be expressed as two 1:1 doublets formed by the outer and inner pairs of lines.

The glutamine γ–CH_2 signal at ca. 2.42 ppm forms a special problem. In its very tightly coupled system, even very small changes in the chemical shifts change the relative positions and intensity ratios of the lines of the multiplet, so that it is not possible to build up a good general structure for the signal. In principle, the only way to do the fitting would be to use an iterative quantum mechanical TLS fitting which properly accounts for the second order effects.

Table 5. The constraints used in the fitting protocol along with corresponding metabolites.

Constraint chemical shift (ppm)	Constraint type	Metabolite
0.84	doublet	α–hydroxyisovalerate
0.90	triplet	α–hydroxybutyrate
1.03	doublet	unknown
1.07	doublet	unknown
1.13	doublet	unknown
1.20	doublet	β–hydroxybutyrate
1.33	doublet	lactate
1.46	doublet	alanine
2.54 + 2.70	slanted doublets	citrate
3.24 + 3.26	doublets	glucose
3.29	triplet	myo-inositol
3.53 + 3.55	doublets	glucose
3.63	triplet	myo-inositol
3.89 + 3.91	doublets	glucose
4.07	triplet	myo-inositol
4.12	quartet	lactate
6.87 + 7.18	AA' BB' multiplets	tyrosine

Quantification: Fitting Protocol

Although the protein concentration of CSF is low, and in the spectral ranges of 6.5 – 8.5 ppm and 0.7-1.3 ppm, it corresponds to great part of the total spectral integral. The protein baseline can be described with a **global** Fourier expansion equation [109]

$$b(v) = \sum_{n}^{N} B_n \sin(nv/\Delta v) + b_0 + slope$$

where Δv = the width of the fitting range or, as in this work, using an n term **local** Fourier-type function

$$b(v) = \sum_{n}^{N} B_n \sin^2 x$$

where $x = [(v-v_n)/\lambda]$, with $\lambda = dv/(N-1)$, for $v_i+\lambda > x > v_i-\lambda$, otherwise sin^2x is set to 0. Although both of the functions give practically the same result with the same number of terms, the local function is easier to visualize, store (in form of constants *B*), and to make continuous when the spectrum is fitted in parts. Because a straight line can be constructed by using equal sin^2-terms, the b_0 and *slope* terms should not be used in local functions. Figure 16 illustrates how the aromatic region hump can be fully described by a 14 terms expansion.

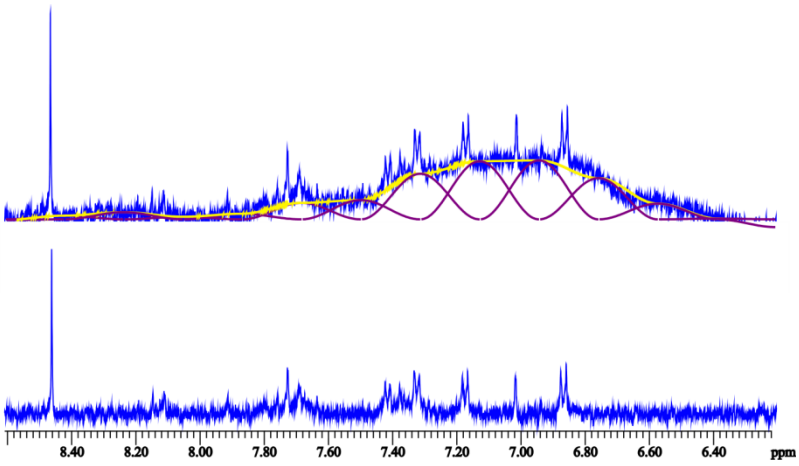

Figure 16. A representation of the local Fourier baseline functions applied for the baseline fit of the aromatic hump. The separate Fourier functions and their sum (the baseline) have been separately indicated.

In this region the signals are clearly separated from the baseline and the hump can be removed by subtracting the baseline contribution before the TLS fitting. On the other hand, the high field (0.7 – 4.5 ppm) hump is not so well-defined, because almost the whole range is covered by some signals. Therefore the baseline must be optimized simultaneously with the TLS fitting.

After the baseline correction, the spectrum is fitted in parts as follows (see Figure 17). An essential question is the number of the baseline terms. When the spectral intensity is formed in large extent by the baseline hump, the number of the terms and also the fitting protocol becomes important: a numerically reasonable fit can be obtained in many ways. The number of baseline terms usually influences the obtained populations; however, when using the same fitting protocol and number of terms for all samples, the bias can be minimized. The following protocol was found to be the most robust:

- Add as many lines as clearly visible to the model.
- Set the number of local Fourier baseline terms to 2 – 20 (depending on the fitting range but 10 is a good guess) and perform the fitting using an option where every line has same line-width.

It is essential that the trial line-width is set to a reasonable value, on the basis of some well-defined typical signal in the range. This should lead to a fairly good fit in this case. If not and there exists clear observed minus calculated differences, additional lines can be added to the model or the number of the baseline terms can be changed.

- Refine the fit using an option that allows different line-widths for lines. If two lines are defined to form, for example, a 1:1 doublet, the line-widths are kept the same; this strongly guides both the baseline function iteration and iteration of overlapping signals to the correct direction. If the baseline is not well-defined, one can use a weighting parameter that forces Fourier terms toward zero.
- Known metabolites are assigned and only clearly resolved signals (if available) are used for quantification. For example, when fitting glutamine, the multiplet at 2.42 ppm was used but the signals at 2.05 ppm ignored.
- Signals that cannot be assigned to any known metabolite can be taken into account by grouping them into well-defined packages that can be treated in the statistical analysis in the same way as the identified compounds. In our data those integrals are marked with Xi (unknown metabolites) and Ai (areas with multiple signals).

The spectral range of 0.70 – 1.3 ppm forms a good example of the fitting strategies when determining how to fix the fitting parameters. Within this range, the three rightmost lines are broad and poorly defined. If the number of baseline terms is too small, the intensity of those lines may become zero or even negative. It is obvious that the intensity of these lines remains somewhat inaccurate, although fair relative values can be obtained when the number of baseline terms is set with same criteria for every spectrum. To test the robustness of the fitting, we performed the fitting with 10, 20 and 30 baseline terms and the obtained populations remained nearly identical with each number of terms. In some cases however, where very small populations were quantified, 30 baseline terms led to erroneous populations for the metabolites. A typical error range was ± 20 % when compared to populations obtained by using 10 – 20 baseline terms and typical metabolites with low concentrations were β–hydroxybutyrate, α–hydroxybutyrate and α–hydroxyisovalerate. This is because of overfitting: the baseline function tries to fit the smallest signals in the spectrum as a part of the baseline.

Anyhow, consideration of the above aspects evidently leads to the conclusion that each CTLS application demands its own validated protocol; our protocol for human CSF is described in detail below. In our final fitting protocol the spectrum was divided into 7 parts, for each of which the fitting was performed independently. An essential point is to perform the fitting for the lines with strong intensities

first (e.g. like lactate at 1.33 ppm), so that its contribution to the signals close to its root can be interpolated in the fitting. This led to the following total fitting protocol:

1. Fit the TSP signal (-0.10 – 0.10 ppm) with 3 – 4 lines and 5 baseline terms. Scale the spectrum so that the area of these signals together is 100.
2. Fit the lactate signal (1.30 – 1.40 ppm), with 5 baseline terms.
3. Fit spectral region 0.6 – 1.75 ppm with 10 – 20 baseline terms.
4. Fit spectral region 1.75 – 2.8 ppm with 10 – 20 baseline terms.
5. Fit spectral region 2.9 – 4.2 ppm with 10 – 20 baseline terms.
6. Fit spectral region 3.57 – 4.3 ppm with 10 – 20 baseline terms.
7. Fit the aromatic range using 10 baseline terms.
8. The protein concentration was estimated by quantifying the protein hump for the spectral region 0.7 – 4.5 ppm. The hump area was obtained by integrating the optimized baseline function.

Figure 17 shows the assigned spectrum of human CSF with assignment of the metabolite signals.

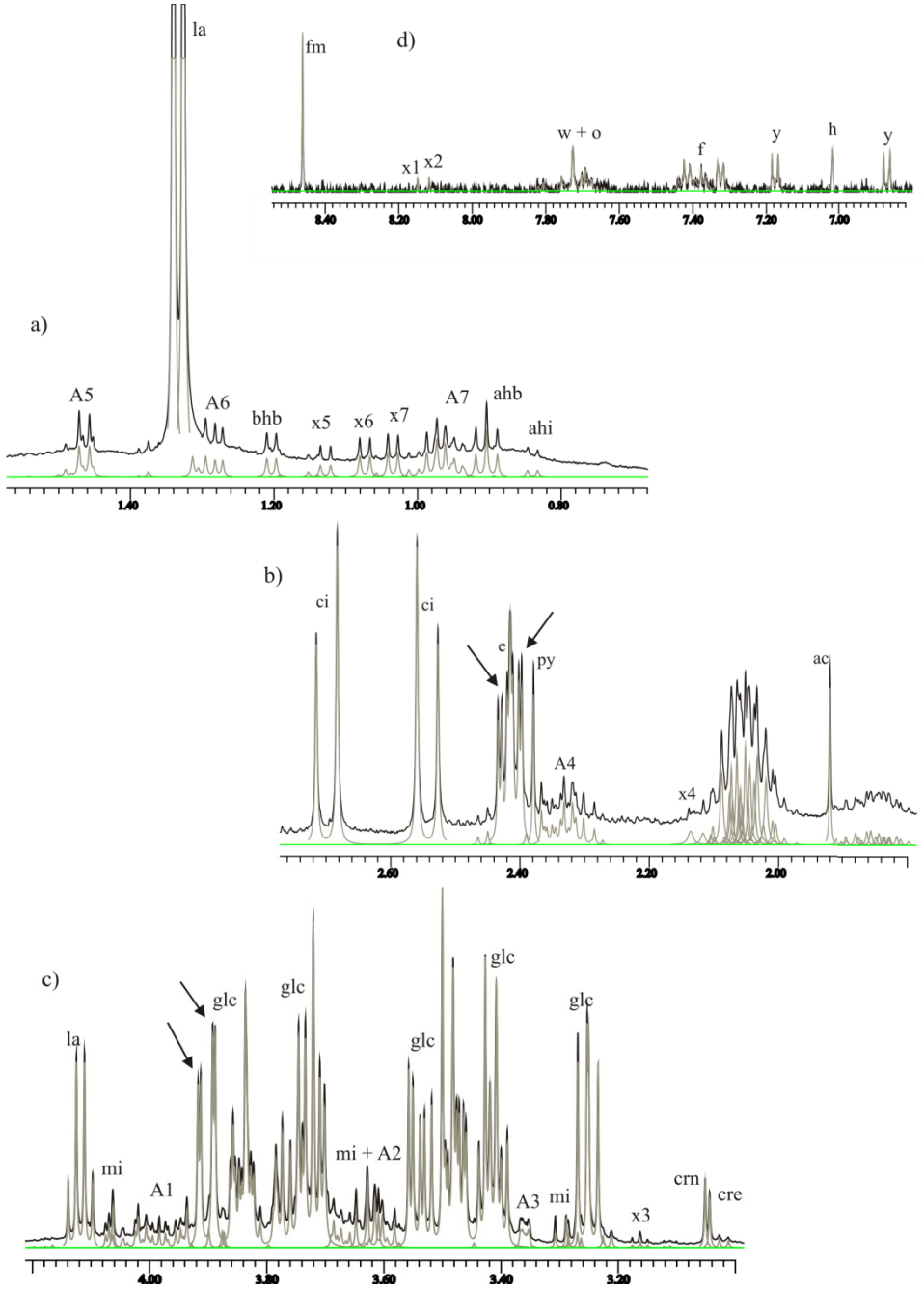

Figure 17. A presentation of a ^{1}H NMR spectrum of human CSF at 500 MHz. a) Higher field aliphatic region, with metabolite markings as follows: la=lactate, ahi=α–hydroxyisovalerate, ahb= α–hydroxybutyrate,bhb= β–hydroxybutyrate, A5 through A7=metabolite areas 5-7, x5 through x7=unknown metabolites. b) Lower field aliphatic region: e=glutamate, ac=acetate, py=pyruvate, ci=citrate, A4=several overlapping metabolites, x4= unknown metabolite. c) Middle region: la=lactate, cre=creatine, crn=creatinine, glc=glucose (α protons not shown), mi=*myo*-inositol, A1 through A3=metabolite areas 1-3, x3=unknown metabolite. d) Aromatic region: h=histidine, f=phenylalanine, w=tryptophan, y=tyrosine, fm=formate, o=others, x1 & x2=unknown aromatic metabolites. For details on the metabolite areas, see Table 4.

For each single line, the frequency, line-width and intensity were optimized during the fitting. For multiplets, the widths of each line were kept equal. The same line-shape [109] was used for every line. The use of macros for the quantification and processing of spectra is highly beneficial in the creation of automatic protocols, thus ensuring that all the analyses are performed in an identical way. All calculations were performed on a standard PC (AMD Athlon MP 2800+, dual CPU). Phase correction was done manually and the baseline was described as shown above. While the above constraints and those defining the structures of multiplets are absolute, further 'soft' least-square constraints on frequencies (to prevent signals moving far from their original positions), line-widths (to force widths into a similar range and to prevent the formation of broad signals to imitate the baseline) and intensities (to level the weights of very high and low intensity lines in the least-squares process) were also applied. For the range 0.7 – 3.0 ppm a weak constraint was applied to force Fourier terms toward zero. For the glutamine γ–CH_2-signal and citrate, it was sometimes necessary to manually adjust the trial positions of lines prior to iteration. Otherwise the program tolerates a few Hz differences between the trial and final positions. The spectral processing and fitting takes less than 2 minutes per spectrum.

Comparison with T_2 editing

The macromolecular baseline can be avoided by T_2 editing [74]. However, this method is complicated by *J*-coupling evolution, diffusion, and selective signal loss due to different T_2 relaxation times [74, 119]. This suggests that while T_2 editing is a valuable tool in detecting small components when creating a metabolomic model, it is not necessarily the best option when absolute quantitative results are desired. In order to assess the performance of CTLS and T_2 editing, the three measured T_2 spectra (not edited, minimally and heavily edited) were fitted in the identical way by using the same metabolite template. When the spectrum was measured so that some protein baseline was still clearly visible (demanding nonlinear baseline), a good correlation of $R^2 = 0.989$ was obtained between the normal 1D and T_2 edited spectra (using $y = ax + b$ type regression equation). Although the good overall correlation is evidence for the robustness of the baseline correction, up to 25 % bias between some concentrations were seen and when the protein signal was fully removed with a 320 ms T_2-filter, the bias in those concentrations increased, while the correlation decreased to $R^2 = 0.859$. For example, the T_2 edited lactate signal was 70 % too large while that of glucose was 35 % too small. Because the protein concentration shows huge variations (Table 8) and because the T_2 artifacts to the intensities can be supposed to be sensitive to them, due to viscosity and metabolite-protein interactions, use of T_2 editing is not ideal in quantification of CSF metabolites.

Chemical shift dependence on Ca^{2+} and Mg^{2+} concentrations

The positions of signal frequencies of some metabolites (e.g. citrate, glutamine and glucose) varied significantly (up to 10 Hz) from one spectrum to another. The good correlation (R=0.96) between the

glutamine γ–CH_2 proton shift and Ca^{2+} concentration suggests that this shift variation arises mainly from Ca^{2+} concentration (see Table 6). The correlation with Mg^{2+} was nearly insignificant. The results also propose that the glutamine γ–CH_2 chemical shift can be used as a Ca^{2+} concentration indicator: a high chemical shift indicates a high Ca^{2+} concentration. Assuming the chemical shift pH dependence zero, the correlation follows the equation, $\delta(\gamma\text{–}CH_2) = 1.4562\ [Ca^{2+}] + 1143.9$, where the shift is given in Hz at 500.13 MHz.

Table 6. Ca^{2+} and Mg^{2+} concentration (mg/ml) vs. glutamine γ–CH_2 signal shift (Hz) at 500 MHz.

Ca^{2+} concentration (mg/l)	Mg^{2+} concentration (mg/l)	Glutamine γ–CH_2 chemical shift in Hz
31.2	16.6	1187.9
32.6	19.6	1192.6
34.0	18.8	1194.1
37.2	26.6	1197.6
39.6	15.2	1201.4

Metabolite concentrations and relevance

The average populations, their standard deviations and ranges of the metabolites are reported in Table 7 and Table 8. The concentrations for metabolites are reported as mM concentrations, and in the case of areas, as signal areas relative to the 2.15 mM TSP in the samples (the TSP signal was scaled to 100), the latter having no specific unit. A single anomalous myo-inositol concentration was observed (56.5 vs. mean 11.4). The data was first subjected to the Grubb's outlier test and the anomalous value was detected as an outlier at probability level $p<0.0001$ and thus excluded. No further outliers were detected.

Table 7 and Table 8 reveal the large variation of the concentrations within the groups. ANOVA results did not indicate average concentration differences between single metabolites (when comparing C_ADP patients and C_NRM patients), with the exception of creatinine ($p = 0.027$). Creatinine concentrations were higher in patients that had an AD marker profile in CSF. This may indicate differences in cerebral energy metabolism, as previously investigated [133]. Additionally, as previously reported to have significance in AD, the concentration of myo-inositol and its ratio to creatinine was also assessed with ANOVA and found to be nearly significant ($p=0.053$ for the ratio). Interestingly, while increased in AD [65], the ratio was now lower in the group having an AD marker profile. The absolute metabolite concentrations in Table 7 were also compared with literature values (if available) obtained from the Human Metabolome Database (HMDB) [36]. It should however be noted that the literature values vary significantly depending on the patient group examined and are therefore not to be absolute-

ly trusted. The concentration ranges in CSF reported for the metabolites in Table 7 are reported normal for adults (>18 years) without standard deviations as follows: tyrosine 6-25 μM, histidine 10-21 μM, phenylalanine 4-18 μM, 1-20 μM, lactate 800-3000 μM, formate 32 μM, myo-inositol 84-175 μM, glucose 1700-5400 μM, creatinine 43-65 μM, creatine 44 μM, 176-400 μM, 425-625 μM, acetate 58-290 μM, β–hydroxybutyrate 34-50 μM, α–hydroxybutyrate 35-85 μM, α–hydroxyisovalerate 4 μM, pyruvate 50-150 μM.

Metabolite concentration correlations and their two-tailed significance were analyzed by using Pearson correlation. The most notable of the correlations detected (all with a significance level <0.0005) were: tyrosine – phenylalanine (0.809), citrate – lactate (0.744), glucose – citrate (0.751), citrate – glutamine (0.679) and x6 – x7 (0.788).

Table 7. Metabolite concentrations (mM) measured from NMR samples in neurological control patients. Standard deviations and concentration ranges for metabolite are also presented. The range is the calculated difference of the maximum and minimum concentration. Metabolite details as in Table 4.

	ABSOLUTE CONCENTRATIONS			NORMALIZED CONCENTRATIONS	
Metabolite	Concentration in C_ADP patients	Range	Concentration in C_NRM patients	Range	Concentration in C_ADP patients	Concentration in C_NRM patients
Tyrosine	0.015 ± 0.008	0.114	0.014 ± 0.005	0.105	0.003 ± 0.001	0.003 ± 0.001
Histidine	0.005 ± 0.001	0.007	0.005 ± 0.001	0.018	0.001 ± 0.000	0.001 ± 0.000
Phenylalanine	0.018 ± 0.010	0.176	0.015 ± 0.005	0.113	0.004 ± 0.002	0.003 ± 0.001
Tryptophan*	0.008 ± 0.003	0.066	0.007 ± 0.002	0.031	0.002 ± 0.001	0.002 ± 0.000
Formate	0.022 ± 0.010	0.036	0.024 ± 0.010	0.040	0.005 ± 0.002	0.005 ± 0.002
Lactate	1.642 ± 0.281	1.041	1.688 ± 0.376	1.295	0.359 ± 0.044	0.355 ± 0.042
Myo-inositol	0.156 ± 0.056	0.840	0.164 ± 0.038	3.372	0.034 ± 0.011	0.035 ± 0.007
Glucose	3.542 ± 0.649	13.995	3.732 ± 0.699	18.639	0.767 ± 0.029	0.785 ± 0.027
Creatinine	0.263 ± 0.052	0.198	0.226 ± 0.042	0.169	0.057 ± 0.008	0.048 ± 0.008
Creatine	0.163 ± 0.035	0.120	0.172 ± 0.038	0.155	0.036 ± 0.007	0.036 ± 0.005
Citrate	0.532 ± 0.158	0.783	0.552 ± 0.141	0.964	0.114 ± 0.020	0.116 ± 0.018
Glutamine	0.409 ± 0.085	0.639	0.388 ± 0.079	0.718	0.089 ± 0.012	0.082 ± 0.013
Acetate	0.191 ± 0.194	1.610	0.179 ± 0.257	3.550	0.038 ± 0.035	0.034 ± 0.045
β–hydroxybutyrate	0.020 ± 0.009	0.090	0.019 ± 0.011	0.183	0.004 ± 0.002	0.004 ± 0.002
α–hydroxybutyrate	0.045 ± 0.017	0.161	0.041 ± 0.014	0.214	0.010 ± 0.003	0.009 ± 0.003
α–hydroxyisovalerate	0.005 ± 0.003	0.049	0.004 ± 0.003	0.082	0.001 ± 0.001	0.001 ± 0.001
Pyruvate	0.046 ± 0.016	0.167	0.042 ± 0.021	0.222	0.010 ± 0.003	0.009 ± 0.004

Table 8. Metabolite areas relative to 2.15 mM TSP when TSP scaled to 100. Standard deviations and concentration ranges for areas are also presented. The range is the calculated difference of the maximum and minimum. Metabolite area details as in Table 4.

	AREA RELATIVE TO TSP			NORMALIZED AREAS		
Metabolite	Areas in C_ADP patients	Range	Areas in C_NRM patients	Range	Areas in C_ADP patients	Areas in C_NRM patients
X1[a]	0.042 ± 0.032	0.097	0.051 ± 0.030	0.122	0.009 ± 0.007	0.011 ± 0.007
X2[b]	0.060 ± 0.040	0.127	0.069 ± 0.039	0.149	0.014 ± 0.010	0.014 ± 0.008
AREA1[c]	11.604 ± 2.576	8.753	11.257 ± 2.583	10.642	2.546 ± 0.525	2.386 ± 0.444
AREA2[d]	10.937 ± 4.001	12.287	10.454 ± 3.413	12.769	2.396 ± 0.842	2.235 ± 0.665
AREA3[e]	3.057 ± 0.810	2.615	3.212 ± 1.231	5.595	0.671 ± 0.163	0.678 ± 0.239
X3[f]	0.622 ± 0.329	1.123	0.566 ± 0.506	2.377	0.140 ± 0.069	0.121 ± 0.105
AREA4[g]	5.248 ± 1.970	5.713	4.995 ± 1.617	6.434	1.118 ± 0.322	1.040 ± 0.253
X4[h]	0.790 ± 1.207	4.556	0.824 ± 0.807	3.172	0.174 ± 0.228	0.177 ± 0.155
AREA5[i]	1.785 ± 0.721	2.685	1.919 ± 0.667	2.615	0.394 ± 0.141	0.399 ± 0.102
AREA6[j]	2.470 ± 2.369	9.068	1.574 ± 0.847	3.855	0.593 ± 0.686	0.345 ± 0.202
X5[k]	0.396 ± 0.153	0.639	0.330 ± 0.130	0.639	0.090 ± 0.039	0.072 ± 0.029
X6[l]	0.981 ± 0.350	1.334	0.916 ± 0.234	1.068	0.212 ± 0.058	0.193 ± 0.040
X7[m]	1.127 ± 0.625	2.503	0.956 ± 0.291	1.165	0.244 ± 0.111	0.201 ± 0.053
AREA7[n]	3.902 ± 1.809	6.870	3.191 ± 0.948	3.659	0.852 ± 0.326	0.668 ± 0.154
Protein	1370.262 ± 1237.306	4721.600	1480.900 ± 1197.683	4814.400	7.692 ± 6.946	8.313 ± 6.723

In general, surprisingly large variations in metabolite concentrations can be seen. In over half of the metabolites quantified, the concentration variances were larger than 30 %, in some cases even over 60 % (x1, x2, x4, acetate and area6 in C_ADP patients and x3, x4, acetate and α–hydroxyisovalerate in C_NRM patients). The overall protein concentration of the samples was also estimated, yielding a very large variability of the concentrations (mean = 1435, range = 260 – 5140). In Table 7 also the relative concentrations of the metabolites are given: the total concentration of the metabolites was set 100 %, which more efficiently reflects the relative variations of the metabolites. Analyses performed on this normalized data resulted in the same conclusions as the analyses done on the relative concentration data.

The principal component analysis revealed that 87 % of variance is explained by the first 10 components and that there are several components that explain ~2 % of variance. This result suggests that significant correlations exist between the metabolites. On the other hand, the ca. 10 independent concentrations variables offer a potential mirror for watching CSF in metabolomic applications.

In order to examine whether the two patient groups can be classified on the basis of the metabolite concentrations, we performed a SOM analysis including age and sex into the multivariate model. The

SOM results clearly indicate that the SOM does not adequately separate the groups. We conclude that the two groups do not differ enough to be separated on the basis of the metabolite concentrations.

Conclusions

In this work a protocol for quantification of a ^{1}H NMR spectrum of hCSF as based on constrained total-line-shape fitting, was developed. The CTLS approach helps to minimize problems arising from signal overlap, chemical shift variations and spectral artifacts, including protein background. In this approach, almost any the spectral regularities can be conveniently incorporated into the spectral model. The inclusion of prior knowledge significantly improves the metabolite population statistics.

Up to 85 % of the non-protein signal area could be explained by 17 metabolites. The rest of the area was grouped into 7 integrals. Although large variations were observed between individual patients, the only difference ($p=0.027$) between control patients and patients with a normal AD marker profile, was the higher creatinine level in the latter group. SOM analysis failed in classification of the patient groups. The large variations, with ca. 10 independent principal components, help to profile patient neural metabolomics on the basis of CSF NMR analysis.

3.3 From concentrations to results

The basic scheme of a metabolomics study is as follows: I) acquire samples, II) measure samples, III) get the concentrations relevant to your study by some form of quantification or integration, IV) process these concentrations to obtain the results. This chapter deals with part IV and focuses on common chemometric ways to get some sense into the large amount of multivariate data from previous analyses. The point is to discover the variables describing the metabolic variation involved in the particular study and to allow categorization and classification of the samples from the study.

The answer to part IV is pattern recognition (PR) methods. PR methods are based on chemometrics and the related multivariate data statistical approaches applied to chemical numerical data [134] and they can be used to reduce the complexity and dimensionality of data sets, thereby facilitating the visualization of patterns in the data set. As an alternative, multiparametric data, such as e.g. the integrals obtained from a series of blood ^{1}H NMR spectra, can be modeled using PR techniques so that the class of an individual sample can be predicted on the basis of a series of mathematical models derived from the original data [2]. A statistical analysis therefore typically consists of two steps referred to as the calibration (or training) and prediction (or test) steps. During the calibration step the characteristics of a set of data are investigated, and an attempt is made to find a mathematical model for its behavior.

There are many ways to achieve the above each of which has their own strengths and weaknesses. Therefore it is vital which method to use for which problem. The mathematic methods commonly used in this type of analyses can be divided into two groups based on the underlying mathematical principle: methods based on regression, and methods based on classification. Another possible way to divide the techniques is whether they leverage the a priori information or not, these referred to as unsupervised and supervised methods. The methods commonly in use in metabolomics are presented in Table 9 along with the method type as well as some advantages and disadvantages.

Due to the nature of metabolomic data, the most enlightening example of regression technique is multiple linear regression (MLR), which is used here to illustrate the basic principle and underlying assumptions of regression techniques. It must however be noted that the linear regression presented here is only the simplest form of regression available and often more complex (including nonlinear and parametric) regression is used. The MLR problem can be stated as follows: different features are measured for m variables x_j (j=1...m) and for variable y with the goal of establishing a linear relationship between them. If there are n samples, the y_i (i=1…n) can be written as a column vector y, the weight vector b remains the same and the vectors x'j form the rows of matrix X. This stated as an equation, results in the form $y = Xb + e$, where the e is an error term, often called the residual.

The matrices referred to in the previous can be graphically presented as:

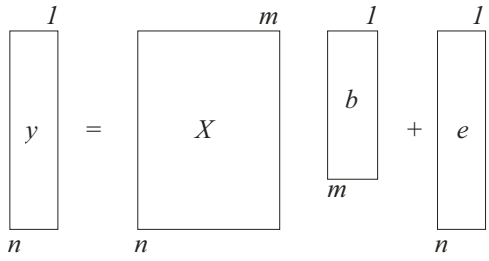

In this case n is the number of samples and m is the number of independent variables. In a regression analysis the input data consists of values of a dependent (response) variable (y) and of one or more independent variables (x), also known as explanatory variables or predictors. The dependent variable in the regression equation is modeled as a mathematical function (which can be generally expressed as $y = f(x) + e$) of the independent variables, corresponding constant parameters, and the error term. The error term is treated as a random variable and represents the unexplained variation in the dependent variable. In an optimal case the residual is zero but in a practical case it is nonzero, though it should remain relatively small when compared to the explained variance.

In contrast to regression techniques the "dependent variable" is not a variable *per se* but a label representing a specific class, which in metabolomics could mean e.g. a specific neurological diagnosis. Thus in classification the independent variables should be considered as properties with which the samples can be associated to the classes. It should also be noted that the classes are discrete entities and as such are not amenable to normal mathematical operations. Thus in classification techniques, all operations take place on the right side of the regression equation.

As stated earlier, another way of dividing PR algorithms is along the line of supervised and unsupervised. In supervised techniques the algorithm is given a set of samples along with the "correct answers" and it is told to formulate a model which most accurately reproduces the given correct answer. The great pitfall of supervised techniques is overfitting which means that by using a powerful enough supervised technique; it is possible to create a near perfect model of almost any data, even random numbers. Thus when using a supervised technique, it is vital that the model is carefully validated to weed out the overfitted models. On the other hand, unsupervised techniques only utilizes a set of samples and tries, without any *a priori* information, to find patterns in the data which could be used to model the internal structure of the data. This means that the unsupervised techniques are more sensitive to noise and artifacts present in the data than supervised techniques. On the other hand, they are more robust as they are not as prone to overfitting as supervised methods. Unsupervised techniques are especially useful for comparing pathological samples with control patients, whereas supervised methods are preferred when the number of classes is large or when there is a lot of noise in the data.

Both unsupervised and supervised methods especially require a second independent data set to test or validate the class predictions made using the training set. Internal (training set) and external (second data set) predictivity are different matters and both must be validated properly. Validation can be done e.g. by using cross-validation (CV) techniques in which one (Leave-One-Out, LOO) or many (Leave-Many-Out, LMO) of the datapoints are excluded from the model building phase to generate an internal test set. Then the model constructed from the remaining data is used to predict the omitted test patients. LOO is the most commonly used CV method, but for large or homogenous data sets it may be necessary to use LMO.

Before the development of any kind of mathematical model, it is often convenient to tailor the calibration set data to make calculations easier. However, in some types of data the methods mentioned below only make the results less accurate and so care must be taken when considering which tailoring methods will be used, if any. Very often the values of each variable are used in mean-centered form meaning that the average value is calculated from the calibration set and then subtracted from each corresponding variable. Quite a few methods for scaling variables also exist, and it is important to note

that the dependent and independent variables can be scaled separately There are essentially three ways of scaling variables: no scaling at all, variance scaling, and weighted scaling. Usually when dealing with data that is measured in the same units in all blocks (such as spectroscopic data), scaling is not needed. Variance scaling on the other hand is mostly used when the variables in different blocks are measured in different units (e.g. ppm, %, and kg) or when the variables have significantly differing values. The scaling itself is done by dividing all the values for a certain variable by the standard deviation for that variable so that the variance for every variable is within the same limits. When using weighted scaling, one must decide which variables are less important than others; these are then given a smaller weight in calculations [135].

Table 9. The main differences, advantages and disadvantages of the methods commonly used in NMR metabolomics. Abbreviations as follows: R=regression, C=classification, S=supervised, U=unsupervised, PCA=principal component analysis, SM=Sammon's mapping, PLS=partial least squares, PLS-DA=partial least squares – discriminant analysis, OPLS=orthogonal projections to latent structures, OPLS-DA= orthogonal projections to latent structures – discriminant analysis, SIMCA= soft independent modeling of class analogy, LVQ=learning vector quantification, SVM=support vector machine, kNN=k-nearest neighbors, DT=decision tree, RF=random forest.

Method	Type	Advantages	Disadvantages
PCA	U, R	Computationally fast Easy interpretation of results Method well understood	Very sensitive to colinearity Relatively sensitive to noise and artifacts
SM	U, C	Computationally relatively fast Easy interpretation of results	Interpreting the results in terms of descriptors is difficult
PLS	S, R	Computationally fast Easy interpretation of results Method well understood	Modestly sensitive to colinearity Relatively sensitive to noise and artifacts Slightly sensitive to misdiagnosed samples
PLS-DA	S, C (R)	Easy interpretation of results	
OPLS	S/R	Relatively insensitive to colinearity, noise, and artifacts	Slightly sensitive to misdiagnosed samples
OPLS-DA	S, C (R)	Combines the strengths of PLS-DA and SIMCA	
SIMCA	S, C	Widely used Method well understood	Interpretation of results challenging Sensitive to misdiagnosed samples
LVQ	S, C	Can handle very heterogeneous data	Computationally challenging for large data sets
SVM	S, C	Results relatively simple to interpret	Fails if classes overlap
kNN	U, C	Computationally fast No specific training step Can handle very heterogeneous data	Results relatively hard to interpret Usually needs variable selection which is not trivial
DT	S, C	Computationally fast Easy interpretation of results	Cannot detect truly multivariate effects
RF	S, C	Computationally fast Runs efficiently on large data sets Gives estimates of what variables are important in the classification	Understanding results can be challenging

3.3.1 Commonly used pattern recognition methods in metabolomics

Principal component analysis

PCA [136] is a mathematical procedure that transforms a number of possibly correlated variables into a (smaller) number of uncorrelated variables called principal components. The principal components (PCs) are linear combinations of the original input descriptors with appropriate weighting coefficients, such that the first PC contains the greatest amount of variance in the data and subsequent PCs contain as much of the variability in the data as possible. By plotting only the first two or three PCs, the original N-dimensional data are effectively compressed into two or three manageable dimensions. Therefore, PCA is actually only a coordinate system transformation where new coordinates are selected so that each of them explains the maximum amount of remaining variance in the data. The loadings are the components of the PC in the variable space, while the score is the eigenvalue of each sample point within the PC. The resulting PCs can be used to visualize any clustering patterns associated with a metabolic response [12]. PCA has been frequently applied in the evaluation of metabolomic data and should be the method of choice for obtaining an overview, find clusters, and to identify outliers. For a few different examples on applications, the reader is referred to publications [13, 21, 22, 54, 73, 137-145].

Sammon's mapping

Sammon's mapping [146] is an iterative non-linear technique for representing n-dimensional data in 2 or 3 dimensions with a minimal overlap of data points in the graphical presentation. This method often provides a better clustering of the samples than PCA but has not been used that much in metabolomics studies.

Partial least squares

Partial least squares (PLS) [135] is an iterative regression method, much like PCA, for modeling the relationship between a set of independent variables and a set of dependent variables. As an example, a patient's neurological state may be defined as a function of neurotransmitter concentrations present in CSF. In principle, PLS uses two PCA analyses, one performed on the dependent variables and the other on the independent variables, to derive the final correlation coefficients. This improves the tolerance for noise and internal correlations in the data. PLS can also be used to examine the influence of time on a data set, which is particularly helpful for biofluid NMR metabolomics because data collected from samples taken over the progression of a disease, therapy or toxic effect, can be studied directly. A discriminant analysis (DA) can be used as an additional step for classification purposes. The DA builds a predictive model for group membership of the samples. The model is composed of discriminant functions based on the linear combinations of the predictor variables that provide the best discrimination

between the groups. The functions are generated from a sample of cases for which group membership is known; the functions can then be applied to new cases that have measurements for the predictor variables but have unknown group membership. The latter method is referred to as partial least squares discriminant analysis (PLS-DA) [147]. For recent examples of the use of PLS and PLS-DA in metabolomics, see references [148-151].

Orthogonal Projections to Latent Structures

Orthogonal Projections to Latent Structures (OPLS) [152-154] is a linear regression method that has been employed successfully for prediction modeling in various biological and biochemical applications [91, 155, 156]. The benefits of OPLS include the ability to model data containing noise as well as multi-collinear variables, such as spectral data from metabolic profiling and other omics platforms [90]. The OPLS method employs the descriptor matrix X to predict the response matrix Y. In fact, OPLS is very much alike PLS, but due to the slightly different mathematical basis it is more noise tolerant than standard PLS. The unique property of this method compared to other linear regression methods is its ability to separate the modeling of co-varying variation from structured noise, defined as the systematic variation of X which does not correlate with Y, while simultaneously maximizing the covariance between X and Y. A recently introduced extension, a kernel based OPLS (K-OPLS) [157] has also been introduced to provide a combination of the strength of kernel based methods (e.g. Support Vector Machine, see below) with the OPLS ability to model structured noise. As is the case with PLS, OPLS can also be coupled with a discriminant analysis and is thus sometimes called OPLS-DA. Several studies using OPLS have already been realized [158-160], but since the method is relatively young, the bulk of applications are yet to be seen.

Soft Independent Modeling of Class Analogy

Soft Independent Modeling of Class Analogy (SIMCA) [161] is a supervised classification method based on PCA. The idea is to construct a separate PCA model for each known class of observations using the observations belonging to that class. For each of the observations, the so called residual or error is computed. These residuals are then analyzed and the 95% confidence interval is determined. Then when an unknown sample is classified, its residual for each of the PCAs is computed and if the residual is within the 95% confidence interval, the sample classified to that class. The SIMCA method is recommended for use for one class cases, i.e. when there is one well-defined class of subjects and all other subjects are inhomogeneous [162]. However, when dealing with a study consisting of several classes (sick/healthy, treated vs. nontreated, etc.) other supervised methods such as PLS-DA or OPLS-DA are preferable. SIMCA has been applied to metabolomic studies, a few examples can be found in references [137, 163-165].

Learning Vector Quantification

LVQ [130] is a supervised form of Vector Quantization which is a feasible method for multi-class classification. It requires predefined classes and pre-classified data to be used in the learning process. The basic idea of LVQ is to cover the sample space with prototype points often called codebook vectors and then use a learning process to optimize the placement of the points, thus locating the most relevant variables for the classification. Most forms of LVQ use derivatives of the competitive learning algorithms utilized by the Self Organizing Maps (SOM). The actual prediction is a fast and rather straightforward process and it is usually performed by finding the nearest codebook vector and assigning the presented sample to the same class with it. Neural network based methods such as LVQ have been extensively used in metabolomics but have recently yielded ground to kernel based methods such as Support Vector Machine (see below).

Support Vector Machine

SVM [166-169] is a newer classification technique which is closely related to neural networks. Instead of optimizing the weight factors of a neural network, SVM uses a statistical learning paradigm to construct a "borderline" (in mathematical terms a parametric hyperplane) in the sample space separating the different classes from each other. The statistical learning is a stable and efficient learning method, being in many ways superior to the traditional neural networks. Furthermore, SVM needs relatively few parameters, and in many cases it can be proven that the statistical learning will inevitably lead to the optimal division [170]. Results of SVM are also usually easier to interpret than those of the traditional neural networks because for SVM there is a clear geometric interpretation available [171]. SVM has found its place in metabolomics and is considered in some cases to be a better option than PLS-DA [172]. Several other studies using SVM have also been published; see references [50, 173-176] for details.

k-Nearest-Neighbors

kNN [177] is probably the simplest and computationally easiest classification technique ever presented as it relies on the simple assumption that the class of an unknown sample can be predicted by a majority voting of the classes nearest to its k neighbors (usually $k = 3, 5, 7, 9\ldots$) [178]. kNN does not require a specific teaching step, nor does it make any other assumptions on the nature of the relationship between the class of a point and its descriptor values. This makes it highly feasible for unevenly distributed datasets as each cluster of samples is automatically used to predict similar samples and other remote clusters do not interfere, which is the case with many other techniques [179]. kNN models generally have more robust external predictivity than the regression models [180]. Even though the actual mechanism of kNN is very simple, it is often very difficult to gain insight to the reasons for the observed regularities and physicochemical conditions [181]. Due to the nature of the kNN analysis, it

requires the data to be variance scaled and mean centered, or the different value ranges may act as implicit weighting factors thus unduly biasing the results. Because the basic kNN assigns equal weight to each descriptor variable, it is very susceptible to noise and co-linearities. It is therefore usually prudent to use some form of variable selection prior to the kNN analysis [182]. This method is quite commonly used in metabolomics, recent examples are in references [174] and [183], but its usage is hampered by the difficulties in gaining an insight for result interpretation.

A method known as simulated annealing (SA) is sometimes used in selecting the appropriate variables for the kNN analysis. The selection is performed by an iterative procedure and commonly leads to rapid elimination of variables with poor signal to noise ratio and it will also drastically reduce the number of co-linear variables included in the kNN analysis. For a descriptor with a high number of poor quality variables, the SA analysis can yield significant improvements in both accuracy and computational speed. The downside of kNN-SA is that if the teaching set is modified, the optimization must be re-run from scratch. The SA optimization is also computationally quite heavy, but the vast majority of computations are performed during the model building phase, and the prediction time computational cost is equivalent to the sum of the separate kNN models which make up the ensemble.

Decision tree

The DT is a recursive partitioning technique which builds up a tree of binary divisions [184]. At each step, the current set of samples is analyzed and the set is divided into two subsets using the variable-value combination which leads to minimal contamination of the subsets with different classes. If desired, this process is repeated using each subset independently as a new current set. Each of these bifurcations becomes a node in the tree and when a subset is no longer divided it becomes a leaf in the tree containing the ID of the most numerous classes in the subset. Prediction of an unknown sample is performed by using the descriptor values, selecting at each bifurcation either the left or right subtree, until a leaf is reached, whereby the sample is classified according to the ID stored in the leaf in question [185].

When constructing a decision tree, it is possible to continue recursive divisions until each subset contains only one class, so that in the extreme case, each set contains only one sample. It is always possible to generate a tree that classifies the current teaching set with 100 % accuracy, but this would lead to overfitting, and the performance of such a tree on external data is usually very poor. In order to avoid overfitting, it is imperative that a cross-validation is used to decide the optimal depth of the tree [186]. The results of decision tree analysis are conceptually very intuitive and it is very easy to see which variables and what values mark the boundaries of the different classes. Therefore it is very easy to link the descriptors to the observed differences in classification [187]. DT is also in common use in the

metabolomic community, even though it is not among the most popular methods used. For examples, see references [173, 187, 188].

Random Forest

Random Forests (RF) is an ensemble learning method which combines two machine learning techniques, *viz.* bagging and random feature subset selection using a large collection of DTs for predictions [189]. The accuracy and computation speed of RF compares favorably with modern machine learning methods e.g. SVMs and neural networks. In contrast with many multivariate classifiers, RF is very resistant to overfitting. Distinctively, RF includes a built-in cross-validation scheme with extensive "Out-of-Bag" data (one third of samples for each tree). The procedure also gives an estimate of the prediction error as a by-product so that there is no need for the use of "external" validation sets.

While RF is originally a classifier, it can be used for distance metric learning [190]. If samples *i* and *j* land in the same terminal node in an individual DT, the similarity (called as proximity in the terminology of RF) between them is increased by one. The final proximity matrix is symmetrized and scaled by the number of trees to the interval [0, 1]. Finally, multidimensional scaling (MDS) produces a map that puts similar cases near to each other, and different cases far apart. This visualization shows the approximate two-dimensional structure of the data, and can provide important insight. For example, it is possible to get a "profile" for each sample by counting the votes in each class. The distribution of votes gives an estimate for the reliability of the prediction. It should be emphasized that RF uses proximity values for clustering instead of original data vectors and thus it may work even if more conventional clustering techniques fail.

RF is a relatively new method in terms of metabolomics and therefore not many applications exist. However, some use has already been found in chemical shift prediction [173], and in the prediction of a metabolic syndrome status based on dietary and genetic parameters [191].

3.3.2 Analytical bias and other considerations

The use of NMR spectroscopy for complex molecular systems has a long history and with the advent of more sensitive NMR spectrometers, the applications are nowadays even more widespread, covering combinatorial chemistry libraries [192], protein structures [193], drug mixture protein binding studies [194] and cell and tissue extracts [195]. Nevertheless, some problems regarding the interpretation of data still remain for metabolomics in particular. A profound example is sorting out the "needles from the haystack" in large sets of NMR spectra of biofluids from a group of animals or humans and then demonstrating various effects, such as normal physiological variation or drug-induced effects [2].

More problems are likely to arise when considering the amounts of data critically. How does e.g. data scaling or normalization affect the final results? What are the main sources of bias in metabolomics and how can these sources be minimized? These are important questions which have been addressed to some extent by research groups (see below). As briefly discussed previously, the data sets in NMR metabolomics yield a wealth of information, but this information is not readily accessible. Furthermore, the data is extensive but redundant: one measurement can result in tens of thousands of data points, but the effective dimensionality is much less due to a smaller amount of NMR visible compounds. These data sets therefore commonly require visualization software and chemometric and bioinformatic methods for interpretation and production of biological fingerprints that have either diagnostic or other classification value [3, 76].

The reproducibility and reliability of results acquired from discovery-based science has been extensively reviewed in the literature [196-199]. For example, many results have been too dataset specific and attempts to reproduce them have been in vain. Furthermore, use of a more rigorous validation approach than the commonly used LOO-CV has been suggested. The kind of bias resulting from e.g. poor validation is a major threat in clinical research and the same applies when dealing with NMR metabolomics. The main problem is the introduction of systematic variations into the data as a result of differential handling and analysis of samples, and the bias may not be immediately obvious. When dealing with e.g. blood plasma samples, bias can result from for example the type of tube used for sample collection or the amount of time the sample has been kept in ice. Sample collection procedure, the time of sampling, diet, exercise and medication can also result in an impact on a clinical chemistry test result. Additional bias can result from e.g. spectral editing and quantification; problems in the form of systematic errors have been detected in the CPMG pulse sequence [118], as well as in curve fitting methods used for quantification [97].

To detect real pathological variance, the preanalytical and analytical variations must be within acceptable limits such that they do not influence the clinical interpretation of the results. Therefore, standard operating procedures should be employed. A study dealing with the impact of analytical bias in metabolomic studies of blood plasma has recently been published [200]. In this report, the lack of available data when dealing with the effects of the sample collection protocol on NMR-derived metabolic profiles of plasma and serum was addressed. The variations in the composition of samples were measured when blood samples were collected onto and in the absence of ice, over a range of serum clot contact times and after freeze-thaw cycling. It was discovered that differences in the abovementioned categories can compromise the pattern recognition analysis of sample sets. Recommendations for the standard operating procedure were also presented. Even though it is essential to minimize bias in every possible way, it is necessary to note that the physiological variation between individual subjects, result-

ing from e.g. diet or other similar factors, is often much larger than the bias introduced by e.g. sample handling.

Another major area of possible bias is the preprocessing of the data prior to mathematical processing: i.e. normalization, variable selection, and scaling. For variable selection, the solution has been sought from genetic algorithms, and has been suggested that these algorithm can be more effective in both sample and variable selection than an independent validation samples set [201]. For the scaling problem, answers have been sought from new scaling methods and recently a protocol for variable stability scaling has been presented [202]. Also, a preprocessing approach that shows promise is a practical methodology for large-scale human studies in which several well-established steps were combined to ensure the minimization of bias, and furthermore, a more rigorous validation was tested and applied [203]. Additionally, an attempt to define an optimum approach for urine NMR spectra has been presented [204]. The results however, were not conclusive and more recently it has been suggested that data preprocessing has to be context dependent [205]. It was discovered that in many cases in NMR metabolomics, the exploratory data analysis is carried out by varying normalization and scaling procedures in order to obtain an optimum separation of two or more sample classes by using PR methods. While this is indeed useful for deriving classification protocols for predicting the class of the subsequent samples, the interpretation of the biochemical factors responsible for the classification is not straightforward. Moreover, with the increased interest in relating and comparing data sets collected from different platforms, or across different levels of molecular biology, it is important to be aware of the effects of preprocessing on statistical outcome and to be conscious of the consequences of a chosen method of preprocessing and, furthermore, the limitations this will place on the interpretation of the chemometric model [205].

To overcome the above problems, the process of standardizing NMR metabolomic sampling and reporting procedures has been realized. In a recently published report by the Standard Metabolic Reporting Structures (SMRS) group, the minimum requirements for designing and recording the results of a metabolic study were proposed [206]. One of the main areas highlighted in the report was the need for standardization of sample collection and preparation protocols for clinical studies. In a more recent report by the Metabolomics Standards Initiative (MSI) group, detailed accounts are reported in the form of various standardization protocols and a significant milestone in publishing a complete set of draft reporting requirements has been reached [207-210]. Hopefully, these guidelines will be respected and utilized in future studies so that the main sources of bias and heterogeneity can be avoided to a maximum extent.

4. NMR METABOLOMICS AND NEUROLOGICAL DISORDERS

Although NMR metabolomics and metabonomics can and are commonly used in many applications, this thesis will only focus on the use of NMR metabolomics in neurological disorders. All in all these are wide topics to discuss since there has been an explosive growth on research performed on the application of metabolomics and metabonomics for the detection or diagnosis of various diseases. A lot of progress has also been made. While the detection of some neurological disorders persistently continues to elude us, several others can readily be detected by using NMR metabolomics.

4.1 Background

Millions of people around the world suffer from mental illnesses or neurodegenerative dementias such as Alzheimer's disease (AD), Parkinson's disease (PD), depression, addiction, schizophrenia, and learning disabilities. These, among other diseases, are in need of better treatments, but unfortunately the comprehensive understanding of the disease specifics is still needed. It is actually likely that most of these disorders are not unitary conditions but may be a combination of various states that are yet to be defined. Some progress has been made in the treatment of psychiatric disorders, but many patients lack response to current therapies. Also, it cannot be predicted who will respond to which treatment. This natural variability in humans, coupled with the fundamental differences in pharmacology, is the underlying factor that affects the inability to perform predictions on how a specific patient may respond to a therapy selected by a physician [211]. These facts result in distress in patients and families who engage repeatedly in *trial-and-error* choices in search of "the right solution" and in physicians thus resorting in a widespread switching of medications [212] and polypharmacy [213]. The high personal and societal burden of inadequate trial-and-error management therefore results in an urgent need for validated biomarkers that establish a diagnosis, guide drug selection and reliably predict the response to treatment [214, 215].

To understand brain function and the complexities within, some new ideas and approaches are needed. The efforts to develop data production and analysis in neuroscience have been increasing. Genomics, including comparative genomics, gene expression databases and the organization of genomic-scale projects, gene microarrays, proteomics, imaging studies, and monitoring the activity of individual neurons using multiple electrode recordings, have all provided useful approaches to the study of neurological disorders [211]. The newest of the omics, metabolomics, also provides powerful tools for the analysis of individual metabolism, as well as for the examination of perturbations in metabolic pathways

and networks in human disease [216-218]. The metabolome defines a metabolic state that is regulated by the net interactions between gene and environment influences and provides information that has the possibility to bridge the gap between genotype and phenotype. It therefore provides the missing link to the study of diseases of the CNS. The knowledge of metabolic signatures for CNS disorders could result in the identification of disease specific biomarkers and in the ability for disease progression or response to therapy analysis. Moreover, as the signatures are the final product of the interactions between gene expression, protein expression and the cellular environment (see Figure 18), metabolomics also provides tools for drug development by providing detailed biochemical knowledge about drug candidates, their mechanism of action, and side effects [211].

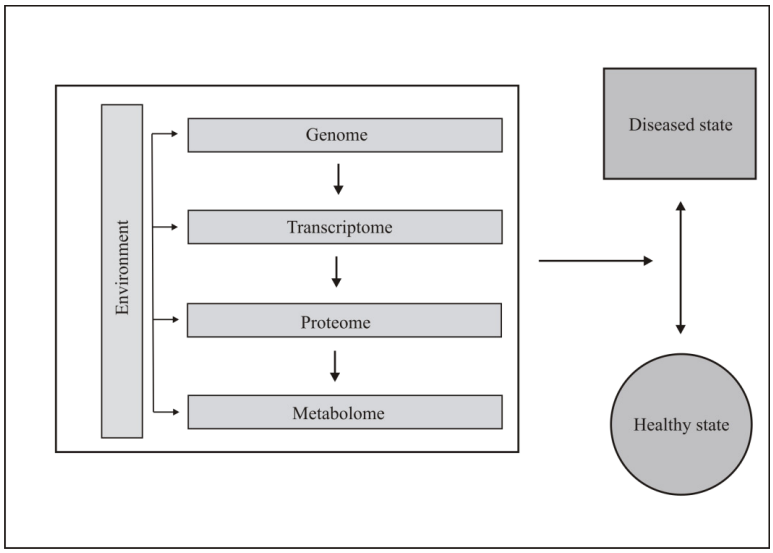

Figure 18. The flow of information from the genetic code to proteins and finally to metabolites. The environment and genetic code affect the end products and therefore influence health and disease states.

As previously discussed, metabolomics can be performed by using various different detection methods such as GC-MS and NMR spectroscopy. In terms of neurodegeneration, the NMR technology has been used extensively, both as an imaging tool to generate anatomical information via the measurement of water molecules in different physiological environments, and as magnetic resonance spectroscopy (MRS), which provides chemical structure information from *in vivo* tissues. Basic magnetic resonance imaging (MRI) has been solidly established as one of the most important clinical diagnostic tools for diseases such as multiple sclerosis (MS) [219, 220] and AD [221]. MRI has also been used for characterization of neural changes in diseases such as Creutzfeldt-Jacob syndrome [222], Huntington's disease (HD) [223], Hallervorden-Spatz disease [224], Alexander's disease [225], Cushing's syndrome [226] and bipolar disorder [227]. Although MRI is an extremely important clinical tool, MRS and

high-resolution NMR spectroscopy of biofluids are more useful in the context of systems biology since they generate multivariate information on a wide range of molecules during a single scan [4].

^{1}H MRS has sufficient sensitivity the detect a range of neurochemicals including amino acids, organic acids, and various phosphorus compounds, and its use has been reported in a number of reviews [228, 229]. Many neurological conditions have also been successfully characterized by MRS; some examples include epilepsy [230], amyotrophic lateral sclerosis (ALS) [231, 232], PD [233], HD [234], and AD [235, 236]. Furthermore, MRS has also been used to increase the specificity of noninvasive diagnosis of brain tumors [237]. Unlike MRS however, high-resolution NMR is not compromised by poor spectral resolution and can routinely access the CNS metabolites present at micromolar concentrations. The use of more specialized NMR probes such as cryoprobes and microprobes offers a further enhancement in sensitivity, lowering the effective detection limit to the nanogram range [4].

4.2 Alzheimer's disease

4.2.1 Introduction

A 51-year old woman with progressive cognitive decline and behavioral changes associated with distinctive neuropathological features was described in 1907 by Alois Alzheimer as the first case of the illness that bears his name [238]. In a more modern era, the leading cause of dementia in the elderly is AD, accounting for 65-75% of all cases. AD is also the fourth most common cause of death in developed nations (after heart disease, cancer, and stroke) [239]. The prevalence of AD is age-dependent and the number of AD patients doubles approximately every 5 years, becoming 2% at age 65, 4% at 70, 8% at 75, 16% at 80, and 32% at 85 [239, 240]. The incidence of the disease also increases with age, and is estimated at 0.5% per year from ages 65 to 69, 1% per year from ages 70 to 74, 2% per year from ages 75 to 79, 3% per year from ages 80 to 84, and 8% per year from age 85 onward [241]. In Helsinki, the prevalence of dementia at ages 75, 80, and 85 has been reported to reach 4.6 %, 13.1 % and 23.3 %, respectively. The cost for institutionalization of these patients alone is expected to reach nearly EUR 1.5 billion in 2030. The disease progression of AD is continuous and gradual but sometimes plateaus may occur. Dementia shortens life expectancy and is classified as a chronic condition, significantly influencing the quality of life [242]. Although the knowledge of molecular background of other dementing diseases has advanced significantly during the recent years, no markers for other dementias are currently available. Due to heterogeneous pathologies and chemical changes in the brain in different dementing diseases, it is highly probable that different markers or marker sets are needed for example for early diagnosis or monitoring of therapeutic responses.

4.2.2 Clinical course

Not all neurological reasons for Alzheimer's disease are clear. An important change in the brain is the neuronal cell death in the inner parts of the temporal lobe, especially near the *hippocampus*. Biochemically, the most significant change is the weakening of acetylcholine activity which can be detected in the lower parts of the frontal lobe. The activity of the *acetylcholinetransferase* enzyme is also decreased, and defects in other signaling systems (noradrenalin, serotonin, and dopamine) have been reported [243].

Some genetic mutations increase the risk of AD. Mutations have been found in the genes encoding the amyloid precursor protein (APP) on chromosome 21 and presenilin-1 and -2 on chromosomes 14 and 1, respectively [244, 245]. Another significant risk factor for AD seems to be an allelic variation of apolipoprotein E (ApoE), especially the ApoE4 allele [246]. Other risk factors include aging, atherosclerosis, stroke, diabetes mellitus, lower education, smoking, alcoholism, high fat intake, transient

ischemic attack, hyperhomocysteinemia, coronary artery disease, thrombogenic factors, migraine, high fibrinogen levels, hemorheologic abnormalities, depression, high serum viscosity, head injury-LOC (loss of consciousness), hypotension, menopause, hypertension, microvessel pathology, cardiac arrhythmias, and high LDL (low density lipoprotein) cholesterol [247].

The first cognitive symptoms usually appear as memory deficits [248]. Early memory loss of everyday events is characteristic for the first stage. In contrast, short-term memory tends to be preserved early in the disease. Language deficits usually occur in the middle stages of the disease, but sometimes they might also appear early for example as difficulties in naming objects or expressing ideas [249]. Visuospatial deficits are often manifested by impairment of topographical memory, when patients easily get lost. Also, deficits in other cognitive abilities such as judgment, attention, abstract reasoning, praxia, and calculation appear in different phases of the progressing disease. Some patients have symptoms like aphasia, visual disorientation, or apraxia [247].

Non-cognitive symptoms are very common in AD and they affect the patients and caregivers quality of life in a large manner [250, 251]. These include symptoms such as personality changes (about 70% have apathy); agitation (60%, this also includes aggressive behavior); manifest depressive features (40%) such as anxiety, irritability, dysphoria, and aberrant motor behavior; delusion and hallucinations (30-60%); and also euphoria (5%) [252, 253]. In AD, neurodegenerative abnormalities are also common affecting such things as sleep, appetite, and libido. The occurrence of abnormal motor behavior, anxiety, sleep disorders, and psychotic symptoms significantly increases with the progression of the illness [247].

AD is a complex syndrome with many subtypes and varieties of clinical patterns. The heterogeneity of the disease is demonstrated in various aspects; age of onset, duration, clinical course, types and patterns of cognitive and non-cognitive symptoms, response to treatments, and neuropathological findings [254]. Several variables are associated with a distinct pattern of symptoms: age at onset, demographics factors (including education, and familial and social network), premorbid personality, and early development of neuropsychiatric or extrapyramidal signs, co-occurrence of physical diseases [255, 256].

Medicinal treatment is available for the symptoms described above, but a definite medicine for AD is yet to be found, if such a medicine even exists. The cognitive symptoms can be lessened with medication. If needed, the disturbing behavior and depression can also be treated with neurological medicine [243].

4.2.3 Biological markers

As a primary degenerative dementia, AD is a proteinopathy [257]. Extracellular deposits of amyloid-beta (Aβ) containing plaques and intracellular neurofibrillary tangles (NFTs) composed of paired helical filaments of hyperphosphorylated tau protein (PHF-tau) are characteristic features in AD brains. It is generally thought that the driving force of AD pathology is the formation of toxic Aβ peptides followed by a cascade of secondary pathologies eventually leading to synaptic dysfunction and loss and neuronal death [258]. CSF β-amyloid$_{42}$ and tau- and phospho-tau proteins reflect AD-associated brain pathology [259]. Changes of these markers appear early during the course of AD [260-262]. The new research criteria (Table 11) for AD include these markers as supporting features for the diagnosis of AD [263]. However, many studies have suggested that the levels of these markers are not sensitive for monitoring the progression of the disease or therapeutic responses [264-266] possibly due to the fact that brain pathology in advanced AD is multifactorial and includes chronic inflammation, oxidative changes, excitoxic damage and the dysfunction of many neurotransmitter systems.

The CSF markers for AD have traditionally included β-amyloid$_{42}$ (Aβ42), total-tau- and phospho-tau proteins [267-269] and these are also discussed in more detail below. The concentration of Aβ42 in AD is lower and that of total-tau is higher when compared with healthy control patients [267, 268] and the concentrations of different phospho-tau epitopes can also be high [270, 271].

APP and its cleavage

The amyloid precursor protein belongs to type 1 membrane spanning glycoproteins and the three major isoforms are APP$_{695}$, APP$_{751}$, and APP$_{770}$. The isoform present in neurons is APP$_{695}$ [272, 273]. APP matures through the secretory pathway. While moving through the *trans*-Golgi network different types of modifications appear: N- and O-glycosylation, and tyrosyl-sulfation. N-glycosylated APP is cleaved in the endoplasmic reticulum (ER) or in *cis*-Golgi and the mature APP is degraded as it is transported to or from the cell surface via either biosynthetic or an endocytic pathway [274].

The APP cleavage pathway classification is divided into two pathways depending on the cleavage by two enzymes called α– and β–secretase [272]. The cleavage of APP by α–secretase appears in the late Golgi or at the plasma membrane in caveolae [274, 275]. The α–secretase pathway results in two fragments: sAPPα and p10 and further cleavage of p10 results in a small fragment called p3 [272]. The β–secretase pathway takes place in the endosomal and secretory compartments of the ER and Golgi [276]. The cleavage produces two fragments: sAPPβ and a fragment of 11.5 kDa which is the intact

Aβ. The β–secretase pathway also includes further cleaving of Aβ by γ–secretase resulting in a smaller fragment called Aβ [272]. An alternative way of cleavage of APP occurs by caspases (apoptotic proteases), and an increased production of Aβ peptides by caspases has been detected during apoptosis. Caspases appear to play a dual role in the proteolytic processing of APP and the resulting proclivity for Aβ peptide formation, as well as in the apoptotic death of neurons [277].

Two main populations of Aβ exist; the $A\beta_{1\text{-}40}$ which represents 90% of secreted Aβ and $A\beta_{1\text{-}42}$ (Aβ42, 10%) [278]. In the AD brain, Aβ42 has a special role since it seems to form senile extracellular plaques and its production in the brain is also increased. The Aβ42 exists in water soluble dimers that may form the building blocks of insoluble Aβ filaments [279]. The variety of different amyloid isoforms and their role in pathogeneity of AD is often explained by C-terminal heterogeneity of Aβ, for example by differences in the amount of hydrophobic amino acids. Additionally, p3 seems to have the corresponding C-terminal and therefore these two C-terminus fragments are the two main constituents of nonfibrillar or diffuse plaques [280].

The cleavage of APP seems to be regulated by several factors during amyloid-metabolism. An example would be the appearance of neurotransmitters acting via certain receptors having effects on the metabolism; e.g. cholinergic agonists show an increase in sAPP release and decrease the production of Aβ in HEK293 cells overexpressing muscarinic acetylcholine receptors [281, 282]. It has also been discussed that APP may have a more important physiological role than Aβ peptides [272]. There also seems to appear some short term activation in intracellular signaling pathways, e.g. activation of protein kinase C (PKC) by phorbol esters increasing the level of sAPP and decreasing the level of Aβ [283]. Also some PKC-independent pathways are involved in the regulation system of APP such as second messenger Ca^{2+}, phopholipase A2 (PLA2), cyclic AMP (cAMP)-dependent protein kinase A (PKA), and unidentified tyrosine kinases [272].

Tau-protein

Extracellular plaques can also be present in healthy individuals, but the presence of intracellular neurofibrillary lesions correlates more accurately with dementia [284]. The intracellular lesions are found in nerve cell bodies and apical dendrites as neurofibrillary tangles (NFTs). The lesions consist structurally of paired helical filaments (PHFs) and related straight filaments (SFs). These filaments are made from the microtubule-associated protein (MAP) tau, in a hyperphosphorylated state [285]. In other forms of dementia, filamentous tau deposits are frequently observed in the absence of amyloid deposits [286]. This might be a severe problem since it will be difficult to separate AD from other forms of dementia.

A single gene located in chromosome 17 expresses all the six isoforms of tau present in the human brain [287]. Within nerve cells tau is mainly present in axons. The morphologically distinct filaments consist of all six tau isoforms or they only comprise three-repeat or four-repeat isoforms, differences depending on the disease. Generally tau isoforms with four repeats are not very common in the human brain [286].

95% of tau filaments in AD are in the form of PHFs with a diameter of 8-20 nm and a periodicity of 80 nm [288]. Stress-activated protein (SAP) kinases, mainly SAP kinase-3 and -4, are responsible for tau-phosphorylation [289]. Additionally, tau in the form of PHFs seems to be hyperphosphorylated as well as abnormally phosphorylated when compared to tau in a healthy adult brain. The result is that tau will not be able to bind microtubules [286]. Incubation of tau with sulphated glycosaminoglycans (like heparin) results in a bulk assembly of tau into AD filaments; so these glycosaminoglycans also stimulate the phosphorylation of tau by a number of protein kinases. Additionally, heparin sulphate is detected in nerve cells in the early state of neurofibrillary generation [290].

4.2.4 Diagnosis

While the patient is still alive, distinction of Alzheimer's disease from other forms of dementia (e.g. VaD and Lewy bodies) rests with clinical assessment. Only a few years ago AD was a diagnosis of inclusion based on patient history, neuropsychological testing, laboratory studies, and physical [239]. This however, has changed due to recent research and the disease can nowadays be characterized more definitively on a phenotypic basis. Several distinct markers of AD are now recognized, as well as structural changes in the brain, observable by MRI. These involve the early and extensive involvement of the medial temporal lobe (MTL), changes in the cerebrospinal fluid biomarkers and molecular neuroimaging changes seen with positron emission tomography (PET) with hypometabolism or hypoperfusion in temporoparietal areas [263].

For the purposes of research, the diagnosis of AD is based on the criteria of the Diagnostic and Statistical Manual of Mental Disorders, fourth edition (DSM-IV-TR) [291] and the National Institute of Neurological Disorders and Stroke‐Alzheimer Disease and Related Disorders (NINCDS‐ADRDA) [292] working group. These accepted criteria are utilized in a two part diagnostic process where there is first an initial identification of a dementia syndrome and then the application of criteria based on the clinical features of the AD phenotype [263]. The original NINCDS‐ADRDA criteria for AD, are shown in Table 10. These criteria have recently been revised and the latest suggested version is presented in Table 11. These revised criteria are the result of a lot of research in the area; the specifics of

AD are nowadays much better known than half a century ago. There is also a need to differentiate e.g. mild cognitive impairment from AD as well as to have some way of defining how far progressed the patient's state is. Specific clinical terms have been proposed for use by Dubois *et al.* [263]; these have been collected in Table 12 for clarification purposes.

A definite AD can still however only be diagnosed by the microscopic examination of brain tissue, either by biopsy, or more commonly, autopsy. The neuropathological criteria require the presence of neurological plaques and neurofibrillary tangles at specified densities [246]. A considerable amount of effort is going into the search for valid, reliable, and easily achieved ways to identify cases very early in the disease, when treatment would be most effective.

The onset of impairment of cognitive functions is not always associated with the diagnosis of dementia. Usually different psychogeriatric or neurological disorders like delirium, major depressive order ("pseudodementia"), psychosis (schizophrenia and paraphrenia), and age-related cognitive decline can be distinguished. Although delirium is often misdiagnosed, it is still especially common in elderly subjects, particularly in inpatient settings and nursing homes. In two thirds of the cases, dementia and delirium coexist. Cognitive decline represents the main risk factor for the development of delirium in elderly subjects. Depression in the elderly is often accompanied by complaints of memory loss, and the presence of mild cognitive deficits in neuropsychological tests. Also depression and dementia often coexist and this may be interpreted as an early sign of a dementia syndrome [239].

If a form of dementia is identified, it is necessary to determine its severity and etiology as the next step. This is because many diseases cause dementia and therefore a differential diagnosis is essential for therapy and prognosis. A popular way is to interview the patient and informant and the history should focus on the general medical condition, with attention to drug use, psychiatric illness, chronic diseases (such as cardiovascular and cerebrovascular diseases, hypertension, neurological diseases, and metabolic disorders), the presence and severity of non-cognitive symptoms, recent trauma or surgical interventions, and the onset and evolution over time of cognitive defects. The family history of dementia, depression, stroke, as well as other related conditions should be evaluated. Also, a comprehensive physical examination, including neurological examination and mental status testing, is essential in all patients [239]. The mental state screening should include an assessment of cognitive and affective status using standardized instruments such as the "Mini Mental State Examination" [293], or the "Blessed Information Concentration" [294].

Table 10. The NINCDS/ADRDA clinical criteria for Alzheimer's disease.

Criteria for the clinical diagnosis of probable Alzheimer's disease:

Presence of dementia established by clinical examination and documented by neuropsychological tests
Deficits in at least two areas of cognition
Progressive deterioration of memory and other cognitive functions
No clouding of consciousness
Onset between ages 40 to 90
Absence of systematic disorders or other brain diseases that could account for the dementia

The diagnosis is supported by:

Progressive deterioration of specific cognitive function
Impaired activities of daily living and altered pattern of behavior
Family history of dementia
Normal lumbar puncture, EEG, and evidence of cerebral cortical atrophy on CT scan with progression documented by serial observation

Features consistent with the diagnosis:

Plateaus in the course of the disease
Associated psychiatric symptoms
Neurological signs, including motor signs, such as increased muscle tone, myoclonus, or gait disorders, especially in advanced disease
Seizures in advanced disease
Normal CT scan

Diagnosis of Alzheimer unlikely if:

Sudden onset
Focal neurological signs, such as hemiparesis, sensory loss, visual field deficit, and incoordination early in the course of the disease
Seizures or gait disturbances early in the disease

Criteria for the clinical diagnosis of possible Alzheimer's disease:

In the presence of atypical onset, presentation, or clinical course
In a presence of a systematic disease sufficient to produce dementia, but not considered to be the cause of the disease
In the presence of a single progressive cognitive deficit

Criteria for diagnosis definite Alzheimer's disease:

Clinical criteria for probable AD
Histopathological evidence of the disorder

Table 11. The revised diagnostic criteria for Alzheimer's disease presented by Dubois *et al.* [263].

Probable AD: A plus one or more supportive features B, C, D, or E

Core diagnostic criteria

A. Presence of an early and significant episodic memory impairment that includes the following features:
1. Gradual and progressive change in memory function reported by patients or informants over more than 6 months
2. Objective evidence of significantly impaired episodic memory on testing: this generally consists of recall deficit that does not improve significantly or does not normalize with cueing or recognition testing and after effective encoding of information has been previously controlled
3. The episodic memory impairment can be isolated or associated with other cognitive changes at the onset of AD or as AD advances

Supportive features

B. Presence of medial temporal lobe atrophy
- Volume loss of hippocampi, entorhinal cortex, amygdala evidenced on MRI with qualitative ratings using visual scoring (referenced to well characterized population with age norms) or quantitative volumetry of regions of interest (referenced to well characterized population with age norms)

C. Abnormal cerebrospinal fluid biomarker
- Low amyloid β1–42 concentrations, increased total tau concentrations, or increased phospho-tau concentrations, or combinations of the three
- Other well validated markers to be discovered in the future

D. Specific pattern on functional neuroimaging with PET
- Reduced glucose metabolism in bilateral temporal parietal regions
- Other well validated ligands, including those that foreseeably will emerge such as Pittsburg compound B or FDDNP

E. Proven AD autosomal dominant mutation within the immediate family

Exclusion criteria

History
- Sudden onset
- Early occurrence of the following symptoms: gait disturbances, seizures, behavioral changes

Clinical features
- Focal neurological features including hemiparesis, sensory loss, visual field deficits
- Early extrapyramidal signs

Other medical disorders severe enough to account for memory and related symptoms
- Non-AD dementia
- Major depression
- Cerebrovascular disease
- Toxic and metabolic abnormalities, all of which may require specific investigations
- MRI FLAIR or T2 signal abnormalities in the medial temporal lobe that are consistent with infectious or vascular insults

Criteria for definite AD

AD is considered definite if the following are present:
- Both clinical and histopathological (brain biopsy or autopsy) evidence of the disease, as required by the NIA-Reagan criteria for the post-mortem diagnosis of AD; criteria must both be present
- Both clinical and genetic evidence (mutation on chromosome 1, 14, or 21) of AD; criteria must both be present

Table 12. A glossary of dementia terms.

Mild cognitive impairment Variably defined but includes subjective memory or cognitive symptoms or both, objective memory or cognitive impairment or both, and generally unaffected activities of daily living; affected people do not meet currently accepted dementia or AD diagnostic criteria
Amnestic mild cognitive impairment A more specified term describing a subtype of mild cognitive impairment, in which there are subjective memory symptoms and objective memory impairment; other cognitive domains and activities of daily living are generally unaffected; affected people do not meet currently accepted dementia or AD diagnostic criteria
Preclinical AD The long asymptomatic period between the first brain lesions and the first appearance of symptoms and which concerns normal individuals that later fulfill AD diagnostic criteria
Prodromal AD The symptomatic predementia phase of AD, generally included in the mild cognitive impairment category; this phase is characterized by symptoms not severe enough to meet currently accepted diagnostic criteria for AD
AD dementia The phase of AD where symptoms are sufficiently severe to meet currently accepted dementia and AD diagnostic criteria

Some studies have been conducted to identify biological markers to confirm AD diagnosis during life. As a result, lower CSF levels of APP, Aβ, and other APP fragments have been found. Altered blood plasma levels of Aβ, hyperhomocysteinemia, elevated CSF levels of tau protein, biological abnormalities in peripheral cells (mainly fibroblasts), and platelets (level of platelet Aβ precursor protein isoforms) have also been found in AD patients [295].

The exponential growth of knowledge in genetics has given rise to some new methods regarding the possibility of using "genetic testing" in the assessment of AD patients. This has raised some moral questions. A good example of genetic methods would be the ApoE genotyping, since the ApoE-ε4 allele has a positive predictive value of 94-98% in an individual with suspicion to AD, this would most likely improve the specificity of the diagnosis.

Research involving gene expression analysis of the hippocampal cornu ammonis 1 (CA1) in AD patients has shown that there are a lot of changes when compared to healthy controls. It is noteworthy to mention that there is a significant down-regulation of RNA encoding synaptic elements (these general deficits in gene expression profiles for structural molecules that define the cytoarchitecture, and thereby the signaling capabilities of the neurons), and RNA encoding metal regulatory factors. Also, a sig-

nificant (over 3 fold) increase in RNA encoding inflammatory, immune, and stress response factors (such as cyclo-oxygenase 2 (COX-2), whose up-regulation may be a specific marker of AD), as well as alterations in expression levels of other RNA encoding chromatin-modifying factors have been detected. Even some intracellular signaling pathways have been found to have deficits [296, 297].

4.3 Metabolomics applications

4.3.1 Applications in general

The key applications in NMR metabolomics include preclinical studies (toxicological and genetic models of neurodegenerative diseases), disease progression monitoring, and drug development studies [4]. There has recently been an explosive growth of research in this area driven by the potential for earlier and earlier disease detection and ultimately for reaching the goal of personalized medicine. Even though early studies have been promising, validation studies are still needed to confirm the biomarkers recognized in various studies. These validation studies commonly include several different sample sets for the same disease with even representation to variation creating factors such as gender, age, ethnicity, comorbidity with other diseases and geographical origin [10].

A majority of metabolomic studies have focused on using a single analytical method, either NMR spectroscopy or MS. Given the complexity of biological systems, it would be more useful to combine both methods and exploit them in parallel, at least in the developmental stages of the protocol in question, to derive more meaningful information on metabolic variations in health and disease. The high reproducibility of NMR and the high sensitivity of MS both provide supplementary and complementary data important for biomarker identification and validation. Combined multivariate analysis of data from both methods is likely to provide data that is more useful and important than using a single approach [10].

Toxicological models

Toxicological studies into numerous neuroactive compounds have given valuable insight into the etiology of several common neurodegenerative disorders. Neurotoxins have been administered to animals to produce many models with clinical phenotypes that are analogous to human disorders. There are some toxins that share the ability to selectively wipe out specific neuroanatomical regions that are primarily associated with specific diseases [4].

PD is one disease that has been extensively studied through toxicological models involving e.g. environmental toxins [298-301], and it would appear that PD is a heterogeneous disease likely to be caused by more than one specific etiological factor. This is further supported by the details such as the clinical and pathological syndromes associated with environmental agents that are remarkable similar when compared to those observed with familial PD cases [4]. Relatively little research has been carried out on the metabolic profiling of toxin-induced PD models given the wealth of information from imaging studies performed [302-304], however, the perturbations of brain metabolites have been analyzed in a primate model of PD [305].

HD is another disease that has been studied through toxicological models and is primarily associated with progressive atrophy and the selective neuronal loss of the medium spiny neurons of the striatum. The postmortem neuropathological analysis of HD brain also demonstrates a reduction of ca. 300-400 g in total brain mass when compared with normal controls. An NMR spectroscopic study was useful in the study of toxin-induced decreases in several metabolites associated with HD [306]. Subsequent studies have been performed to assess the possible therapeutic strategies in toxin models of HD, including drugs to correct brain energy deficits [234], striatal allografts [307], and neurotrophic factors [308].

The potential neurotoxic effects of xenobiotics on animals have also been explored by NMR spectroscopy, even though it was found to be debatable, whether the use of neurotoxic compounds can be regarded as truly neurodegenerative. And furthermore, animal models are limited by their capacity to imitate only certain characteristics of a neurodegenerative condition; they can only simulate specific aspects of pathogenic, histological, biochemical, or behavioral features. Animal models may however be of use in improving the understanding of neurodegenerative mechanisms [4].

Genetic models

These models are transgenic animal models of several neurodiseases that have been created to simulate a neuropathologically and clinically similar environment to the clinical disorder in question. One example is a transgenic (TG) mouse model overexpressing human α−synuclein which is a major component in the formation of Lewy bodies observed in PD. These mice showed α−synuclein positive cytoplasmic inclusions, but also revealed motor impairments and a loss of nigrostriatal dopaminergic terminals in the striatum [309]. Other examples include a TG rat model overexpressing human mutant G93A-SOD1 (these rats develop a motor neuron disease similar to human ALS), and a TG model containing a doubly mutated form of the human α−synuclein gene, which has been shown to exhibit age-related reductions in dopamine concentrations and impairments in motor co-ordination [310]. Further TG models exist for e.g. HD [310, 311] and Machado-Joseph disease [312] and in both cases NMR spectroscopy based data has provided either a good class differentiation between diseased and healthy [313], or important metabolite concentrations relevant to the disease studied [312, 314].

Disease progression monitoring

Current research is frantically searching for biomarkers that are hoped to provide more insight into neuronal dysfunction, disease progression and response to treatment. To be truly useful, a biomarker must be quantifiable, reproducible, and analytically simple to measure. Additionally, it is preferred that biomarkers are unaffected by comorbid factors. Biomarkers that can help the detection of neurodegenerative diseases in an early or even presymptomatic stage are essential. There is a scarcity of suitable biomarkers for assessing disease progression especially in this group of disorders. At this time, the

ongoing development of many potential disease modifying therapies, for which biomarkers are urgently needed, will soon lead to an evaluation in clinical trials. For the study of possibly useful therapies the biomarker needs to change with disease progression, also closely correlating with the established clinicopathological parameters of disease [315]. There may be situations in which a single metabolite or protein will fulfill this requirement, but unfortunately, most diseases are polygenic in origin and often have strong environmental influences attached. It is therefore likely that a complex fingerprint of molecular markers is associated with the disease state, and that the efficacy or toxicity of administered drug will evolve through time. Thus, in reality, combinations of biomarkers are far more likely to form the basis of a reliable diagnostic test. The capability of metabolomics to generate a metabolic fingerprint is uniquely suited for the recognition of such combinations of biomarkers. Therefore, as a method, it can be placed next to the more traditional clinical protocols encompassing specific cognitive and neurophysiological testing supplemented with genomic and proteomic profiling. Many different approaches are currently being undertaken to recognize biomarkers; these include imaging, neurophysiological and cognitive testing, in addition to newer technologies such as biochemical, proteomic, metabolomic, and gene array profiling of tissue and biofluids from patients. The metabolomic analysis of biofluids is also relatively noninvasive and is a rapid profiling tool. Therefore it is highly suitable for monitoring disease progression that requires a multisampling practice [4].

Because AD is the most common form of dementia and is also difficult to diagnose in the very early stages, the early detection is an urgent challenge, likely demanding a combination of different strategies and methods. The methods based solely on clinical features and exclusions of other possible causes are not sufficient for early diagnoses. The common CSF β-amyloid$_{42}$ and tau- and phospho-tau proteins reflect AD-associated brain pathology but do not fulfill the criteria for the ideal biomarker [316]. Additionally, at this moment, an approved small molecule metabolomic approach for AD and several other neurological states is not available. One likely reason to this is the large variation of the personal CSF metabolic profiles [26] which hide the possible metabolic characteristics. In recent years more attention has been focused in the clinical manifestation of mild cognitive impairment (MCI), which may represent an early form of AD in some patients [317]. Currently, no clinical method exists for the determination of whether a patient with MCI has incipient AD or has a benign form of MCI without progression [318]. Thus there is a great need for diagnostic biomarkers to identify incipient AD in MCI cases so that early symptomatic or disease-modifying treatments may be given early in the course of disease. Several studies based on NMR spectroscopic methods to better understand the progression and nature of AD have been reported [235, 236, 319, 320].

PD is another disease that can be very difficult to diagnose in its early stages, partly due to the fact that it may be mimicked by other diseases such as essential tremor, progressive supranuclear palsy, and

multiple system atrophy. Furthermore, when the patient reaches a point when there is evidence of the clinical features of PD, there is already a ~50% reduction in dopaminergic nigral cells [321]. It also appears that the preclinical phase of PD lasts for ca. 5 years [322]. It is therefore clear that the treatment in the preclinical phase would be essential in halting the progressing disease. The role of NMR metabolomics in the case of PD is essentially the same as in other similar diseases; measuring the relative concentrations of relevant metabolites in biofluids or brain areas.

There is a clear genetic test for HD, but the clinical trials remain challenging and only a few double-blind phase III trials have been conducted. Because the current method of assessment of clinical disease progression (the Unified Huntington's Disease Rating Scale) lacks sensitivity and specificity particularly over short periods of time, the identification of biomarkers that could also be used to track disease progression would be invaluable. In addition, markers capable of detecting disease related changes in presymptomatic HD gene carriers are likely to be essential for future detection and monitoring of treatments that can delay disease onset. Several NMR spectroscopic studies have been reported in the research field of HD [223, 234, 307, 308, 314, 323-328].

MS is characterized by the degeneration of the myelin sheath that leads to neuronal damage and loss which ultimately results in the irreversibility of the debilitating disorder. NMR spectroscopy has revealed alterations in the levels that are specific for axonal damage, demyelination, and inflammation and have been monitored during the remitting-relapsing phases typical for this disease [219, 329, 330]. Additionally, numerous *in vivo* ^{1}H MRS studies in patients with MS have also been conducted [232, 331-334].

In addition to the diseases mentioned above, metabolomics has also been used to study several other common disorders, the most prominent ones being cancer (e.g. [164, 335-344]), diabetes [345-347], and coronary heart disease [3, 45, 348-351]. Inborn errors of metabolism have also been studied and so and it has become increasingly clear that especially NMR metabolomics has become a certified method of choice in many areas of study [10].

Drug development

NMR spectroscopy has a long history in the investigation of drug metabolism [134, 352]. Both biofluid and ^{1}H MAS NMR analyses have been used to characterize toxicity profiles of several toxins and drug candidates and to generate knowledge on important metabolic pathways. NMR spectroscopy is therefore also useful as a tool in drug development. Moreover, recent studies have shown that the predose metabolic profile can in some instances be used to predict the dominant metabolism of pharmaceutical compounds [4].

4.3.2 Neurological state visualizing protocol based on NMR metabolomics

(This chapter is loosely based on Jukarainen, N. M., Korhonen, S. P., Laakso, M. P., Korolainen, M. A., Tuppurainen, K., Pirttila, T., Laatikainen, R. Classification of Dementia Disorders Based on Cerebrospinal Fluid Metabolite Profiling: a Multivariate ^{1}H NMR Study. Manuscript, **2009**.)

Background

At this moment, an approved small molecule metabolomic approach for AD and other neurological states is not available. NMR methods have been used to some extent for the analysis of metabolites in CSF [4]. The most commonly used methods have however been based on MRI [319, 353] or *in vivo* methods [320]. However, as a solution state method, NMR is better suited for the analysis because it generates multivariate information on a wide range of molecules with sufficient sensitivity [4] and thus allows the harvesting of a combination of numerous metabolite concentrations with just a single scan. In NMR metabolomics, experiments can also be performed without complex sample treatment and instrumental calibration. Furthermore, the low protein and lipid content of CSF is advantageous because the spectrum is relatively simple due to the rather low number (ca. 50) of components [354].

In our recent work, we used 1D ^{1}H NMR spectroscopy for the metabolic profiling of CSF and developed a CTLS approach for NMR quantification of CSF metabolites [26]. At this time, it was also discovered that the variations of metabolite concentrations in the personal CSF profiles of two control groups with no dementia, were very large. The purpose of this study was to examine if it is possible to classify neurological patients on the basis of their CSF metabolic profiles in spite of these large personal variations. We therefore assessed the performance of the CTLS protocol, together with other commonly used spectral integration methods and, secondly, tested several common mathematical tools to find optimal classification approaches for patients with various types of dementia. The multivariate classification methods assessed were kNN, kNN-SA, PCA, PLS-DA, SVM, DT, and RF. The resulting metabolite profiles and disease specific points are discussed.

Methods

CSF samples of patients with dementia and neurological controls

The control group of 45 patients consisted of individuals examined for various neuropsychiatric symptoms, such as depression or headache, but who did not have cognitive decline or a chronic neurological disease. These controls were further divided into two groups: patients with an AD marker profile (low β-amyloid$_{42}$ and/or high tau protein) present in CSF (control class abbreviation: C/ADP) and patients

that do not have an AD marker profile in CSF (control class abbreviation: C). The C/ADP group consisted of 11 patients and the C group consisted of 34 patients. No other confounding neurological disease states were associated with these patients. Other patient groups included in this study were 76 patients with probable AD, 59 patients with mild cognitive impairment (MCI), including 22 patients with an early stage AD (EAD), 16 patients with vascular dementia (VaD), 9 patients with Lewy body disease (LBD), and 16 patients with frontotemporal dementia (FTD). For additional details on patient age, sex and other relevant demographics, see Table 13.

Table 13. Demographics of study participants displaying group sizes, sex, means, and standard deviations (SD) for patient age and Mini-Mental State Examination (MMSE) score.

		Sex		Age		MMSE	
Group	N	Female	Male	Mean	SD	Mean	SD
AD[a, d]	76	52	24	72	± 7.7	19	4.4
C/ADP[b]	11	8	3	67	± 8.2	26	2.6
C[b]	34	19	15	66	± 9.5	25	3.2
FTD[c]	16	9	7	54	± 11.1	23	4.8
LBD[d]	9	4	5	76	± 6.0	18	5.7
EAD	22	13	9	71	± 6.8	24	2.8
MCI	37	20	17	71	± 6.8	24	2.4
VAD[d]	16	5	11	77	± 4.6	19	4.0

[a]The AD patient class contained more women than expected (significance, $P<0.05$) and, conversely, the VAD patient class contained more men than expected (asymptomatic significance, $P<0.05$), as assessed with the χ^2–test.
[b]The control patients are significantly ($P<0.01$) younger than other patient groups (excluding FTD), as assessed with ANOVA.
[c]The FTD patients are significantly ($P<0.001$) younger than all other patients, as assessed with ANOVA.
[d]The AD, VAD, and LBD patients have significantly ($P<0.05$ for LBD and $P<0.001$ for AD and VAD) lower MMSE scores than other patient groups, as assessed with ANOVA.

This study was approved by the local ethics committee of Kuopio University Hospital, and informed consent for participation in the study was obtained from all participants and caregivers of the demented patients. The diagnosis of probable AD was made according to the consensus criteria of the National Institute of Neurological and Communicative Disorders and Stroke-Alzheimer's Disease and Related Disorders Association (NINCDS-ADRDA) [292]. The individuals with MCI were diagnosed based on

criteria presented by Mayo Clinic Alzheimer's Disease Research Center [355]. The early AD group (henceforth referred to as the EAD group) consisted of individuals with MCI who developed AD during the follow-up examination which lasted up to 168 months. Those individuals with MCI for whom the diagnosis remained as MCI, are hereafter referred to as MCI.

VaD refers to patients in whom the cause of dementia symptoms was associated with a cerebrovascular disorder. VaD was diagnosed according to National Institute of Neurological Disorders and Stroke and Association Internationale pour la Recherché et l'Enseignement en Neurosciences (NINDS-AIREN) criteria [356]. FTD was diagnosed by using the Lund-Manchester diagnostic criteria [357], and LBD was diagnosed according to the consensus criteria for LBD [358].

Statistical analysis

To provide an overview of differences between the neurological classes, an ANOVA analysis with two-tailed significance was performed by using patient age and Mini-Mental State Examination (MMSE) score as variables. Additionally, a χ^2–test with two-tailed significance was performed on patient sex. See Table 13 for details.

Sample preparation

Lumbar CSF samples were obtained by using a standardized protocol and the samples were stored at -70°C until use. The samples were prepared according to the protocol described by Maillet [1]. First, 1800 µl of each sample was subjected to an identical lyophilization protocol for 40 hours. The freeze-dried samples were then stored at -20° C in sealed vials until analysis. Prior to the NMR measurements, the samples were reconstituted in 600 µl of D_2O (99.98%-D, Merck) and 450 µl of this liquid was transferred to a separate vial followed by addition of 50 µl of 21.5 mM 3-(trimethylsilyl)-propionic-d4 acid in D_2O to be used as an internal standard of known concentration. The pH of the samples was not adjusted, being typically around 7.00±0.05. This pH can be defined as pH*, which is the reading of the pH meter as measured with a standard pH electrode. The pD value is ca. 0.4 units higher than pH*.

NMR Spectroscopy

The classification was based on standard 1D ^{1}H NMR spectra. All spectra were measured by using a Bruker AVANCE DRX 500 instrument operating at 500 MHz (i.e. 11.4 Tesla) (Bruker-Biospin GmbH, Karlsruhe, Germany), equipped with a quadronuclear probe. The Bruker XWIN-NMR software version 3.5pl8 running on a standard PC was used for acquisition of all spectra. The relevant parameters used in the 1D experiments, were calibrated and used as follows: recycling delay 45 s, acqui-

sition time 6.5 s, number of scans 128, and a sweep width of 9.5 ppm. A calibrated 90° pulse was used for all spectra and all acquisitions were performed on non-spinning samples.

Quantification

Quantification for the different models used for classification purposes was performed by using the same 31 metabolites and/or signal areas as previously reported as the CTLS protocol [26]. As an extension, a combined model with metabolite areas and buckets was created. In this model the non-assigned lines were combined into buckets to form additional variables to reduce the chemical shift variation effects. This model is hereafter referred to as CTLSB. All spectral model creation and quantification was performed by using PERCH NMR Software version 2008.1 (PERCH Solutions Ltd., Kuopio, Finland).

Validation

To remove the influence of the large differences in the metabolite concentrations levels, we used mean centering of the data (mean = 0) together with variance scaling, in which the variance of each sample value was scaled to have a maximum of 1. In conjunction with the scaling procedure, a variance analysis was performed and metabolites with variance of less than 20% of the total variance were omitted resulting in total of 27 metabolites (including several buckets) which were used in further analyses. All of the classification methods used in this study employed either standard LOO CV or a more rigorous method known as out-of-bag (OOB) CV in which several data points are removed in the model building phase.

Random Forest

Random Forests (RF) is an ensemble learning method which combines two machine learning techniques, *viz.* bagging and random feature subset selection using a large collection of DTs for predictions [189]. The accuracy of RF compares favorably with modern machine learning methods e.g. SVMs and neural networks. In contrast with many multivariate classifiers, RF is very resistant to overfitting. Distinctively, RF includes a built-in CV scheme with extensive OOB data (one third of samples for each tree). The procedure also gives an estimate of the prediction error as a by-product so that there is no actual need for the use of "external" validation sets.

While RF is originally a classifier, it can be used for distance metric learning [190]. RF is a good choice as a classifier for many reasons; it has excellent accuracy among current algorithms, it runs efficiently on large data sets, it can handle thousands of input variables without variable deletion and it gives estimates of what variables are important in the classification. Furthermore, RF generates an internal unbiased estimate of the generalization error (OOB) as the forest building progresses and it is

also very resistant to overfitting. Multidimensional scaling (MDS) performed on RF data produces a map that puts similar cases near to each other, and different cases far apart.

All calculations were done with the R package *randomForest*, which is freely available on the Internet at http://cran.cnr.berkeley.edu/src/contrib/Descriptions/randomForest.html.

Results and discussion

Group Demographics

The control patients were significantly younger than the patient groups (see Table 13), save for frontotemporal dementia (FTD) ($F = 6.789$, $P < 0.05$). The FTD patients were significantly ($F = 61.749$, $P < 0.001$) younger than all the other patients, as assessed with ANOVA. This is expected because it is typical for FTD to have an early onset.

The groups were comparable for sex, except for AD and vascular dementia (VaD). The AD group contained significantly more women than men ($\chi^2 = 4.632$, $P < 0.05$) and, conversely, the VaD patient class contained significantly more men than women ($\chi^2 = 5.299$, $P < 0.05$).

The AD and VaD patients had significantly ($F = 57.319$ (AD), $F = 7.875$ (VaD), $P < 0.001$ in both cases) lower Mini-Mental State Examination (MMSE) scores compared with the other groups.

Dementia RF maps

Classification problems with many weak and overlapping inputs are becoming more common in e.g. medical diagnostics - the present task provides a challenging example of these. Initially, a large number of different classification techniques (kNN, PLS, LVQ …etc.) were tested, but their performance proved limited (data not shown). Interestingly, DT qualified best, prompting us to test its advanced version, known as Random Forest (a.k.a. Decision Forest). When performing the neurological classification, the inclusion of demographic variables such as sex, age and MMSE score improved the discrimination of the neurological groups.

Previously, it has been shown that RF has the ability to work even with very weak classifiers, in particular if their correlation is low [189]. Although this condition was not completely fulfilled for this data set, it appeared that RF was superior to other methods, including DT. However, it was still not sensitive enough for a complete classification with eight classes. The OOB estimate of error rate was considerably large (44%), and most small classes including other dementias (LBD, VAD, FTD) were predicted incorrectly. The cluster near the origin mainly consisted of these other dementias, together with a few samples from all classes, probable AD being the most abundant. This cluster obviously caused most of the prediction errors, and contained altogether about 70 samples.

A more reasonable model could be derived with three classes: controls (C, C/ADP, MCI), ADs (EAD and AD), and other dementias (VAD, LBD, and FTD). In this case it can be considered as an analysis between controls, AD-type patients, and other forms of dementia. The OOB estimate of error rate is reasonable (28%), and the structure of the RF/MDS map is compact (Figure 19). Note, however, that there is still a considerable overlap between ADs and other dementias, and ODs will be predicted largely as AD. The corresponding confusion matrix is given in Table 14. The correctly classified patients are on the diagonal and the other patients and their amount in each case can be seen under the class they were classified to.

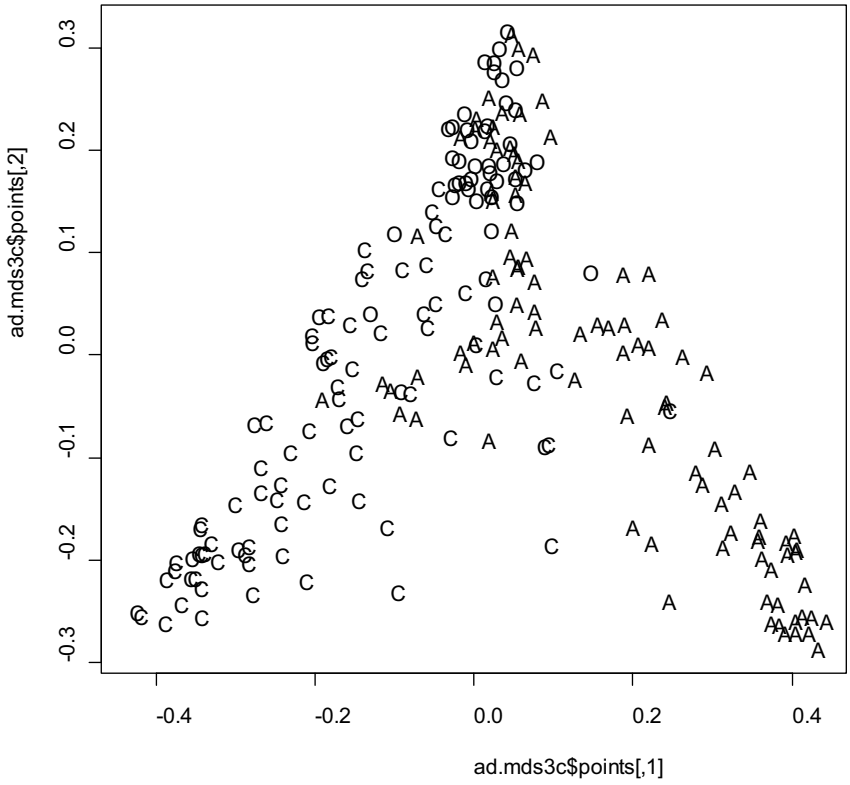

Figure 19. RF classification with three classes (C, A, and O). Abbreviations as follows: C=control (C/ADP, C, MCI), A=AD (EAD, AD), O=other dementia (VAD, FTD, LBD).

Table 14. The confusion matrix for the RF classification with 3 neurological classes. O=other dementia. The correctly classified patients are on the diagonal and the other patients and their amount in each case can be seen under the class they were classified to by the RF method.

	AD	C	O	Classification error
AD	79	13	6	0.194
C	14	66	2	0.195
O	16	10	15	0.634

An alternative model included four classes: controls (C and C/ADP), M (MCI, including EAD), A (probable ADs) and other dementias (O) (Figure 20). The OOB error is slightly larger (30%) than with the three-class model, and the confusion statistics are shown in Table 15. Interestingly, the MDS map for this model (Figure 20) is symmetric about the origin, and thus its interpretation is easy: the predictions for the samples near the origin cannot be regarded as reliable, while the samples far from the origin represent "sure" cases.

Table 15. The confusion matrix for the RF classification with 4 neurological classes. O=other dementia. The correctly classified patients are on the diagonal and the other patients and their amount in each case can be seen under the class they were classified to by the RF method.

	AD	C	M	O	Classification error
AD	64	0	6	6	0.159
C	4	31	7	3	0.311
M	12	4	41	2	0.305
O	18	1	4	18	0.561

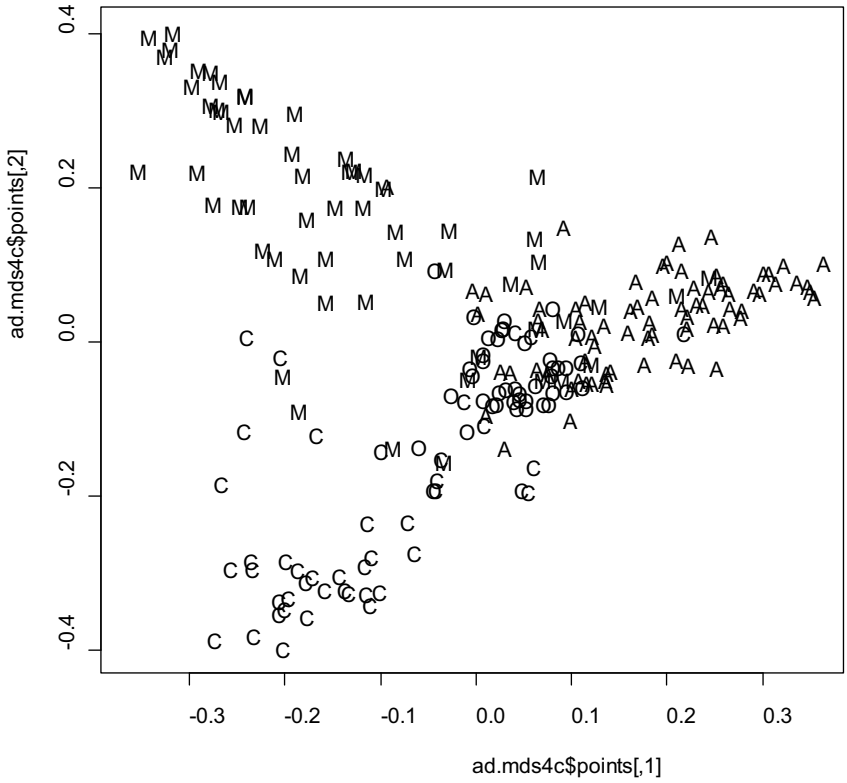

Figure 20. Classification with four classes (C, M, A, and O). Abbreviations as follows: C=control (C/ADP, C), A=probable AD, M=MCI, including EAD, O=other dementia (VAD, FTD, LBD).

A practically useful model can be derived by separating the cluster containing ODs (the O cluster in the 4 class model, Figure 20) from the rest of the samples to its own category already in the teaching phase. The OOB error is 23% and the overall confusion statistics are reasonable (Table 16). Moreover, the form of the corresponding RF/MDS map (Figure 21) is highly symmetric, although the O cluster (patients with diagnosis X, fourth "arm", right center) not fully manifested. By this way it is possible to distinguish the other forms of dementia from AD almost completely: if a patient belongs in the cluster X, he/she is almost surely demented and the right diagnosis is likely LBD, VAD or FTD, rather than AD. Admittedly, the model is conceptually somewhat questionable.

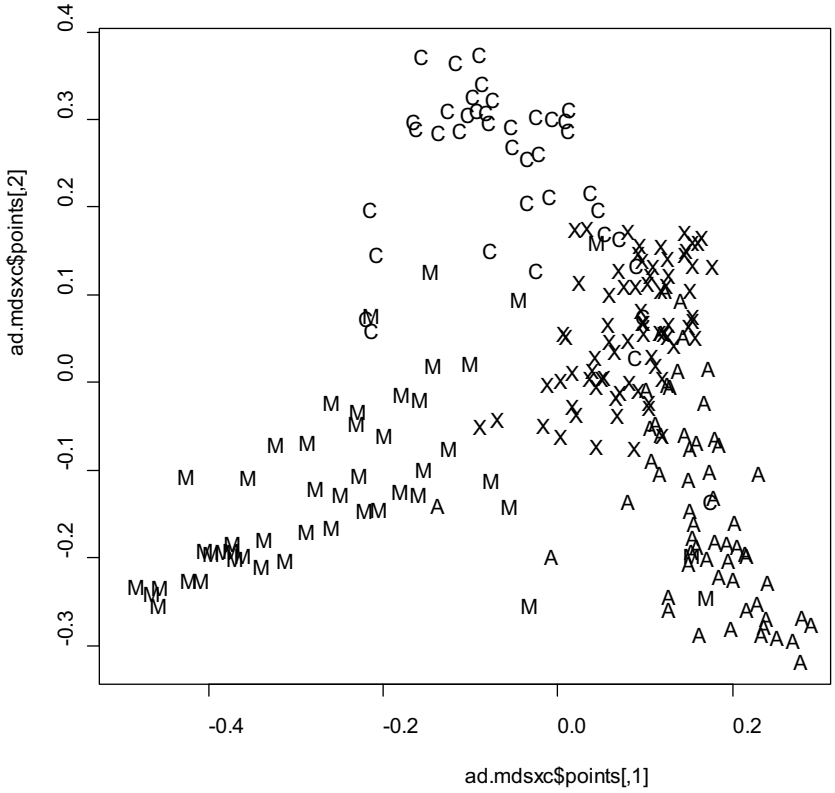

Figure 21. Classification with the X cluster as its own class in the training phase. Abbreviations as follows: A=AD, C=control, M=EAD or MCI, X=VAD, FTD or LBD.

Table 16. The confusion matrix for the RF classification with class X as a separate class in the training phase. A=AD, C=control, M=EAD or MCI, X=VAD, FTD or LBD. The correctly classified patients are on the diagonal and the other patients and their amount in each case can be seen under the class they were classified to by the RF method.

	A	C	M	X	Classification error
A	43	0	2	13	0.259
C	2	29	3	6	0.275
M	4	3	35	6	0.271
X	8	0	4	63	0.160

A very simple predictive model can be constructed with only two classes, i.e. dividing samples to non-demented subjects (C, C/ADP, MCI, and EAD) and demented (AD, VAD, FTD and LBD). Now the OOB error is only about 18%; the confusion statistics are given below (Table 17 EAD group in the non-demented class and Table 18 EAD group in the demented class) from which the sensitivity and specificity have also been calculated (see below). Interestingly, the members of the class EAD are responsible for the most prediction errors - be they in the non-demented or demented group, about half of them will be misclassified. In general, it should be emphasized that the controls in this particular data set are not really healthy persons, but have neurological symptoms, even though no neurodegenerative disease was diagnosed. Thus the border between the classes is necessarily more diffuse than usual, which is reflected both to sensitivity (79%) and specificity (88%). If the EAD patients are placed to the class demented, sensitivity is 80% and specificity is 83% respectively. Overall, the predictive ability of the two-class model is encouraging, suggesting that it may be of help even in practical diagnostics. An additional two-class model was also tried out in which EAD and AD patients (group A) were compared to all other patients (group O). This model should show if it is possible to separate AD and EAD in particular from patients that have no AD symptoms at all. This model resulted in an OOB error of only 18.5% and 87% of the group O patients were classified correctly (75% group A). The sensitivity and specificity in this model were 75% and 87%, respectively, so this is another clinically interesting two-class model. The RF/MDS map for this model is shown in Figure 22 with all 8 patient classes shown.

Table 17. The confusion matrix for the RF classification with 2 neurological classes and with the EAD patients in the control group. C=control, D=dementia. The correctly classified patients are on the diagonal and the other patients and their amount in each case can be seen under the class they were classified to by the RF method.

	C	D	Classification error
C	81	23	0.221
D	10	107	0.085

Table 18. The confusion matrix for the RF classification with 2 neurological classes and with the EAD patients in the dementia group. C=control, D=dementia. The correctly classified patients are on the diagonal and the other patients and their amount in each case can be seen under the class they were classified to by the RF method.

	C	D	Classification error
C	52	30	0.366
D	8	131	0.058

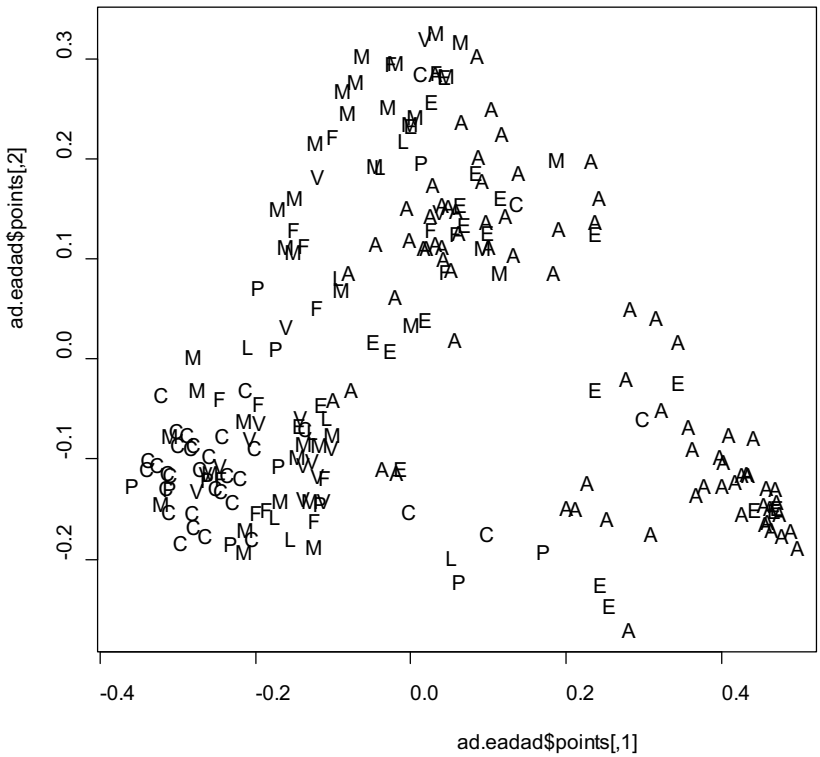

Figure 22. The RF/MDS map of the two-class model in which EAD and AD patients were combined as one group and compared against the other patients. Patient abbreviation codes are shown as 8 classes for clarification even though there were only 2 classes in the classification step. Abbreviations: C=C/NRM, P=C/ADP, F=FTD, L=LBD, V=VAD, E=EAD, A=AD, M=MCI.

Finally, it should be emphasized that RF provides a means for "profiling" of an individual patient, simply by counting the votes in each class. This is exemplified in Figures 23-27; the profile of an individual patient can be compared to the average profile in each class. Thus the analysis gives the whole profile of CSF changes in an individual patient and makes it possible to judge the most probable cause for the symptoms.

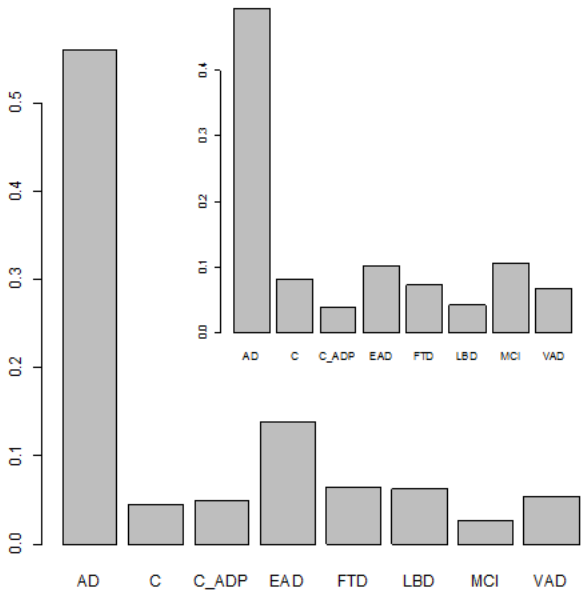

Figure 23. A typical "voting" profile for AD patients (main) and class average for AD patients (inset).

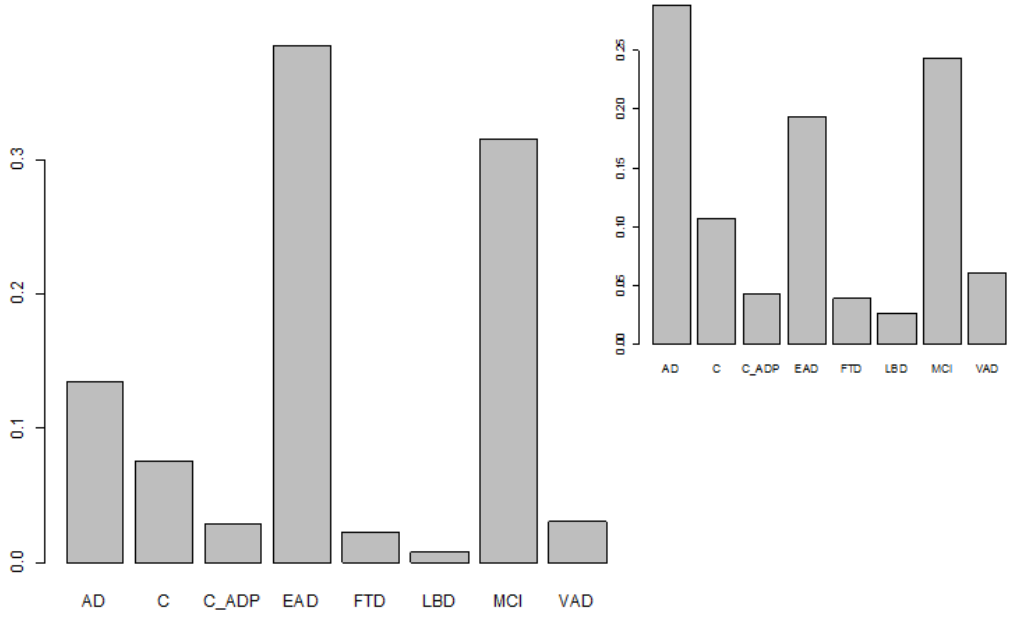

Figure 24. A typical "voting" profile for EAD patients (main) and class average for EAD patients (inset).

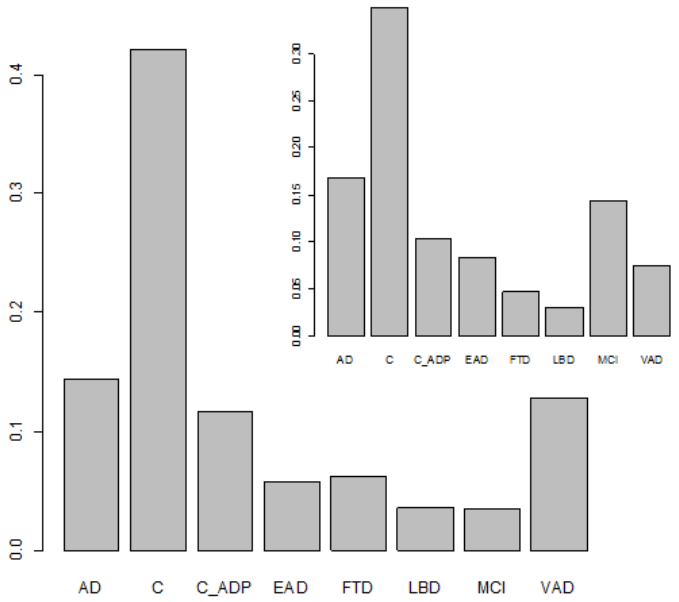

Figure 25. A typical "voting" profile for control patients (main) and class average for control patients (inset).

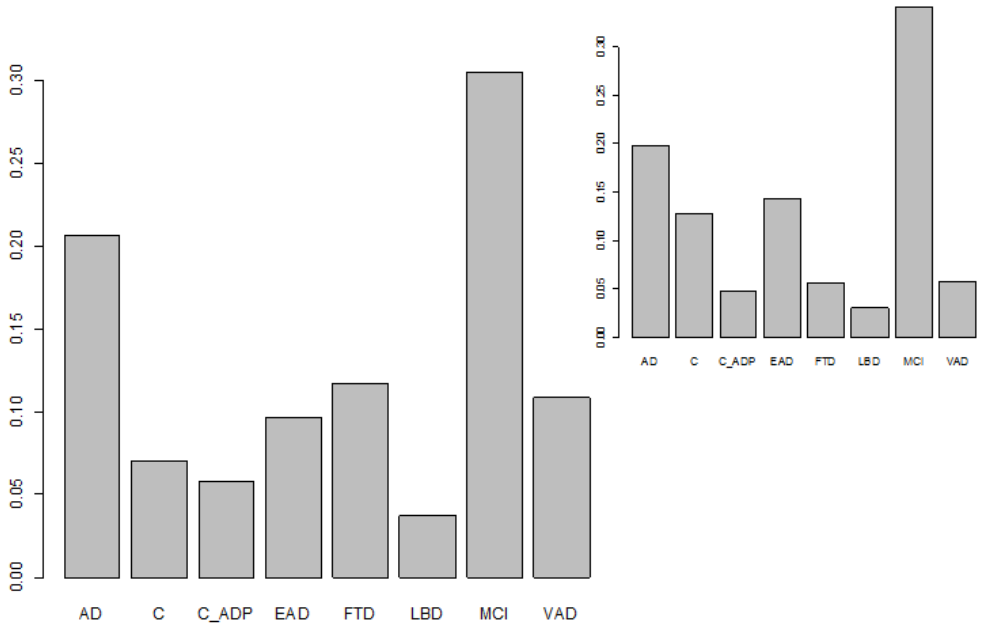

Figure 26. A typical "voting" profile for MCI patients (main) and class average for MCI patients (inset).

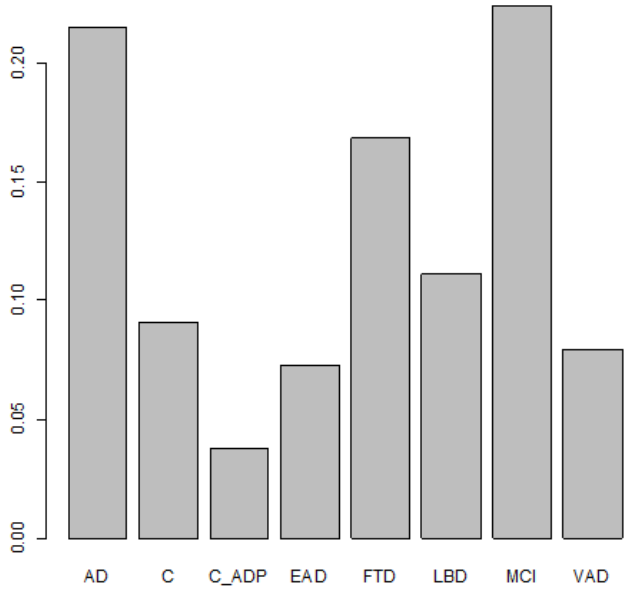

Figure 27. A typical “voting” profile for an unreliable patient.

Another useful property of RF is the variable importance plot, which reveals the most important variables employing two different performance indices with slightly different results (Figure 28). In this case, these variables are the metabolites responsible for the differences in the neurological state making classification possible. The shown metabolites in Figure 28 represent the results for the 4 class model (Figure 20 and Table 15) which is likely the one with the most clinical significance. The most important metabolites contributing to the variability were glucose, acetate, citrate, glutamine and three unknown metabolites.

The variable importance measure of RF is based on the following heuristic: when a descriptor that contributes to the prediction accuracy is "noised up" (e.g. replaced with random noise or permutation), the accuracy should degrade considerably. On the other hand, if a descriptor is irrelevant, noising it up should have little effect on the performance. A number of specific variable importance measures based on this heuristic have been proposed by Breiman [184, 189], Mean Decrease Accuracy (MDA) and Mean Decrease Gini (MDG) being the most popular. The MDA is constructed by permuting the values of each variable of the test set, recording the prediction and comparing it with the unpermuted test set prediction of the variable (normalized by the standard error). The MDG measures the quality of a split for every variable (node) of a tree by means of the Gini Index [359]. Every time a split of a node is made on a variable the Gini impurity criterion for the two descendent nodes is less than the parent

node. Adding up the gini decreases for each individual variable over all trees in the forest gives a fast variable importance that is often very consistent with the permutation importance measure.

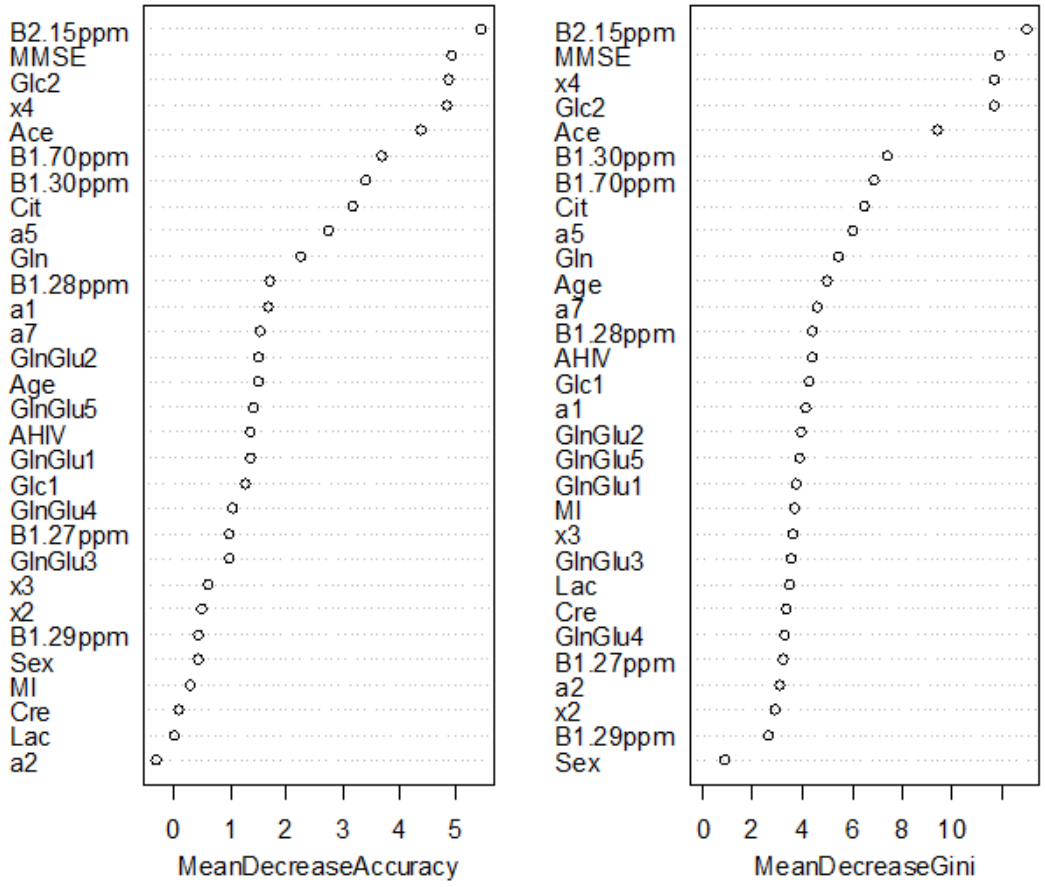

Figure 28. Variable importance plots with two different indices. The topmost variables are the ones that have the largest contribution in the RF model. Abbreviations as follows x2=unknown aromatic signal at ca. 8.13 ppm, Lac=lactate, MI=myo-inositol, a1=several overlapping amino acid α–protons between 4.05 and 3.95 ppm, Glc=glucose, a2=metabolites in the 3.70-3.56 ppm range, not including myo-inositol, x3=a triplet + underlying signals at 3.16 ppm, Cre=creatine, Cit=citrate, Gln=glutamine, x4=unknown signal at 2.13 ppm, Ace=acetate, a5=the spectral region 1.56-1.40 ppm, AHIV=α–hydroxyisovalerate, a7=the spectral region 1.02-0.93 ppm, GlnGlu=glutamine/glutamate, Bx.yzppm=bucket at x.yz ppm.

ANOVA results

1. The CMA-model

   In this model, the control patients were compared to both AD and M (MCI+EAD) patients. Several statistically significant metabolite concentration variations were detected, most of them were between the control patients and AD patients or between M (MCI+EAD) and AD patients, i.e. only one significant variable (age) was found between the control and M groups (Table 19). Patients

belonging to the M group were significantly older than control patients. The average metabolite concentrations, including standard deviations, for the groups discussed here are shown in Table 20. For details on the role of the statistically significant metabolites in neurodegenerative disorders see Table 23.

In the case of control patients vs. AD patients, the following metabolite concentration differences were statistically significant: histidine, formate, lactate, glucose, area2, creatine, glutamate, area5, area6, BHB, x5, x6, and area7. Differences in patient age and the MMSE score were also significant.

The statistically significant concentration between AD patients and M group patients were histidine, formate, area1, glucose, area2, creatinine, creatine, citrate, glutamate, acetate, area5, area6, x5, area7, and pyruvate. The MMSE score of these patients was also significant, whereas patient age was not.

2. Other dementias

In the other dementia model FTD, LBD, and VAD patients were compared to control patients. Several statistically significant metabolite concentration variations were detected. Additionally, the patient's age in all comparisons was significant, and, furthermore, the MMSE score was significant for LBD and VAD patients (Table 21). The average metabolite concentrations, including standard deviations, for the groups discussed here are shown in Table 22. The metabolites that had statistically significant concentration differences have been assessed in more detail in Table 23.

When comparing controls with FTD patients, the following metabolite concentration differences were statistically significant: formate, lactate, glucose, area2, creatine, citrate, glutamate, acetate, area5, BHB, x6, AHB, AHIV, and area7.

In the case of control patients vs. LBD patients the concentrations of histidine, glucose, glutamine, glutamate, acetate, area5, BHB, x5, x6, AHIV, area7, and pyruvate were statistically significant.

When VAD patients were compared with control patients the relevant metabolites were formate, x2, lactate, area1, glucose, area2, creatinine, creatine, citrate, glutamine, glutamate, acetate, area5, BHB, x5, x6, x7, AHB, and area7.

Table 19. The level of statistical significance of the metabolite concentrations between control, MCI and AD patients (the CMA-model, Figure 20). The significances are presented as is (ANOVA). The group column designates the groups between which the significance exists, e.g. C/A means that there is a significant variance between the C and A group patients in the level of the metabolite in question. Abbreviations: C=control (C/NRM+C/ADP), M=MCI (MCI+EAD), A=AD. Area and unknown metabolites (X) as in Table 4 footnote.

Statistical significance (ANOVA)			
Metabolite	F	Sig.	Groups
Age	7.56	0.00	C/A + C/M
MMSE	57.20	0.00	C/A + A/M
Tyrosine	2.34	0.10	
Histidine	8.59	0.00	C/A + A/M
Phenylalanine	1.30	0.28	
Tryptophan	2.68	0.07	
Formate	8.83	0.00	C/A + A/M
X1	0.40	0.67	
X2	2.12	0.12	
Lactate	5.25	0.01	C/A
Myo-inositol	1.97	0.14	
AREA1	6.79	0.00	A/M
Glucose	5.72	0.00	C/A + A/M
AREA2	9.93	0.00	C/A + A/M
AREA3	2.96	0.05	
X3	0.07	0.92	
Creatinine	3.75	0.02	A/M
Creatine	10.65	0.00	C/A + A/M
Citrate	4.09	0.02	A/M
Glutamine	0.39	0.68	
Glutamate	4.60	0.01	C/A + A/M
X4	1.49	0.23	
Acetate	5.25	0.01	A/M
AREA5	14.86	0.00	C/A + A/M
AREA6	6.02	0.00	C/A + A/M
β–hydroxybutyrate	4.19	0.02	C/A
X5	9.57	0.00	C/A + A/M
X6	3.92	0.02	C/A
X7	0.23	0.79	
α–hydroxybutyrate	2.64	0.08	
α–hydroxyisovalerate	0.71	0.49	
AREA7	5.53	0.01	C/A + A/M
Pyruvate	8.02	0.00	A/M

Table 20. Average metabolite concentrations relative to TSP (TSP=100) and standard deviations in the CMA-model. Abbreviations: C=control (C/NRM+C/ADP), M=MCI (MCI+EAD), A=AD. Area and unknown metabolites (X) as in Table 4 footnote.

Metabolite	Average Concentration (±StDev)		
	C	M	A
Tyrosine	0.9 ± 0.4	0.7 ± 0.2	0.9 ± 0.7
Histidine	0.2 ± 0.1	0.1 ± 0.1	0.2 ± 0.1
Phenylalanine	1.3 ± 0.5	1.2 ± 0.5	1.3 ± 0.7
Tryptophan	0.6 ± 0.2	0.5 ± 0.1	0.6 ± 0.3
Formate	0.4 ± 0.2	0.3 ± 0.1	0.4 ± 0.2
X1	0.1 ± 0.0	0.1 ± 0.0	0.1 ± 0.0
X2	0.1 ± 0.0	0.1 ± 0.0	0.1 ± 0.0
Lactate	26.1 ± 5.2	27.3 ± 7.2	29.8 ± 6.5
Myo-inositol	10.9 ± 7.4	9.3 ± 3.2	10.5 ± 2.8
AREA1	11.3 ± 2.7	10.7 ± 2.5	12.4 ± 2.8
Glucose	348.0 ± 67.9	349.0 ± 92.4	392.8 ± 91.9
AREA2	10.8 ± 3.3	10.0 ± 3.5	12.9 ± 4.4
AREA3	3.2 ± 1.2	3.0 ± 1.2	3.7 ± 2.0
X3	0.6 ± 0.5	0.6 ± 0.3	0.6 ± 0.3
Creatinine	3.7 ± 0.7	3.7 ± 0.8	4.0 ± 1.0
Creatine	2.6 ± 0.6	2.5 ± 0.6	3.0 ± 0.6
Citrate	16.9 ± 4.3	16.8 ± 4.9	18.9 ± 5.1
Glutamine	12.4 ± 2.7	11.7 ± 3.0	11.9 ± 5.4
Glutamate	5.2 ± 1.7	5.5 ± 1.9	9.5 ± 13.8
X4	0.8 ± 0.9	0.6 ± 0.3	0.8 ± 0.6
Acetate	9.6 ± 12.1	6.5 ± 12.7	14.7 ± 17.7
AREA5	1.9 ± 0.7	2.3 ± 1.0	3.0 ± 1.3
AREA6	1.9 ± 1.6	1.0 ± 0.8	1.8 ± 1.9
β–hydroxybutyrate	0.9 ± 0.5	1.1 ± 0.5	1.2 ± 0.6
X5	0.3 ± 0.1	0.3 ± 0.1	0.5 ± 0.4
X6	0.9 ± 0.3	1.0 ± 0.3	1.1 ± 0.5
X7	1.0 ± 0.4	1.0 ± 0.5	1.1 ± 0.7
α–hydroxybutyrate	2.0 ± 0.7	2.0 ± 0.8	2.3 ± 1.1
α–hydroxyisovalerate	0.4 ± 0.3	0.4 ± 0.2	0.5 ± 0.5
AREA7	3.4 ± 1.3	3.6 ± 1.7	4.3 ± 1.8
Pyruvate	1.9 ± 0.9	1.7 ± 0.8	2.4 ± 1.1

Table 21. The level of statistical significance of the metabolite concentrations between control patients and FTD, LBD, and VAD patients (the other dementias-model, Figure 20). The significances are presented as is (ANOVA). Area and unknown metabolites (X) as in Table 4 footnote.

Metabolite	Statistical significance (ANOVA)					
	FTD		LBD		VAD	
	F	Sig.	F	Sig.	F	Sig.
Age	18.71	0.00	8.48	0.01	21.13	0.00
MMSE	3.87	0.06	22.66	0.00	46.61	0.00
Tyrosine	0.00	0.95	1.21	0.28	0.36	0.55
Histidine	0.03	0.87	4.32	0.04	1.19	0.28
Phenylalanine	0.42	0.52	0.09	0.77	0.08	0.77
Tryptophan	0.20	0.66	1.30	0.26	0.40	0.53
Formate	6.72	0.01	3.61	0.06	10.66	0.00
X1	0.38	0.54	1.74	0.19	2.84	0.10
X2	0.25	0.62	0.16	0.69	4.37	0.04
Lactate	8.60	0.01	2.44	0.12	25.76	0.00
Myo-inositol	0.07	0.78	0.06	0.81	0.00	1.00
AREA1	1.04	0.31	1.25	0.27	7.07	0.01
Glucose	8.15	0.01	4.96	0.03	9.97	0.00
AREA2	4.18	0.05	3.59	0.06	7.95	0.01
AREA3	3.87	0.05	2.24	0.14	1.44	0.23
X3	0.08	0.78	0.40	0.53	2.67	0.11
Creatinine	0.00	0.92	0.53	0.47	13.93	0.00
Creatine	8.70	0.01	3.14	0.08	8.83	0.00
Citrate	12.88	0.00	2.61	0.11	7.69	0.01
Glutamine	1.13	0.29	11.05	0.00	5.94	0.02
Glutamate	18.84	0.00	23.77	0.00	30.50	0.00
X4	2.02	0.16	1.53	0.22	2.35	0.13
Acetate	16.21	0.00	6.46	0.01	8.61	0.01
AREA5	24.78	0.00	19.29	0.00	25.18	0.00
AREA6	0.13	0.72	0.38	0.54	0.56	0.46
β–hydroxybutyrate	4.80	0.03	11.84	0.00	19.07	0.00
X5	1.00	0.32	12.40	0.00	8.48	0.01
X6	17.04	0.00	8.90	0.00	24.82	0.00
X7	2.56	0.12	0.67	0.42	4.37	0.04
α–hydroxybutyrate	8.34	0.01	3.86	0.06	12.25	0.00
α–hydroxyisovalerate	4.20	0.05	9.14	0.00	0.36	0.55
AREA7	9.55	0.00	9.66	0.00	24.31	0.00
Pyruvate	0.13	0.72	5.85	0.02	1.33	0.25

Table 22. Average metabolite concentrations relative to TSP (TSP=100) and standard deviations in the other dementia-model. Area and unknown metabolites (X) as in Table 4 footnote.

Metabolite	Average Concentration (±StDev)			
	C	FTD	LBD	VAD
Tyrosine	0.9 ± 0.4	0.9 ± 0.7	0.7 ± 0.3	0.8 ± 0.3
Histidine	0.2 ± 0.1	0.2 ± 0.1	0.2 ± 0.0	0.2 ± 0.1
Phenylalanine	1.3 ± 0.5	1.4 ± 0.6	1.2 ± 0.2	1.3 ± 0.4
Tryptophan	0.6 ± 0.2	0.6 ± 0.3	0.5 ± 0.1	0.6 ± 0.1
Formate	0.4 ± 0.2	0.5 ± 0.1	0.5 ± 0.1	0.5 ± 0.2
X1	0.1 ± 0.0	0.0 ± 0.0	0.0 ± 0.0	0.1 ± 0.0
X2	0.1 ± 0.0	0.1 ± 0.0	0.1 ± 0.0	0.1 ± 0.0
Lactate	26.1 ± 5.2	30.5 ± 5.2	29.8 ± 10.9	34.4 ± 6.7
Myo-inositol	10.9 ± 7.4	11.4 ± 3.3	10.3 ± 2.8	10.9 ± 2.5
AREA1	11.3 ± 2.7	12.4 ± 5.3	12.6 ± 4.8	13.4 ± 2.5
Glucose	348.0 ± 67.9	413.3 ± 103.7	412.8 ± 126.7	411.1 ± 70.9
AREA2	10.8 ± 3.3	13.0 ± 4.6	13.4 ± 5.7	13.6 ± 3.3
AREA3	3.2 ± 1.2	4.1 ± 2.2	4.0 ± 2.4	3.6 ± 1.6
X3	0.6 ± 0.5	0.6 ± 0.4	0.7 ± 0.4	0.8 ± 0.3
Creatinine	3.7 ± 0.7	3.7 ± 0.6	3.9 ± 1.0	4.4 ± 0.6
Creatine	2.6 ± 0.6	3.1 ± 0.5	3.0 ± 0.5	3.1 ± 0.5
Citrate	16.9 ± 4.3	21.5 ± 4.7	19.5 ± 4.6	20.6 ± 5.3
Glutamine	12.4 ± 2.7	11.2 ± 6.5	8.0 ± 6.7	9.7 ± 6.2
Glutamate	5.2 ± 1.7	8.6 ± 4.5	10.4 ± 6.2	11.2 ± 6.7
X4	0.8 ± 0.9	0.5 ± 0.3	0.4 ± 0.2	0.4 ± 0.1
Acetate	9.6 ± 12.1	32.8 ± 33.2	25.5 ± 33.0	22.9 ± 22.6
AREA5	1.9 ± 0.7	3.2 ± 1.3	3.3 ± 1.6	3.3 ± 1.5
AREA6	1.9 ± 1.6	1.7 ± 1.4	1.6 ± 0.8	1.6 ± 0.8
β–hydroxybutyrate	0.9 ± 0.5	1.2 ± 0.6	1.6 ± 0.7	1.6 ± 0.7
X5	0.3 ± 0.1	0.4 ± 0.2	0.5 ± 0.2	0.5 ± 0.2
X6	0.9 ± 0.3	1.3 ± 0.3	1.2 ± 0.2	1.3 ± 0.3
X7	1.0 ± 0.4	1.3 ± 0.7	1.1 ± 0.5	1.3 ± 0.7
α–hydroxybutyrate	2.0 ± 0.7	2.6 ± 0.7	2.5 ± 0.5	2.8 ± 0.9
α–hydroxyisovalerate	0.4 ± 0.3	0.6 ± 0.4	0.8 ± 0.5	0.5 ± 0.1
AREA7	3.4 ± 1.3	4.9 ± 2.3	4.8 ± 0.7	5.5 ± 1.9
Pyruvate	1.9 ± 0.9	1.8 ± 0.8	2.9 ± 1.8	2.3 ± 1.5

Table 23. Statistically significant metabolites in FTD, LBD and VAD. see Table 22 for details in metabolite concentrations and Table 21 for details in statistical significance. Abbreviations: CAC=citric acid cycle, NS=not statistically significant. Detected levels are reported relative to control patients.

Metabolite	Role in metabolism	Detected levels	References
Formate	-Oxidative stress -Radical scavenger	FTD: elevated LDB: elevated VAD: elevated	[360, 361]
Lactate	-Energy metabolism, a product of anaerobic glycolysis -Increased levels reported in neurodegenerative diseases	FTD: elevated LDB: NS VAD: elevated	[362, 363]
Glucose	-Energy metabolism, fuels CAC cycle -Concentration changes reported in neurodegenerative diseases	FTD: elevated LDB: elevated VAD: elevated	[364-367]
Creatine	-Energy storage -Has been reported to decrease neurodegeneration	FTD: elevated LDB: NS VAD: elevated	[368, 369]
Citrate	-Energy metabolism, CAC cycle metabolite -Decrease in processing enzymes reported in neurodegenerative diseases	FTD: elevated LDB: NS VAD: elevated	[365, 370]
Glutamate	-Most abundant neurotransmitter in mammals -Lowered levels may suggest neuronal loss or damage -Excessive activation of glutamate receptors can result in neuronal dysfunction and cell death, resulting in excitotoxicity	FTD: elevated LDB: elevated VAD: elevated	[371-373]
Acetate	-Energy metabolism, fuels CAC cycle -Concentration changes reported in neurodegenerative diseases	FTD: elevated LDB: elevated VAD: elevated	[364-366]
β–hydroxybutyrate	-Brain ketone body energy metabolism -Can be used as an alternative source of energy lowering the effect of glucose depletion in neurodegenerative diseases thus preventing neurodegeneration	FTD: elevated LDB: elevated VAD: elevated	[374, 375]

Metabolite	Role in metabolism	Detected levels	References
α–hydroxybutyrate	-Energy metabolism -Oxidative stress	FTD: elevated LDB: NS VAD: elevated	[36, 64]
α–hydroxyisovalerate	-Metabolite related to Phenylketonuria and several other disease states	FTD: elevated LDB: elevated VAD: NS	[376, 377]
Glutamine	-Energy metabolism -Precursor for neurotransmitters -Formed from α–ketoglutarate via glutamate -α–ketoglutarate dehydrogenase complex is known to be deficient in many neurodegenerative disorders and is thought to be critical in the formation of potentially neurotoxic glutamate -Decreased levels of glutamine reflect the defective glutamate detoxification into glutamine in astrocytes - Previous studies have indicated that glutamine synthase activity and glutamate-glutamine cycling are altered in neurodegenerative disorders	FTD: NS LDB: decreased VAD: decreased	[378-380]
Pyruvate	-Energy metabolism -Pyruvate dehydrogenase deficits during brain aging may result in higher levels of pyruvate in neurodegeneration -Has been shown to slow disease progression of ALS in mouse models	FTD: NS LDB: elevated VAD: NS	[381, 382]
Histidine	-Histidine derivatives (e.g. carnosine and homocarnosine) have been shown to have neuroprotective and antioxidative properties that could be of use in treating neurodegenerative disorders	FTD: NS LDB: elevated VAD: NS	[383-385]
Creatinine	- Cerebral energy metabolism	FTD: NS LDB: NS VAD: elevated	[386]

ANCOVA results

The ANCOVAs were run with patient age as a covariate, thus removing the effect of age from the results. The CMA-model and the other dementias model are the same as in the ANOVA results.

1 The CMA-model

Most of the statistically significant metabolite concentration variations were between the AD patients and M (MCI+EAD) group patients (Table 24). In addition to the MMSE score, the significant metabolites were histidine, formate, lactate, area1, glucose, area2, area3, creatinine, creatine, citrate, glutamate, acetate, area5, area6, x5, x6, area7, and pyruvate. As an interesting detail, the significance of area3 was only detected when the effect of patient age was removed. Only two significant variables were found between the control patients and M group patients, these being tyrosine and area6.

2 Other dementias

As in the ANOVAs, several statistically significant metabolite concentration variations were found when the other dementias were compared to controls. The MMSE score, as well as the levels of glutamate, acetate, BHB, x6, and area7 were significant for all classes (Table 25). Class specific metabolite concentrations (in addition to the ones mentioned above) that were statistically significant were as follows:

- formate, lactate, glucose, creatine, citrate, x7, AHB, and AHIV for FTD patients
- histidine, glutamine, x5, and AHIV for LBD patients
- formate, lactate, area1, glucose, citrate, glutamine, x5, and AHB in VAD patients

Table 24. The level of statistical significance of the metabolite concentrations between control, MCI and AD patients (the CMA-model, Figure 20). The significances are presented as is (ANCOVA) with patient age as a covariate. The group column designates the groups between which the significance exists, e.g. C/A means that there is a significant variance between the C and A group patients in the level of the metabolite in question. Abbreviations: C=control (C/NRM+C/ADP), M=MCI (MCI+EAD), A=AD. Area and unknown metabolites (X) as in Table 4 footnote.

Statistical significance (ANCOVA/age)			
Metabolite	F	Sig.	Groups
MMSE	51.73	0.00	A/M
Tyrosine	3.21	0.04	C/M
Histidine	8.54	0.00	A/M
Phenylalanine	1.38	0.25	
Tryptophan	2.34	0.10	
Formate	8.74	0.00	A/M
X1	0.40	0.67	
X2	1.82	0.17	
Lactate	4.27	0.02	A/M
Myo-inositol	1.89	0.15	
AREA1	6.58	0.00	A/M
Glucose	5.40	0.01	A/M
AREA2	9.71	0.00	A/M
AREA3	3.26	0.04	A/M
X3	0.54	0.58	
Creatinine	3.20	0.04	A/M
Creatine	10.22	0.00	A/M
Citrate	3.83	0.02	A/M
Glutamine	0.32	0.73	
Glutamate	3.92	0.02	A/M
X4	1.32	0.27	
Acetate	5.05	0.01	A/M
AREA5	12.87	0.00	A/M
AREA6	5.73	0.00	C/M + A/M
β–hydroxybutyrate	3.34	0.04	!
X5	9.93	0.00	A/M
X6	3.30	0.04	A/M
X7	0.12	0.89	
α–hydroxybutyrate	2.43	0.09	
α–hydroxyisovalerate	0.71	0.49	
AREA7	4.44	0.01	A/M
Pyruvate	7.73	0.00	A/M

!No significance *post hoc* Sidak

Table 25. The level of statistical significance of the metabolite concentrations between control patients and FTD, LBD, and VAD patients (the other dementias-model, Figure 20). The significances are presented as is (ANCOVA) with patient age as a covariate. Area and unknown metabolites (X) as in Table 4 footnote.

Metabolite	Statistical significance (ANCOVA/age)					
	FTD		LBD		VAD	
	F	Sig.	F	Sig.	F	Sig.
MMSE	8.87	0.01	22.66	0.00	22.46	0.00
Tyrosine	0.00	0.99	2.49	0.12	1.70	0.20
Histidine	0.02	0.89	3.16	0.08	0.36	0.55
Phenylalanine	1.48	0.23	1.06	0.31	0.55	0.46
Tryptophan	0.02	0.88	1.30	0.26	0.47	0.50
Formate	6.51	0.01	3.05	0.09	8.93	0.00
X1	0.17	0.68	1.76	0.19	1.36	0.25
X2	0.45	0.51	0.07	0.79	2.44	0.12
Lactate	9.46	0.00	0.52	0.48	15.01	0.00
Myo-inositol	0.04	0.85	0.00	0.97	0.07	0.79
AREA1	1.00	0.32	0.55	0.46	4.90	0.03
Glucose	10.86	0.00	2.31	0.14	4.21	0.05
AREA2	3.98	0.05	1.85	0.18	3.15	0.08
AREA3	1.18	0.28	2.84	0.10	2.78	0.10
X3	0.77	0.38	0.01	0.94	0.46	0.50
Creatinine	1.08	0.30	0.01	0.94	3.70	0.06
Creatine	12.09	0.00	0.46	0.50	1.42	0.24
Citrate	14.52	0.00	1.26	0.27	5.21	0.03
Glutamine	1.21	0.28	9.91	0.00	6.74	0.01
Glutamate	17.80	0.00	19.05	0.00	22.48	0.00
X4	2.44	0.12	0.89	0.35	1.07	0.31
Acetate	10.21	0.00	5.15	0.03	3.50	0.07
AREA5	18.47	0.00	12.20	0.00	15.62	0.00
AREA6	0.36	0.55	0.15	0.70	0.09	0.77
β–hydroxybutyrate	7.04	0.01	6.24	0.02	11.10	0.00
X5	1.09	0.30	8.15	0.01	5.95	0.02
X6	22.53	0.00	4.12	0.05	11.11	0.00
X7	4.01	0.05	0.00	0.97	0.70	0.41
α–hydroxybutyrate	10.51	0.00	1.71	0.20	6.38	0.01
α–hydroxyisovalerate	4.58	0.04	6.86	0.01	0.13	0.72
AREA7	10.25	0.00	4.78	0.03	11.91	0.00
Pyruvate	0.02	0.89	2.89	0.10	0.57	0.46

The neurological relevance of the results

Our results show that the CSF metabolite profiles can be used to discriminate between controls, subjects with MCI, and subjects with dementia. While differences in metabolite concentrations were detected between the diseases well enough to gain reasonably good classification, there was some overlap between the groups.

The early diagnosis of AD has become increasingly important due to evolving and possibly disease-modifying therapies. Recently CSF β-amyloid$_{42}$ and tau- and phospho-tau proteins are increasingly used for the support of early diagnosis since they are known to reflect AD-type brain pathology [259]. However, the non-demented elderly may show a heavy burden of AD pathology in autopsy, while showing no cognitive decline whatsoever pre mortem [387]. Many studies have suggested that this subclinical pathology may be reflected in CSF as well [388, 389]. Thus the current CSF markers do not reflect the clinical symptoms of the subjects very well. Our results suggest that the CSF NMR profiles are able to discriminate cognitively intact study subjects from cognitively affected subjects including subjects with early AD even though part of cognitively intact subjects had a CSF AD profile. These results suggest that the onset of clinical symptom in AD involves distinctive brain systems that are associated with cognitive decline and can be detected with NMR. Another interesting finding was that subjects with MCI formed a separate group from both controls and from demented subjects. Most of these subjects had a form of MCI that did not show progression during the extended follow up. The reason for mild cognitive decline remained unclear. It is well-known that etiology of MCI is heterogeneous and may be related to reversible causes [390]. Our results may suggest that the pathophysiological processes including neurotransmitter deficits that are associated with cognitive decline differ between subjects with dementing diseases and those with MCI due to other reasons.

The most important metabolites contributing to the variability in the four class model were glucose, acetate, citrate, glutamine and three unknown metabolites. The levels of glucose, acetate, citrate, and glutamate tended to be higher and glutamine lower in the demented when compared to controls and MCI without cognitive decline (Figure 29). All the known metabolites are related to energy metabolism. Glucose and acetate act as fuel for the CAC cycle. The increased tendency of the levels of these metabolites in the demented may indicate that they are not used efficiently for energy repair for example due to enzymatic deficiencies in the metabolic pathways known to exist in dementia [364-366]. Citrate is a metabolite in the CAC cycle and the activities of the enzymes processing citrate to alpha-ketoglutarate have been shown to be decreased in post-mortem AD brain [365]. The increase in citrate levels may be related to the lack of processing it due to deficiencies occurring in the CAC cycle. Glutamine is formed from alpha-ketoglutarate via glutamate. The alpha-ketoglutarate dehydrogenase

complex is known to be deficient in many neurodegenerative disorders and is thought to be critical in the formation of potentially neurotoxic glutamate [378]. The decreased levels of glutamine reflect the defective glutamate detoxification into glutamine in astrocytes. Previous studies have indicated that glutamine synthase activity and glutamate-glutamine cycling are altered in neurodegenerative disorders [379]. Glutamate did not significantly contribute to the classifications. However, the trend was that the amount was increased in the demented but not in EAD. This may mean different pathomechanisms taking place in early disease when compared to advanced stages. Our data together with the current literature supports the hypotheses that mitochondrial dysfunction, glutamate excitotoxicity, and alterations in the glutamate-glutamine cycling are related to different forms of dementia [378, 379].

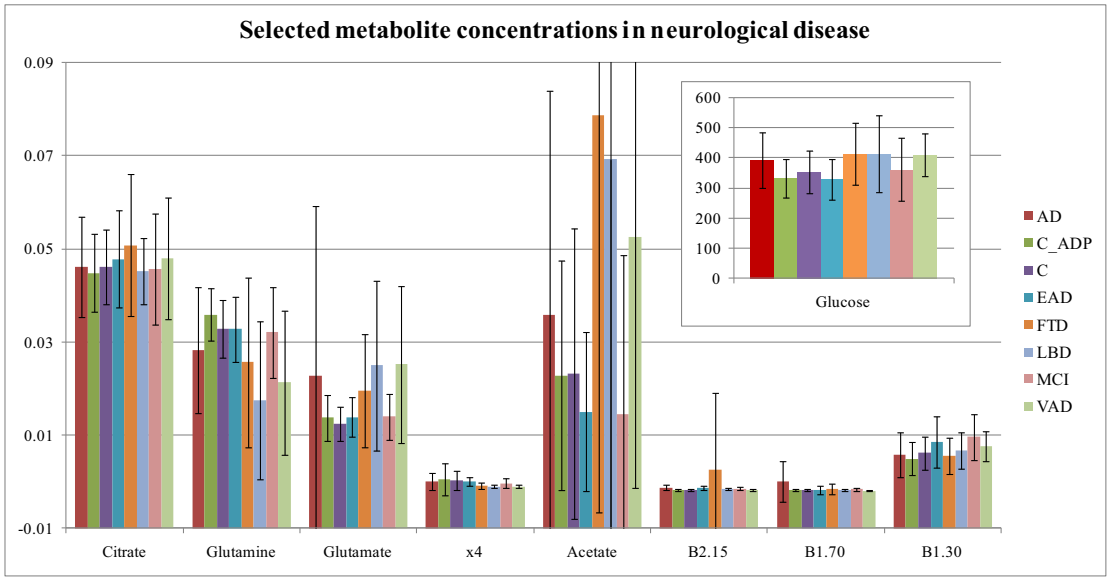

Figure 29. Metabolite concentrations for selected metabolites with neurological significance in control and demented patients. All concentrations are relative to TSP and were mean centered and variance scaled (variance=1), except glucose which is reported relative to TSP (TSP concentration=100). The error bars are based on standard deviations. Abbreviations: x4=unknown metabolite 4 (2.13 ppm), B2.15=10 Hz bucket at 2.15 ppm, B1.70=10 Hz bucket at 1.70 ppm, B1.30=10 Hz bucket at 1.30 ppm.

There was overlap between different dementing diseases and many subjects with other dementias were classified as having AD. These results suggest that the metabolite variations are as complex as the disease processes. Many studies have shown that various forms of dementia share brain pathologies and mixed pathology is common in subjects with cognitive decline [391, 392]. Particularly in the very old subjects dementia may develop in the absence of clear neuropathological sequelae and a significant proportion of the very old demented subjects do not meet the pathological criteria for AD [393-397]. AD patients often have heterogeneous brain pathology and a considerable number of patients also exhibits brain changes indicating the presence of other concomitant neurodegenerative disorders [398].

Patients with clinical diagnoses of VAD or LBD also frequently show AD type neuropathological changes [399, 400]. This is likely to explain the least accurate diagnostic accuracy of other dementias in this study.

Marker profiling may offer advantages over the use of single markers in complex diseases such as neurodegenerative diseases. Many studies have suggested that for example diagnostic CSF AD markers do not perform well in monitoring the disease progression [264, 265]. Previous studies have mainly applied different proteomic methods. These studies have suggested that the use of multiple marker panels may improve the discrimination between the different diseases [401-405]. A panel of five individual markers were shown to distinguish AD from healthy controls with high specificity [405] and larger panel of 17 different markers predicted the progression of MCI to AD [404]. One recent study reported the classification error rate of 14 % for AD in comparison with various neurological diseases using a panel of 23 protein spots [403]. However, there are only few studies that have included relevant pathological control groups, i.e. patients with other types of dementia providing the differential diagnostic challenges in clinical routine. Abdi et al. [402] found eight unique markers that discriminated AD, Parkinson's disease and LBD with high sensitivity and specificity in different combinations. To the best of our knowledge, this is only the second study having used ^{1}H NMR of CSF to study dementia and the first one to feature over 200 patients with several different forms of dementia included. The first study, which tapped metabolic alterations in multiple sclerosis and dementia, seems not to have gained much interest in scientific community [406]. The proteomics methods used in the previous studies are a laborious two-dimensional gel electrophoresis [403], protein chip arrays requiring multiple steps [401, 404, 405] or isobaric Tagging for Relative and Absolute protein Quantification (iTRAQ) requiring most complex sample handling [402]. Compared to these, the advantages of an NMR method are comprehensible: the measurements can be done with minimal sample preparation and instrument calibration. The protocol created here is ultimately aimed for use in neurological screening of suspected and existing dementia patients. The acquired metabolic profile of the patient may be used when assessing the need for e.g. pre emptive medication and its forthcoming effects and possibly monitoring the disease process.

In terms of classification, the results for the SVM and DT/RF methods were clearly superior when compared to the performance of PCA, PLS-DA, kNN, kNN-SA and Sammon's mapping. Between the two best methods, the SVM results were slightly inferior when compared to the DT/RF results, but some classification profiles (e.g. AD) were not discriminated at all, leaving the DT/RF as the only realistic choice of method. Unfortunately, the definitive answer as to why the DT/RF gives best results is unclear. The most likely explanation is that the DT/RF uses a recursive decision making process and is thus capable of successfully handling very complex datasets. This flexibility does not come without a

price as the DT/RF is also prone to overfitting and needs careful validation to ensure the reliability of the results. This superiority of DT is directly reflected in the performance of the RF method which ultimately provided the results with best clarity and possibilities of visualization, together with a firm CV (OOB).

Our study suffers from some limitations that are common to the vast majority of biomarker studies. The diagnoses of AD and other diseases were based on the clinical criteria without pathological confirmation. However, neuropathologically verified accuracy of clinical diagnosis of AD in our clinic has been reported to exceed 90 % [407]. Even though most controls were free of chronic neurological disease, they had neurological symptoms and do not represent a healthy population. These factors most likely lead to a situation in which the control patients overlap with other neurological groups, which in turn creates errors in the classification process. Learning techniques, such as DT/RF, attempt to derive a consistent model based on the input data and are therefore particularly sensitive to misdiagnosed patients. Potential additional problems may arise from physiological variation within human CSF, including variations due to genetics, aging, gender, dietary variation, smoking, stress, exercise, and other similar factors. It is well known that intra- and interindividual biological variation increases with ageing. The number of control patients is small and therefore sensitive to the effects of such sources of variation. Moreover, despite the good classification results obtained with the use of 30 variables (metabolites with buckets + age, sex and MMSE score), the number of metabolic variables could, and in the future should, be increased in order to improve the diagnostic accuracy. Another issue to be addressed in the future is how the results provided in this study are converted into clinical practice to study individual patients presenting memory disorders.

In brief, the objective of this study was to find a method for profiling neurological states and to study the suitability of these profiles for diagnosis of AD and other forms of dementia based on quantitative ^{1}H NMR spectra of human CSF. A wide variety of models and mathematical classification methods were examined for the purpose of finding the optimal combination. Based on our results, we can conclude that the large differences of the metabolite profiles in CSF, hidden under complex relationships of the partly unidentified components, reflect the real significant variance of the neurological states in the patients under scrutiny. The results suggest that the metabolic profile related to cognitive decline is shared between different diseases. AD seems to be a heterogeneous disease and some patients share common features with other dementias. As a conclusion, we believe that CSF profiling, based on NMR information, offers an invaluable method for studies to understand and probe neural system biology and metabolomic intricacies through CSF, the reasons underlying dynamics for the metabolic variations and, for example, the response to medical intervention.

4.3.3 Animal models in NMR metabolomics

(This chapter is loosely based on Jukarainen, N. M., Korhonen, S. P., Puoliväli, J., Ahtoniemi, T., Koistinaho, J., Vepsäläinen, J. Central nervous system disorders studied by ^{1}H NMR metabolomics of rat cerebrospinal fluid. Manuscript, **2009**.)

Background

The purpose of this study was to assess the applicability of NMR metabolomics on rat samples especially in the context of various neurological symptoms or diseases. More specifically, whether or not the information on e.g. the neurometabolism gained from the study of animal models would bring more insight into the respective human cases. The effects of various drugs was also assessed in the case of ischemic and PD rats; specific drug names cannot however be mentioned due to corporate constraints.

NMR spectroscopy was the method of choice, since NMR metabolomics has been proven as an efficient, inexpensive and cost efficient method of analyzing numerous metabolites following disease progression [10, 50].

Methods

All animal studies were carried out with permission of The Institutional Animal Care and Use Committee of the University of Kuopio and the Provincial Government according to the National Institute of Health guidelines for the care and use of laboratory animals. Rats and mice were housed in groups of 2-3 rats in one cage in light and temperature controlled environment with ad libitum water and standard laboratory rodent chow.

CSF samples of rats (Stroke)

Transient focal cerebral ischemia was produced by middle cerebral artery (MCA) occlusion in male Sprague Dawley (SD) rats according to Longa and co-workers [408]. The right carotid arteries were exposed through a mid-line cervical incision and sterile silk sutures (5/0) were looped around the common carotid, external carotid, and internal carotid arteries. The arterial braches of the external carotid artery were all exposed and divided using diathermy forceps leaving a stump of ~2-3 mm in length, and a microvascular clip was placed on the end of the stump to assist haemostasis. The pterygopalatine artery was exposed by developing a plane alongside the internal carotid artery, and ligated at its origin with fine silk (5/0) leaving the extracranial carotid circulation contiguous. Aneurysm clips were placed across the common carotid and internal carotid arteries, and an arteriotomy was made in the external carotid artery stump allowing the introduction of a blunted, rounded length of monofila-

ment nylon suture. This was secured in place with a silk suture and the aneurysm clip on the internal carotid artery was removed. The suture was advanced into the internal carotid artery and placed into the intracranial circulation to lodge in the narrower lumen of the proximal anterior cerebral artery, approximately 17-21 mm distal to the carotid bifurcation, thereby occluding the origin of the MCA. The cervical wound was then closed using sutures.

90 min post occlusion the rats were re-anesthetized and the skin sutures were removed. An aneurysm clip was re-applied to the common carotid artery and the filament slowly and completely was withdrawn. The arteriotomy was closed with diathermy and haemostasis rechecked. The cervical wound was then sutured.

Following MCA occlusion and induction of reperfusion, anaesthesia was discontinued and the animals were allowed to regain consciousness and righting reflex under strict observation. The rats were fed with standard laboratory diet suspended in tap water on days 0-7 after the tMCAO. To prevent dehydration all rats were given an i.p. injection of saline (5 ml per rat) once-a-day for 14 days.

Two months after the tMCAO, the rats were deeply anesthetized with pentobarbital (60 mg/kg Mebunat, Orion Pharma, Finland). A rat was placed prone on the stereotaxic instrument. A sagittal incision of the skin was made inferior to the occiput. After blunt dissection of the tissue and neck muscles through the midline, the dura was penetrated between the third and fourth vertebra by a 26G needle, and 100µl of CSF was collected.

The term “sham” is generally used for sham-operated rats. This means normal rats operated as a control, but not the same mutants as the test or not treated in the same way.

CSF samples of rats (PD)

In order to generate partial retrograde degeneration into the substantia nigra pars compacta (SNc), 6-OHDA lesioning was carried out according to Sauer and Oertel with modifications [409]. Male Wistar rats were anesthetized with ketamine/xylazine and placed in a stereotaxic frame. The rectal temperature was maintained at 37.0 ± 1.0°C with a homeothermic blanket system. The right brain hemisphere was exposed through a small craniectomy to the skull. The dura mater was carefully removed with fine forceps and a stereotaxic injection of 6-OHDA (4 µg/µl) was made into the right striatum. A total of 8 µl of 6-OHDA was infused at a speed of 0.5 µl/min and was equally distributed between 4 sites at the following coordinates: AP +1.0, ML +2.8, DV –6.0, -5.5, -5.0 and –4.4 mm. The cannula was left in place for another 5 min before being withdrawn. The hole in the skull was subsequently filled with repair material and the skin was closed and disinfected. The rats were allowed to recover from anesthe-

sia and were carefully monitored for possible post surgical complications. The animals were returned to the home cages with ad libitum access to food and water.

Six weeks (44 days) after the 6-OHDA injections, animals were, one by one, anaesthetized and placed prone on the stereotaxic instrument. A sagittal incision of the skin was made inferior to the occiput. After blunt dissection of the tissue and neck muscles through the midline, the dura was penetrated between the third and fourth vertebra by a 26G needle, and 100µl of CSF was collected.

CSF samples of rats (ALS)

ALS is a neurodegenerative disease characterized by the combined degeneration of central motor neurons and peripheral motor neurons, whose cell bodies are located in the motor cortex, and in the spinal cord and brainstem, respectively [410, 411]. Only one specific biomarker has so far been found and is known as the TAR DNA binding protein (TARDBP, also known as TDP-43) [412]. Due to the lack of specific biomarkers, the clinical diagnosis for ALS is based on medical history, clinical examination, electromyography, and exclusion of alternative differential diagnoses [413]. This inevitably leads to diagnosis difficulties because of the phenotypic heterogeneity of the disease and conditions similar to ALS that represent about 7% in population-based studies [414]. Several concentration changes of CSF molecules, as well as smaller (NMR-detectable) metabolites have also been reported. These include the changes in concentrations of glutamate and N-acetylaspartate (NAA) and its ratio with choline containing compounds and creatine [415-418].

TG rats expressing human mutant G93A-SOD1 [Tac:N:(SD)]-TgN(SOD1G93A)L26H [Emerging Models, sponsored by Amyotrophic Lateral Sclerosis Association, Taconic, Hudson, NY, USA] develop a motor neuron disease similar to human ALS [419]. Hemizygous rats over-express human mutant G93A-SOD1 at levels increasing from 8-fold over endogenous superoxide dismutase (SOD1) in presymptomatic rats to 16-fold in end stage animals. Disease onset is determined by limb gait and occurs on average at 115 days (16 weeks). From the onset the disease progresses rapidly to end stage within 11 days. The end stage of the disease was determined by righting reflex test, where the animal was placed on its side and if the rat was not able to right itself in 30 seconds, it was scored as death and sacrificed. Righting reflex failure typically coincides with complete paralysis of both hind limbs and one forelimb as a result of substantial loss of spinal cord motor neurons, as well as marked increases in gliosis and degeneration of muscle integrity and function.

The TG and wild type (WT) were aged (and sacrificed) as follows: TG presymptomatic: 3 males, ages 12w, 16w, 16w; 3 females, ages 14w, 14w, 15w, TG end stage: 3 males, ages 19w, 20w, 20w; 3 females, ages 19w, 21w, 21w, TG PDTC end stage: 3 males, ages 18w, 18w, 20w; 3 females, ages 14w, 14w, 15w, WT: 3 males, ages 14w, 16w, 16w; 3 females, ages 21w, 21w, 21w. Sacrificed animals

were anaesthetized with 40mg/kg pentobarbital and perfused transcardially with saline and extracted tissues were frozen in liquid nitrogen and stored at –80°C. G93ASOD1 rats were also treated with pyrrolidine dithiocarbamate (PDTC) on a dose of 50 mg/kg/day (for females) 25 mg/kg/day (for males) and starting at 70 days of age. The TG_PS, TG_ES, and WT rats received plain water. PDTC treated or untreated animals were anesthetized with 40mg/kg pentobarbital, perfused transcardially with saline and extracted tissues were either frozen in liquid nitrogen and stored at –80C or post-fixed with 4% paraformaldehyde for 24 h, cryoprotected with 30% sucrose for three days and then frozen in liquid nitrogen and stored at –80°C.

A rat was anaesthetized and placed prone on the stereotaxic instrument. A sagittal incision of the skin was made inferior to the occiput. After blunt dissection of the tissue and neck muscles through the midline, the dura was penetrated between the third and fourth vertebra by a 26G needle, and 100µl of CSF was collected.

Statistical analysis

To provide an overview of the amount of rats in each disease category, the sample amounts are presented in Table 26. Furthermore, an ANOVA analysis with multiple comparisons was performed on the data. The results are presented in Table 27 (stroke), Table 29 (PD), and Table 31 (ALS) with significances flagged according to *post hoc* tests. Additionally, average metabolite concentrations relative to TSP (TSP=100) were calculated and are presented along with standard deviations in Table 28 (stroke), Table 30 (PD), and Table 32 (ALS).

Table 26. Rat sample amounts showing class and group sizes for the different rats that were analyzed. Abbreviations: TG_PS= TG presymptomatic, TG_ES=TG end stage, TG_PDTC=TG PDTC treated, WT=wild type.

Diagnosis	Number of samples	
ALS	Total	24
	TG_PS	6
	TG_ES	6
	TG_PDTC	6
	WT	6
Stroke	Total	50
	Sham	11
	Vehicle	14
	Drug1	13
	Drug2	12
PD	Total	81
	Sham	10
	Vehicle	15
	Drug1	15
	Drug2	14
	Drug3	11
	Drug4	16

NMR Spectroscopy

The NMR samples were prepared according to the following protocol: The original samples with a volume of ca. 100 µl were subjected to an identical lyophilization protocol for ca. 24 hours. The freeze-dried samples were then stored at -20°C in sealed vials until analysis. Prior to NMR measurements, all samples were reconstituted in 75 µl of D_2O (99.98%-D, Merck). Five microliters of 21.5 mM TSP-d4 (3-(trimethylsilyl)-propionic-2,2,3,3-d_4 acid) in D_2O was added and used as an internal standard of known concentration. All spectra were measured using a Bruker AVANCE DRX 500 instrument operating at 500.13 MHz (Bruker-Biospin GmbH, Karlsruhe, Germany) equipped with a broadband inverse probe (2.5 mm BBI BB, ^{1}H, Z-Grad). The Bruker XWIN-NMR software version 3.5 pl 6 was used for acquisition of all spectra. The pH of the samples was not adjusted, being typically around 7.00±0.05. This pH can be defined as pH*, which is the reading of the pH meter as measured with a standard pH electrode. The pD value is ca. 0.4 units higher than pH*. The relevant parameters used in the 1D experiments, were calibrated and used as follows: recycling delay 45 s, acquisition time 6.5 s, number of scans 128, and a sweep width of 9.5 ppm. A calibrated 90° pulse was used for all spectra and all acquisitions were performed on non-spinning samples. The metabolite concentrations used in the analyses were derived from standard 1D ^{1}H NMR spectra.

Quantification

Quantification for the different models used for classification purposes was performed by using the CTLS protocol previously used in human studies [26]. A slightly different collection of metabolites was however used because of a) the presence of anesthetic metabolites in the CSF and, b) because of the fewer amount of metabolites present in rat CSF (when compared with human CSF). All spectral model creation and quantification was performed by using PERCH NMR Software version 2008.1 (PERCH Solutions Ltd., Kuopio, Finland).

Results and discussion

Stroke

No statistically significant differences between the vehicle and sham groups were detected in ischemic rats (Table 27). This is likely due to the experimental conditions; the vehicle (i.e. "diseased") samples were acquired two months after tMCAO. The rats recovered spontaneously from the blood loss in the brain resulting in nearly identical metabolite concentrations than in the sham (i.e. control) rats.

Statistically significant differences in formate and area1 metabolite concentrations were still discovered between vehicle rats and rats belonging to drug group 2 (Table 27). Rats treated with drug2 had significantly lower levels of formate and area1 metabolites (Table 28). This little tidbit of information is however not very useful in determining disease progression and neurologically significant metabolite correlations.

Table 27. The level of statistical significance of the metabolite concentrations in stroke rats. The significances are presented as is (ANOVA). The group column designates the groups between which the significance exists (if significance still exists *post hoc* Sidak), e.g. V/D1 means that there is a significant variance between the V and D1 group rats in the level of the metabolite in question. Abbreviations as follows: S=sham, V=vehicle, Dn=drug group n.

ANOVA/STROKE			
Metabolite	F	Sig.	Groups
β–hydroxybutyrate	1.87	0.15	
Lactate	0.33	0.80	
AREA1 (1.25-1.30 ppm)	3.43	0.02	V/D2
AREA2 (1.05-1.10 ppm)	2.06	0.12	
AREA3 (1.38-1.48 ppm)	0.45	0.72	
Leucine/Lysine	0.51	0.68	
Acetate	3.26	0.03	!
Glutamine/Glutamate	0.09	0.97	
γ–aminobutyrate	2.25	0.10	
Pyruvate	1.42	0.25	
Glutamate	0.34	0.79	
Glutamine	0.05	0.98	
Citrate	0.03	0.99	
AREA4 (2.98-3.03 ppm)	0.15	0.93	
Creatine	0.49	0.69	
Creatinine	0.44	0.73	
Glucose	0.14	0.94	
Myo-Inositol	0.06	0.98	
Hippurate	0.69	0.56	
Formate	7.73	0.00	S&V/D2

!No significance *post hoc* Sidak in sham/vehicle groups

Table 28. Average metabolite concentrations relative to TSP (TSP=100) and standard deviations in stroke rats. Abbreviations as in Table 27.

Metabolite	Average Concentration (±StDev)			
	Sham	Vehicle	Drug1	Drug2
β–hydroxybutyrate	0.3 ± 0.3	1.0 ± 1.3	0.9 ± 0.8	0.5 ± 0.5
Lactate	206.6 ± 77.3	251.4 ± 171.5	268.7 ± 223.7	228.2 ± 128.3
AREA1 (1.25-1.30 ppm)	4.1 ± 1.1	4.7 ± 3.2	4.2 ± 3.4	1.6 ± 1.8
AREA2 (1.05-1.10 ppm)	1.5 ± 0.8	2.1 ± 1.6	3.0 ± 2.5	3.0 ± 1.8
AREA3 (1.38-1.48 ppm)	7.0 ± 3.6	8.9 ± 5.9	9.9 ± 8.3	8.9 ± 5.1
Leucine/Lysine	5.6 ± 3.5	4.8 ± 2.7	4.8 ± 3.5	3.9 ± 3.0
Acetate	2.3 ± 0.8	2.4 ± 1.2	2.3 ± 1.7	4.1 ± 2.6
Glutamine/Glutamate	37.2 ± 11.6	37.9 ± 23.5	38.3 ± 30.0	34.1 ± 20.2
γ–aminobutyrate	1.5 ± 0.7	1.1 ± 0.6	2.6 ± 2.6	1.6 ± 1.2
Pyruvate	4.7 ± 2.0	5.2 ± 3.2	6.0 ± 5.1	3.2 ± 2.4
Glutamate	2.3 ± 1.6	2.7 ± 2.1	2.3 ± 2.0	2.9 ± 1.4
Glutamine	23.5 ± 8.2	23.8 ± 14.8	23.1 ± 17.6	21.7 ± 13.1
Citrate	12.1 ± 5.9	12.7 ± 7.5	12.3 ± 9.6	12.8 ± 6.4
AREA4 (2.98-3.03 ppm)	3.4 ± 1.5	3.5 ± 2.3	3.0 ± 2.3	3.4 ± 2.0
Creatine	5.3 ± 2.2	4.2 ± 2.1	4.9 ± 3.3	4.9 ± 2.3
Creatinine	0.8 ± 0.3	1.0 ± 0.8	0.8 ± 0.8	0.7 ± 0.4
Glucose	827.4 ± 309.5	757.1 ± 461.5	792.4 ± 613.0	711.5 ± 373.6
Myo-Inositol	6.9 ± 2.9	6.8 ± 4.2	7.5 ± 5.5	7.2 ± 3.9
Hippurate	9.8 ± 3.6	11.3 ± 7.3	13.2 ± 10.1	13.7 ± 6.6
Formate	85.6 ± 20.3	76.3 ± 40.7	79.0 ± 55.9	21.0 ± 8.2

PD

As in the stroke rats, no statistically significant differences between the vehicle and sham groups were detected in PD rats (see Table 29). This is again likely due to the experimental conditions; the vehicle samples were acquired 6 weeks after treatment. Statistically significant concentration differences were detected when comparing the sham and vehicle groups with several drug groups: area1 metabolite concentrations were significantly higher in the sham and vehicle groups than in drug groups, area3 concentrations were higher in vehicle rats than in drug2 treated rats, leucine and lysine concentrations were higher in sham and vehicle rats than in drug2 and drug4 treated rats, acetate concentrations were higher in sham rats than in drug2 treated rats, and γ–aminobutyrate (GABA) concentrations were higher in vehicle rats than in drug4 treated rats (Table 30). Still, without knowledge of the drug names or types of effect, one can only conclude that the drugs do have an effect on some aspects of the disease, but no specifics can be deduced on the basis of this limited knowledge.

Table 29. The level of statistical significance (ANOVA) of the metabolite concentrations in PD rats. Details and abbreviations as in Table 27.

	ANOVA/PD		
Metabolite	F	Sig.	Groups
β–hydroxybutyrate	1.83	0.12	
Lactate	2.04	0.08	
AREA1 (1.25-1.30 ppm)	12.81	0.00	S & V/ALL DRUG G
AREA2 (1.05-1.10 ppm)	1.29	0.28	
AREA3 (1.38-1.48 ppm)	3.70	0.01	V/D2
Leucine/Lysine	5.21	0.00	S&V/D2 + S&V/D4
Acetate	3.03	0.02	S/D2
Glutamine/Glutamate	1.91	0.10	
γ–aminobutyrate	3.68	0.01	V/D4
Pyruvate	0.32	0.90	
Glutamate	1.80	0.12	
Glutamine	2.43	0.04	!
Citrate	2.10	0.08	
AREA4 (2.98-3.03 ppm)	2.19	0.06	
Creatine	0.53	0.75	
Creatinine	1.53	0.19	
Glucose	1.67	0.15	
Myo-Inositol	1.48	0.21	
Hippurate	1.41	0.23	
Formate	1.13	0.35	

!No significance *post hoc* Sidak in sham/vehicle groups

Table 30. Average metabolite concentrations relative to TSP (TSP=100) and standard deviations in PD rats. Abbreviations as in Table 27.

Metabolite	Average Concentration (±StDev)					
	Sham	Vehicle	Drug1	Drug2	Drug3	Drug4
β–hydroxybutyrate	0.9 ± 0.6	0.9 ± 0.5	0.6 ± 0.3	0.5 ± 0.3	0.7 ± 0.3	0.8 ± 0.3
Lactate	281.1 ± 124.3	313.6 ± 141.9	282.2 ± 94.5	202.9 ± 76.2	259.8 ± 67.5	245.6 ± 77.4
AREA1 (1.25-1.30 ppm)	7.2 ± 3.4	5.9 ± 2.3	3.3 ± 1.3	2.9 ± 1.2	3.2 ± 1.8	2.6 ± 0.7
AREA2 (1.05-1.10 ppm)	3.0 ± 1.0	3.2 ± 1.2	3.0 ± 1.2	2.4 ± 0.9	3.3 ± 1.4	2.9 ± 0.8
AREA3 (1.38-1.48 ppm)	13.5 ± 7.2	15.1 ± 6.6	12.6 ± 5.1	7.9 ± 3.3	12.3 ± 4.0	9.8 ± 3.7
Leucine/Lysine	8.8 ± 4.9	8.9 ± 4.0	7.1 ± 3.0	4.3 ± 2.1	5.8 ± 2.4	4.6 ± 2.5
Acetate	4.8 ± 2.5	4.7 ± 2.5	5.0 ± 2.2	2.8 ± 1.2	4.2 ± 1.5	3.4 ± 1.2
Glutamine/Glutamate	38.9 ± 14.3	41.4 ± 15.2	38.3 ± 12.8	28.7 ± 10.9	37.4 ± 12.8	32.8 ± 10.0
γ–aminobutyrate	0.9 ± 0.3	1.0 ± 0.2	0.9 ± 0.4	0.8 ± 0.3	0.8 ± 0.1	0.7 ± 0.1
Pyruvate	3.4 ± 1.3	3.7 ± 2.5	3.6 ± 2.2	3.1 ± 1.9	2.9 ± 2.2	3.3 ± 1.3
Glutamate	5.5 ± 3.6	5.3 ± 2.6	4.9 ± 2.2	4.1 ± 1.6	5.9 ± 1.9	6.6 ± 2.8
Glutamine	24.7 ± 10.9	25.1 ± 9.0	24.7 ± 7.6	17.3 ± 5.7	22.8 ± 7.8	19.2 ± 6.6
Citrate	18.4 ± 6.3	18.2 ± 7.1	19.4 ± 7.1	13.1 ± 4.8	16.7 ± 5.7	14.8 ± 5.9
AREA4 (2.98-3.03 ppm)	3.7 ± 1.5	3.8 ± 1.5	3.8 ± 1.5	2.6 ± 0.8	3.6 ± 1.6	2.9 ± 1.0
Creatine	5.2 ± 1.7	5.8 ± 2.1	5.7 ± 2.1	5.2 ± 6.6	4.7 ± 1.3	4.2 ± 1.2
Creatinine	0.8 ± 0.3	0.7 ± 0.3	0.6 ± 0.3	0.5 ± 0.2	0.8 ± 0.5	0.7 ± 0.2
Glucose	958.0 ± 386.0	967.4 ± 358.9	925.2 ± 311.9	691.7 ± 263.7	915.9 ± 301.5	801.9 ± 251.8
Myo-Inositol	8.7 ± 3.7	9.4 ± 3.9	9.4 ± 4.1	6.5 ± 2.6	8.4 ± 3.7	8.0 ± 2.4
Hippurate	12.1 ± 6.5	15.0 ± 6.6	13.6 ± 6.6	9.9 ± 4.9	15.1 ± 6.0	12.7 ± 5.5
Formate	0.8 ± 0.4	0.7 ± 0.2	0.7 ± 0.2	0.6 ± 0.2	0.7 ± 0.3	0.7 ± 0.3

ALS

In the ALS rats, many statistically significant concentration differences between groups were found (Table 31); most of these were between the TG_PS and TG_ES groups (β–hydroxybutyrate, lactate, glutamine, glutamate, citrate, area4, and creatine). Differences in concentrations were also detected between TG_PS and TG_PDTC groups (area2, glutamine, citrate, glucose, and myo-inositol), between TG_PS and WT groups (glutamine and formate), and also between TG_ES and WT groups (β–hydroxybutyrate). The variations of the metabolite concentrations can also be seen in Table 32 with standard deviations included. The statistically significant metabolites are nearly the same as in human neurodegenerative disease models (Table 23) even though there was no ALS model in the human studies performed. The only exceptions were myo-inositol and hippurate which have not so far been reported as significant metabolites in ALS [413]. Additionally, the WT type animals have rather different metabolite concentrations than the TG groups (Table 32) which might reflect the genetic modification of the animals.

Table 30. The level of statistical significance (ANOVA) of the metabolite concentrations in ALS rats. Abbreviations as follows: TG_PS=TG presymptomatic, TG_ES=TG end stage, TG_PDTC=TG PDTC treated end stage, WT=wild type.

	ANOVA/ALS		
Metabolite	F	Sig.	Groups
β–hydroxybutyrate	5.11	0.01	TG_PS/TG_ES + TG_ES/WT
Lactate	3.50	0.03	TG_PS/TG_ES
AREA1 (1.25-1.30 ppm)	1.20	0.34	
AREA2 (1.05-1.10 ppm)	3.94	0.02	TG_PS/TG_PDTC
AREA3 (1.38-1.48 ppm)	3.00	0.06	
Leucine/Lysine	2.37	0.10	
Acetate	1.17	0.35	
γ–aminobutyrate	1.45	0.26	
Pyruvate	1.20	0.33	
Glutamate	2.68	0.08	
Glutamine	7.70	0.00	TG_PS/TG_ES + TG_PS/TG_PDTC + TG_PS/WT
Citrate	6.18	0.00	TG_PS/TG_ES + TG_PS/TG_PDTC
AREA4 (2.98-3.03 ppm)	3.93	0.02	TG_PS/TG_ES
Creatine	3.91	0.02	TG_PS/TG_ES
Creatinine	2.19	0.12	
Glucose	3.96	0.02	TG_PS/TG_PDTC
Myo-Inositol	3.74	0.03	TG_PS/TG_PDTC
Hippurate	1.08	0.38	
Formate	3.99	0.02	TG_PS/WT

Table 31. Average metabolite concentrations relative to TSP (TSP=100) and standard deviations in ALS rats. Abbreviations as in Table 31.

Metabolite	Average Concentration (±StDev)			
	TG_PS	TG_ES	TG_PDTC	WT
β–hydroxybutyrate	0.3 ± 0.2	3.2 ± 2.6	1.3 ± 1.2	0.4 ± 0.1
Lactate	96.3 ± 20.0	207.0 ± 101.9	165.9 ± 55.1	139.8 ± 30.7
AREA1 (1.25-1.30 ppm)	1.3 ± 0.5	1.8 ± 0.6	1.6 ± 0.5	1.6 ± 0.3
AREA2 (1.05-1.10 ppm)	1.1 ± 0.3	1.2 ± 0.4	1.6 ± 0.3	1.5 ± 0.3
AREA3 (1.38-1.48 ppm)	3.3 ± 1.0	5.0 ± 0.8	5.1 ± 1.8	4.1 ± 1.0
Leucine/Lysine	2.6 ± 1.2	4.0 ± 0.6	3.3 ± 1.1	3.5 ± 0.8
Acetate	2.7 ± 0.6	3.6 ± 1.3	3.5 ± 0.8	3.4 ± 0.9
Glutamine/Glutamate	12.5 ± 3.1	19.5 ± 3.4	16.9 ± 4.0	16.8 ± 2.6
γ–aminobutyrate	0.3 ± 0.1	0.4 ± 0.1	0.5 ± 0.2	0.5 ± 0.1
Pyruvate	0.9 ± 0.2	2.3 ± 2.6	1.5 ± 0.8	1.0 ± 0.7
Glutamate	5.5 ± 3.8	5.8 ± 3.7	2.6 ± 1.1	2.4 ± 0.5
Glutamine	4.0 ± 3.6	11.6 ± 4.3	12.0 ± 2.3	11.6 ± 3.1
Citrate	6.5 ± 1.7	11.5 ± 2.3	11.0 ± 3.9	6.8 ± 2.1
AREA4 (2.98-3.03 ppm)	1.0 ± 0.5	2.0 ± 0.6	1.4 ± 0.5	1.5 ± 0.3
Creatine	1.6 ± 0.4	2.7 ± 0.7	2.5 ± 0.6	2.3 ± 0.6
Creatinine	0.3 ± 0.1	0.4 ± 0.1	0.4 ± 0.1	0.4 ± 0.1
Glucose	303.1 ± 36.7	336.8 ± 113.1	473.3 ± 121.1	418.9 ± 86.5
Myo-Inositol	2.5 ± 0.5	3.3 ± 0.8	4.1 ± 1.3	4.0 ± 0.9
Hippurate	4.5 ± 3.3	4.3 ± 4.0	6.7 ± 2.5	6.7 ± 2.7
Formate	0.2 ± 0.0	0.2 ± 0.0	0.2 ± 0.0	0.2 ± 0.1

Conclusions

On the basis of the results, it can be concluded that NMR metabolomics is an efficient method of acquiring metabolite concentrations to be used in further analyses. A further advantage in the use of animal models in metabolomics studies is that the variation between samples is not as great as in human studies because of inbred animals with a standardized environment. And even though the number of NMR detectable metabolites is lower in rats than in human, several key metabolites related to neurodegenerative disorders can relatively easily be detected and quantified.

5. FUTURE PROSPECTS

Metabolomics is still a relatively new but rapidly (if not exponentially) growing field that has the potential to impact our understanding of the molecular mechanism of disease. A state of disease commonly disrupts metabolism and leaves behind signatures that can be identified and defined by using metabolomics protocols. A deeper understanding of global perturbations in biochemical pathways in complex diseases such as AD, and upon treatment with drugs, could provide valuable insight to the mechanisms of disease, drug effects, and variation in drug response and provide needed diagnostic, prognostic and surrogate biomarkers. Additionally, metabolomics could provide biochemical labels to the diverse clinical manifestations of CNS diseases leading to a more extensive and thorough classification of disease based on different etiologies and biochemical perturbations. This could in turn streamline clinical trials and improve outcomes. It should however be noted that this is still the learning phase and therefore the research at this stage represents the first steps toward the development of a metabolic signature as a biomarker for a disease or its treatment [211, 420]. Many confounding factors exist and the sample sizes have been relatively small so far. The proper matching of patients and controls for age, gender, ethnic background, and many other factors should be considered carefully because a change or difference in only one of these factors (e.g. a different ethnic background if several patients) can result in a large effect in the final results. All of the above, and furthermore, drugs and environment, immensely contribute to human biocomplexity and identification of subtle metabolic variations associated with various diseases is a great challenge. A close monitoring of diet and exercise and the possible effects of medication should also be considered along with other possible disease states. Longitudinal studies are required to confirm and expand on these initial findings, and furthermore, replication studies and blinded studies are needed to validate the markers identified. Connecting central and peripheral changes in CNS disorders could be the key to defining if and how biochemical changes in plasma are related to changes in the brain. Combining metabolomics with imaging approaches and other omics approaches might be powerful ways to achieve these goals [211].

Currently, the metabolomics applications of NMR spectroscopy and MS to diseases have provided better insights into the altered metabolic pathways and disease pathogenesis. However, for applications in early diagnosis the technology is still in its evolutionary stages. Further studies focused on the deconvolution of confounding effects are required. NMR generally detects relatively highly concentrated metabolites and it is normally thought to lack sufficient sensitivity to detect more specific biomarkers featuring a low concentration. Although the latest technological advancements have demonstrated a dramatic reduction in the detection limit of NMR using pure substances, such methods are still not considered high throughput for routine biological sample analysis. By combining the latest advance-

ments in NMR methods and targeted metabolite profiling using sensitivity enhanced approaches, such as isotope labeling or others, a breakthrough in biomarker detection may be achieved. While MS is more sensitive than NMR, it may not be the solution at this stage since there are problems with reproducibility arising from the chromatography of biofluids and with factors such as matrix effects and ion suppression. Anyhow, due to recent technological advancements, the future outlook for NMR and MS based metabolomics does look promising [10, 421].

The future is therefore likely to bring a significant role for metabolomics into different areas of disease and drug research. This can in turn help us toward the ultimate goal in personalized medicine: providing the right medicine to the right patient at the right time [422]. Combining different techniques and omics can also lead to an even more widespread application base for metabolomics, hopefully resulting in more accurate disease progression monitoring and diagnosis.

References

1. Maillet, S., et al., *Experimental protocol for clinical analysis of cerebrospinal fluid by high resolution proton magnetic resonance spectroscopy.* Brain Research. Brain Research Protocols, 1998. **3**(2): p. 123-34.
2. Lindon, J.C., E. Holmes, and J.K. Nicholson, *Peer Reviewed: So whats the deal with metabonomics?* Analytical Chemistry, 2003. **75**(17): p. 384A-391A.
3. Ala-Korpela, M., *Critical evaluation of H-1 NMR metabonomics of serum as a methodology for disease risk assessment and diagnostics.* Clinical Chemistry and Laboratory Medicine, 2008. **46**(1): p. 27-42.
4. Holmes, E., T.M. Tsang, and S.J. Tabrizi, *The Application of NMR-Based Metabonomics in Neurological Disorders.* NeuroRX, 2006. **3**: p. 358-372.
5. Wishart, D.S., *Applications of metabolomics in drug discovery and development.* Drugs in R&D, 2008. **9**(5): p. 307-322.
6. Wilson, I.D., et al., *HPLC-MS-based methods for the study of metabonomics.* Journal of Chromatography B-Analytical Technologies in the Biomedical and Life Sciences, 2005. **817**(1): p. 67-76.
7. Chen, H., et al., *Neutral desorption sampling of living objects for rapid analysis by extractive electrospray ionization mass spectrometry.* Angewandte Chemie-International Edition, 2007. **46**(40): p. 7591-7594.
8. Takats, Z., et al., *Mass spectrometry sampling under ambient conditions with desorption electrospray ionization.* Science, 2004. **306**(5695): p. 471-473.
9. Cody, R.B., J.A. Laramee, and H.D. Durst, *Versatile new ion source for the analysis of materials in open air under ambient conditions.* Analytical Chemistry, 2005. **77**(8): p. 2297-2302.
10. Gowda, G.A.N., et al., *Metabolomics-based methods for early disease diagnostics.* Expert Review of Molecular Diagnostics, 2008. **8**(5): p. 617-633.
11. Lenz, E.M. and I.D. Wilson, *Analytical strategies in metabonomics.* Journal of Proteome Research, 2007. **6**(2): p. 443-458.
12. Potts, B.C.M., et al., *NMR of biofluids and pattern recognition: assessing the impact of NMR parameters on the principal component analysis of urine from rat and mouse.* Journal of Pharmaceutical and Biomedical Analysis, 2001. **26**(3): p. 463-476.
13. Keun, H.C., et al., *Analytical reproducibility in H-1 NMR-based metabonomic urinalysis.* Chemical Research in Toxicology, 2002. **15**(11): p. 1380-1386.
14. Dunn, W.B., N.J.C. Bailey, and H.E. Johnson, *Measuring the metabolome: current analytical technologies.* Analyst, 2005. **130**(5): p. 606-625.
15. Lindon, J.C., et al., *Contemporary issues in toxicology - The role of metabonomics in toxicology and its evaluation by the COMET project.* Toxicology and Applied Pharmacology, 2003. **187**(3): p. 137-146.
16. Tate, A.R., S.J.P. Damment, and J.C. Lindon, *Investigation of the metabolite variation in control rat urine using H-1 NMR spectroscopy.* Analytical Biochemistry, 2001. **291**(1): p. 17-26.
17. Bailey, N.J.C., et al. *An NMR-based metabolomic approach to the analysis of the effects of xenobiotics on endogenous metabolite levels in plants*. 2004.
18. Zuppi, C., et al., *H-1 NMR spectra of normal urines: Reference ranges of the major metabolites.* Clinica Chimica Acta, 1997. **265**(1): p. 85-97.
19. Zuppi, C., et al., *Influence of feeding on metabolite excretion evidenced by urine H-1 NMR spectral profiles: a comparison between subjects living in Rome and subjects living at arctic latitudes (Svaldbard).* Clinica Chimica Acta, 1998. **278**(1): p. 75-79.
20. Nicholson, J.K., et al., *Monitoring metabolic disease by proton NMR of urine.* Lancet, 1984. **2**(8405): p. 751-752.

21. Lenz, E.M., et al., *A H-1 NMR-based metabonomic study of urine and plasma samples obtained from healthy human subjects.* Journal of Pharmaceutical and Biomedical Analysis, 2003. **33**(5): p. 1103-1115.
22. Lenz, E.M., et al., *Metabonomics, dietary influences and cultural differences: a H-1 NMR-based study of urine samples obtained from healthy British and Swedish subjects.* Journal of Pharmaceutical and Biomedical Analysis, 2004. **36**(4): p. 841-849.
23. Beckonert, O., et al., *Metabolic profiling, metabolomic and metabonomic procedures for NMR spectroscopy of urine, plasma, serum and tissue extracts.* Nature Protocols, 2007. **2**(11): p. 2692-2703.
24. Holmes, E., et al. *The identification of novel biomarkers of renal toxicity using automatic data reduction techniques and PCA of proton NMR spectra of urine*. 1998.
25. De Meyer, T., et al., *NMR-based characterization of metabolic alterations in hypertension using an adaptive, intelligent binning algorithm.* Analytical Chemistry, 2008. **80**(10): p. 3783-3790.
26. Jukarainen, N.M., et al., *Quantification of H-1 NMR spectra of human cerebrospinal fluid: a protocol based on constrained total-line-shape analysis.* Metabolomics, 2008. **4**(2): p. 150-160.
27. Crockford, D.J., et al., *Curve-fitting method for direct quantitation of compounds in complex biological mixtures using H-1 NMR: Application in metabonomic toxicology studies.* Analytical Chemistry, 2005. **77**(14): p. 4556-4562.
28. Eads, C.D., et al., *Molecular factor analysis applied to collections of NMR spectra.* Analytical Chemistry, 2004. **76**(7): p. 1982-1990.
29. Bhat, H., B.R. Sajja, and P.A. Narayana, *Fast quantification of proton magnetic resonance spectroscopic imaging with artificial neural networks.* Journal of Magnetic Resonance, 2006. **183**(1): p. 110-122.
30. Richards, S.E., et al., *Self modeling curve resolution recovery of temporal metabolite signal modulation in NMR spectroscopic data sets: Application to a life-long caloric restriction study in dogs.* Analytical Chemistry, 2008. **80**(13): p. 4876-4885.
31. Asiago, V.M., et al., *Use of EDTA to minimize ionic strength dependent frequency shifts in the H-1 NMR spectra of urine.* Metabolomics, 2008. **4**(4): p. 328-336.
32. Pearce, J.T.M., et al., *Robust algorithms for automated chemical shift calibration of 1D H-1 NMR spectra of blood serum.* Analytical Chemistry, 2008. **80**(18): p. 7158-7162.
33. Tiziani, S., et al., *Optimized metabolite extraction from blood serum for H-1 nuclear magnetic resonance spectroscopy.* Analytical Biochemistry, 2008. **377**(1): p. 16-23.
34. Nicholson, J.K., et al., *750-MHz H-1 and H-1-C-13 NMR-spectroscopy of human blood plasma.* Analytical Chemistry, 1995. **67**(5): p. 793-811.
35. Lindon, J.C., et al., *Metabonomics: Metabolic processes studied by NMR spectroscopy of biofluids.* Concepts in Magnetic Resonance, 2000. **12**(5): p. 289-320.
36. Wishart, D.S., et al., *HMDB: the human metabolome database.* Nucleic Acids Research, 2007. **35**: p. D521-D526.
37. Bell, J.D., J.C.C. Brown, and P.J. Sadler, *NMR studies of body fluids.* Nmr in Biomedicine, 1989. **2**: p. 246-256.
38. Nowick, J.S., et al., *DSA: A new internal standard for NMR studies in aqueous solution.* Organic Letters, 2003. **5**(19): p. 3511-3513.
39. Daykin, C.A., et al., *The comparison of plasma deproteinization methods for the detection of low-molecular-weight metabolites by H-1 nuclear magnetic resonance spectroscopy.* Analytical Biochemistry, 2002. **304**(2): p. 220-230.
40. Pers, T.H., et al., *Prediction of fat oxidation capacity using H-1-NMR and LC-MS lipid metabolomic data combined with phenotypic data.* Chemometrics and Intelligent Laboratory Systems, 2008. **93**(1): p. 34-42.
41. Beger, R.D., et al., *Metabonomic models of human pancreatic cancer using 1D proton NMR spectra of lipids in plasma.* Metabolomics, 2006. **2**(3): p. 125-134.

42. Beckwith-Hall, B.M., et al., *A metabonomic investigation of hepatotoxicity using diffusion-edited H-1 NMR spectroscopy of blood serum.* Analyst, 2003. **128**(7): p. 814-818.
43. Solanky, K.S., et al., *Application of biofluid H-1 nuclear magnetic resonance-based metabonomic techniques for the analysis of the biochemical effects of dietary isoflavones on human plasma profile.* Analytical Biochemistry, 2003. **323**(2): p. 197-204.
44. Huq, S.M., et al. *High glucose and low lactate: a metabolic signature of hypertension in human serum?* 2008.
45. Brindle, J.T., et al., *Rapid and noninvasive diagnosis of the presence and severity of coronary heart disease using H-1-NMR-based metabonomics.* Nature Medicine, 2002. **8**(12): p. 1439-1444.
46. Barba, I., et al., *Nuclear magnetic resonance-based metabolomics predicts exercise-induced ischemia in patients with suspected coronary artery disease.* Magnetic Resonance in Medicine, 2008. **60**(1): p. 27-32.
47. Lucas, L.H., et al., *Progress toward automated metabolic profiling of human serum: Comparison of CPMG and gradient-filtered NMR analytical methods.* Journal of Pharmaceutical and Biomedical Analysis, 2005. **39**(1-2): p. 156-163.
48. Barton, R.H., et al., *High-throughput H-1 NMR-based metabolic analysis of human serum and urine for large-scale epidemiological studies: validation study.* International Journal of Epidemiology, 2008. **37**: p. 31-40.
49. Holmes, E., et al., *750 MHz H-1 NMR spectroscopy characterisation of the complex metabolic pattern of urine from patients with inborn errors of metabolism: 2-hydroxyglutaric aciduria and maple syrup urine disease.* Journal of Pharmaceutical and Biomedical Analysis, 1997. **15**(11): p. 1647-1659.
50. Bertini, I., et al., *The Metabonomic Signature of Celiac Disease.* Journal of Proteome Research, 2009. **8**(1): p. 170-177.
51. Qiu, Y., et al., *Multivariate classification analysis of metabolomic data for candidate biomarker discovery in type 2 diabetes mellitus.* Metabolomics, 2008. **4**(4): p. 337-346.
52. Wei, L., et al., *Toxicological effects of cinnabar in rats by NMR-based metabolic profiling of urine and serum.* Toxicology and Applied Pharmacology, 2008. **227**(3): p. 417-429.
53. Craig, A., et al., *Systems toxicology: Integrated genomic, proteomic and metabonomic analysis of methapyrilene induced hepatotoxicity in the rat.* Journal of Proteome Research, 2006. **5**(7): p. 1586-1601.
54. Waters, N.J., et al., *Metabonomic deconvolution of embedded toxicity: Application to thioacetamide hepato- and nephrotoxicity.* Chemical Research in Toxicology, 2005. **18**(4): p. 639-654.
55. Gartland, K.P.R., et al., *Application of pattern-recognition methods to the analysis and classification of toxicological data derived from proton nuclear-magnetic-resonance spectroscopy of urine.* Molecular Pharmacology, 1991. **39**(5): p. 629-642.
56. Crockford, D.J., et al., *H-1 NMR and UPLC-MSE Statistical Heterospectroscopy: Characterization of drug metabolites (xenometabolome) in epidemiological studies.* Analytical Chemistry, 2008. **80**(18): p. 6835-6844.
57. Keun, H.C., et al., *Heteronuclear F-19-H-1 statistical total correlation spectroscopy as a tool in drug metabolism: Study of flucloxacillin biotransformation.* Analytical Chemistry, 2008. **80**(4): p. 1073-1079.
58. Ebbels, T.M.D., et al., *Prediction and classification of drug toxicity using probabilistic modeling of temporal metabolic data: The Consortium on Metabonomic Toxicology screening approach.* Journal of Proteome Research, 2007. **6**(11): p. 4407-4422.
59. Skordi, E., et al., *Characterization and quantification of metabolites of racemic ketoprofen excreted in urine following oral administration to man by H-1-NMR spectroscopy, directly coupled HPLC-MS and HPLC-NMR, and circular dichroism.* Xenobiotica, 2004. **34**(11-12): p. 1075-1089.

60. Wishart, D.S., *Metabolomics: A complementary tool in renal transplantation*, in *Proteomics in Nephrology - Towards Clinical Applications*. 2008. p. 76-87.
61. Dunne, V.G., et al., *Metabolites from cerebrospinal fluid in aneurysmal subarachnoid haemorrhage correlate with vasospasm and clinical outcome: a pattern-recognition H-1 NMR study.* NMR in Biomedicine, 2005. **18**(1): p. 24-33.
62. Holmes, E., et al., *Metabolic profiling of CSF: Evidence that early intervention may impact on disease progression and outcome in schizophrenia.* Plos Medicine, 2006. **3**(8): p. 1420-+.
63. Lutz, N.W., et al., *A branched-chain organic acid linked to multiple sclerosis: First identification by NMR spectroscopy of CSF.* Biochemical and Biophysical Research Communications, 2007. **354**(1): p. 160-164.
64. Wishart, D.S., et al., *The human cerebrospinal fluid metabolome.* Journal of Chromatography B-Analytical Technologies in the Biomedical and Life Sciences, 2008. **871**(2): p. 164-173.
65. Hancu, I., et al., *1H MR Spectroscopy Using TE Averaged PRESS: A More Sensitive Technique to Detect Neurodegeneration Associated with Alzheimer's Disease.* Magnetic Resonance in Medicine, 2005. **53**: p. 777-782.
66. Pfeuffer, J., et al., *Towards an in vivo neurochemical profile: quantification of 18 metabolites in short-echo-time 1H NMR spectra of the rat brain.* Journal of Magnetic Resonance, 1999. **141**: p. 104-120.
67. Schulte, R.F., et al., *Improved two-dimensional J-resolved spectroscopy.* NMR in Biomedicine, 2006. **19**(2): p. 264-270.
68. Yue, Q., et al., *New observations concerning the interpretation of magnetic resonance spectroscopy of meningioma.* European Radiology, 2008. **18**(12): p. 2901-2911.
69. Lauridsen, M., et al., *Application of the FLIPSY pulse sequence for increased sensitivity in H-1 NMR-based metabolic profiling studies.* Analytical Chemistry, 2008. **80**(9): p. 3365-3371.
70. Claridge, T.D.W., *High-Resolution NMR Techniques in Organic Chemistry*. Tetrahedron Organic Chemistry Series. 1999: Pergamon Press.
71. Carr, H.Y. and E.M. Purcell, *Effects of Diffusion on Free Precession in Nuclear Magnetic Resonance Experiments.* Physical Review, 1954. **94**: p. 630-638.
72. Meiboom, S. and D. Gill, *Modified spin-echo method for measuring nuclear relaxation times.* Review of Scientific Instruments, 1958. **29**: p. 688-691.
73. Wang, Y.L., et al., *Spectral editing and pattern recognition methods applied to high-resolution magic-angle spinning H-1 nuclear magnetic resonance spectroscopy of liver tissues.* Analytical Biochemistry, 2003. **323**(1): p. 26-32.
74. Tang, H.R., et al., *Use of relaxation-edited one-dimensional and two dimensional nuclear magnetic resonance spectroscopy to improve detection of small metabolites in blood plasma.* Analytical Biochemistry, 2004. **325**(2): p. 260-272.
75. Maher, A.D., et al., *Optimization of Human Plasma 1H NMR Spectroscopic Data Processing for High-Throughput Metabolic Phenotyping Studies and Detection of Insulin Resistance Related to Type 2 Diabetes.* Anal Chem, 2008. **80**(19): p. 7354-7362.
76. Lindon, J.C. and J.K. Nicholson, *Analytical technologies for metabonomics and metabolomics, and multi-omic information recovery.* TrAC-Trends in Analytical Chemistry, 2008. **27**(3): p. 194-204.
77. Stejskal, E.O. and J.E. Tanner, The Journal of Chemical Physics, 1965. **42**.
78. Tanner, J.E., The Journal of Chemical Physics, 1970. **52**.
79. Liu, M.L., J.K. Nicholson, and J.C. Lindon, *Analysis of drug-protein binding using nuclear magnetic resonance based molecular diffusion measurements.* Analytical Communications, 1997. **34**(8): p. 225-228.
80. Ma, Y.H., et al., *NMR spectroscopic diffusion, chemical shift and linewidth measurements of low-affinity binding of ibuprofen enantiomers to human serum albumin.* Magnetic Resonance in Chemistry, 1999. **37**(4): p. 269-273.

81. Liu, M.L., et al., *Measurement of biomolecular diffusion coefficients in blood plasma using two-dimensional H-1-H-1 diffusion-edited total-correlation NMR spectroscopy.* Analytical Chemistry, 1997. **69**(8): p. 1504-1509.
82. Rooney, O.M., et al., *High-resolution diffusion and relaxation-edited magic angle spinning H-1 NMR spectroscopy of intact liver tissue.* Magnetic Resonance in Medicine, 2003. **50**(5): p. 925-930.
83. Smith, L.M., et al., *Statistical correlation and projection methods for improved information recovery from diffusion-edited NMR spectra of biological samples.* Analytical Chemistry, 2007. **79**(15): p. 5682-5689.
84. Wang, Y., et al., *Magic angle spinning NMR and H-1-P-31 heteronuclear statistical total correlation spectroscopy of intact human gut biopsies.* Analytical Chemistry, 2008. **80**(4): p. 1058-1066.
85. Mierisova, S. and M. Ala-Korpela, *MR spectroscopy quantitation: a review of frequency domain methods.* NMR in Biomedicine, 2001. **14**(4): p. 247-259.
86. Vogels, J., et al. *Partial linear fit: A new NMR spectroscopy preprocessing tool for pattern recognition applications*. 1996.
87. Forshed, J., I. Schuppe-Koistinen, and S.P. Jacobsson, *Peak alignment of NMR signals by means of a genetic algorithm.* Analytica Chimica Acta, 2003. **487**(2): p. 189-199.
88. Lee, G.C. and D.L. Woodruff, *Beam search for peak alignment of NMR signals.* Analytica Chimica Acta, 2004. **513**(2): p. 413-416.
89. Torgrip, R.J.O., et al., *Peak alignment using reduced set mapping.* Journal of Chemometrics, 2003. **17**(11): p. 573-582.
90. Cloarec, O., et al., *Statistical total correlation spectroscopy: An exploratory approach for latent biomarker identification from metabolic H-1 NMR data sets.* Analytical Chemistry, 2005. **77**(5): p. 1282-1289.
91. Cloarec, O., et al., *Evaluation of the orthogonal projection on latent structure model limitations caused by chemical shift variability and improved visualization of biomarker changes in H-1 NMR spectroscopic metabonomic studies.* Analytical Chemistry, 2005. **77**(2): p. 517-526.
92. Stoyanova, R., et al., *Automatic alignment of individual peaks in large high-resolution spectral data sets.* Journal of Magnetic Resonance, 2004. **170**(2): p. 329-335.
93. Weljie, A.M., et al., *Targeted profiling: Quantitative analysis of H-1 NMR metabolomics data.* Analytical Chemistry, 2006. **78**(13): p. 4430-4442.
94. Weljie, A.M., et al., *Evaluating Low-Intensity Unknown Signals in Quantitative Proton NMR Mixture Analysis.* Analytical Chemistry, 2008. **80**(23): p. 8956-8965.
95. Torgrip, R.J.O., et al., *New modes of data partitioning based on PARS peak alignment for improved multivariate biomarker/biopattern detection in 1H-NMR spectroscopic metabolic profiling of urine.* Metabolomics, 2006. **2**(1): p. 1-19.
96. Ammann, L. and M. Merritt, *StePSIM - a method for stepwise peak selection and identification of metabolites in 1H NMR spectra.* Metabolomics, 2007. **3**(1): p. 1-11.
97. Viles, J.H., et al., *Potential bias in NMR relaxation data introduced by peak intensity analysis and curve fitting methods.* Journal of Biomolecular NMR, 2001. **21**(1): p. 1-9.
98. *LCModel, Steven Provencher, http://s-provencher.com/pages/lcmodel.shtml*. 2009.
99. Provencher, S.W., *Automatic quantitation of localized in vivo H-1 spectra with LCModel.* NMR in Biomedicine, 2001. **14**(4): p. 260-264.
100. Provencher, S.W., *Estimation of metabolite concentrations from localized in-vivo proton NMR-spectra.* Magnetic Resonance in Medicine, 1993. **30**(6): p. 672-679.
101. *AMIX, Bruker Biospin GmbH, http://www.bruker-biospin.com/amix.html*. 2009.
102. *Chenomx NMR Suite, Chenomx Inc., http://www.chenomx.com.* 2009.
103. Saude, E.J., C.M. Slupsky, and B.D. Sykes, *Optimization of NMR analysis of biological fluids for quantitative accuracy.* Metabolomics, 2006. **2**(3): p. 113-123.

104. Gipson, G.T., et al., *Weighted least-squares deconvolution method for discovery of group differences between complex biofluid H-1 NMR spectra.* Journal of Magnetic Resonance, 2006. **183**(2): p. 269-277.
105. Xu, Q.W., et al., *Quantification and identification of components in solution mixtures from 1D proton NMR spectra using singular value decomposition.* Analytical Chemistry, 2006. **78**(20): p. 7175-7185.
106. Zhang, F.L. and R. Bruschweiler, *Robust deconvolution of complex mixtures by covariance TOCSY spectroscopy.* Angewandte Chemie-International Edition, 2007. **46**(15): p. 2639-2642.
107. *PERCH NMR Software, http://www.perchsolutions.com*. 2009.
108. Stoer, J. and S. Bulirsch, *Introduction to Numerical Analysis*. 1983, Springer New York. p. 209-215.
109. Laatikainen, R., et al., *A computational strategy for the deconvolution of NMR spectra with multiplet structures and constraints: Analysis of overlapping C-13-H-2 multiplets of C-13 enriched metabolites from cell suspensions incubated in deuterated media.* Magnetic Resonance in Medicine, 1996. **36**(3): p. 359-365.
110. Soininen, P., et al., *Strategies for organic impurity quantification by H-1 NMR spectroscopy: Constrained total-line-shape fitting.* Analytica Chimica Acta, 2005. **542**(2): p. 178-185.
111. Ala-Korpela, M., et al., *The inherent accuracy of 1 H NMR spectroscopy to quantify plasma lipoproteins is subclass dependent.* Atherosclerosis, 2007. **190**: p. 353-358.
112. Holmes, E., et al., *Detection of urinary drug metabolite (Xenometabolome) signatures in molecular epidemiology studies via statistical total correlation (NMR) spectroscopy.* Analytical Chemistry, 2007. **79**(7): p. 2629-2640.
113. Holmes, E., O. Cloarec, and J.K. Nicholson, *Probing latent biomarker signatures and in vivo pathway activity in experimental disease states via statistical total correlation spectroscopy (STOCSY) of biofluids: Application to HgCl2 toxicity.* Journal of Proteome Research, 2006. **5**(6): p. 1313-1320.
114. Sands, C.J., et al., *Statistical Total Correlation Spectroscopy Editing of H-1 NMR Spectra of Biofluids: Application to Drug Metabolite Profile Identification and Enhanced Information Recovery.* Analytical Chemistry, 2009. **81**(15): p. 6458-6466.
115. Crockford, D.J., et al., *Statistical heterospectroscopy, an approach to the integrated analysis of NMR and UPLC-MS data sets: Application in metabonomic toxicology studies.* Analytical Chemistry, 2006. **78**(2): p. 363-371.
116. Viant, M.R., *Improved methods for the acquisition and interpretation of NMR metabolomic data.* Biochemical and Biophysical Research Communications, 2003. **310**(3): p. 943-948.
117. Rubtsov, D.V. and J.L. Griffin, *Time-domain Bayesian detection and estimation of noisy damped sinusoidal signals applied to NMR spectroscopy.* Journal of Magnetic Resonance, 2007. **188**(2): p. 367-379.
118. Ross, A., M. Czisch, and G.C. King, *Systematic errors associated with the CPMG pulse sequence and their effect on motional analysis of biomolecules.* Journal of Magnetic Resonance, 1997. **124**(2): p. 355-365.
119. de Graaf, R.A. and K.L. Behar, *Quantitative 1H NMR Spectroscopy of Blood Plasma Metabolites.* Analytical Chemistry, 2003. **75**(9): p. 2100-2104.
120. Fan, T.W.M. and A.N. Lane, *Structure-based profiling of metabolites and isotopomers by NMR.* Progress in Nuclear Magnetic Resonance Spectroscopy, 2008. **52**: p. 69-117.
121. Evilia, R.F., *Quantitative NMR spectroscopy.* Analytical Letters, 2001. **34**(13): p. 2227-2236.
122. Bharti, S.K., et al., *Improved quantification from H-1-NMR spectra using reduced repetition times.* Metabolomics, 2008. **4**(4): p. 367-376.
123. Van, Q.N., G.N. Chmurny, and T.D. Veenstra, *The depletion of protein signals in metabonomics analysis with the WET-CPMG pulse sequence.* Biochemical and Biophysical Research Communications, 2003. **301**(4): p. 952-959.

124. Ghauri, F.Y., et al., *NMR spectroscopy of human post mortem cerebrospinal fluid: distinction of Alzheimer's disease from control using pattern recognition and statistics.* NMR Biomed., 1993. **6**(2): p. 163-167.
125. Koschorek, F., et al., *High-resolution 1H NMR spectroscopy of cerebrospinal fluid in spinal diseases.* Neurosurg.Rev., 1993. **16**(4): p. 307-315.
126. Bollard, M.E., et al., *NMR-based metabonomic approaches for evaluating physiological influences on biofluid composition.* Nmr in Biomedicine, 2005. **18**(3): p. 143-162.
127. Forshed, J., et al., *A comparison of methods for alignment of NMR peaks in the context of cluster analysis.* Journal of Pharmaceutical and Biomedical Analysis, 2005. **38**(5): p. 824-832.
128. Fan, T.W.M., *Metabolite profiling by one- and two-dimensional NMR analysis of complex mixtures.* Prog Nucl Mag Res Sp, 1996. **28**: p. 161-219.
129. Govindaraju, V., K. Young, and A. Maudsley, *Proton NMR chemical shifts and coupling constants for brain metabolites.* NMR Biomed, 2000. **13**: p. 129-153.
130. Kohonen, T., *Self-Organizing Maps*. Springer Series in Information Sciences. 2001.
131. Tiainen, M., et al., *Spectral Analysis of 1H Coupled 13C Spectra of the Amino Acids: Adaptive Spectral Library of Amino Acid 13C Isotopomers and Positional Fractional 13C Enrichments.* Magn Reson Chem, 2007. **In Press**.
132. Laatikainen, R., et al., *General strategies for total-lineshape-type spectral analysis of NMR spectra using integral-transform iterator.* Journal of Magnetic Resonance Series A, 1996. **120**(1): p. 1-10.
133. Agren, H. and F. Niklasson, *Creatinine and Creatine in Csf - Indexes of Brain Energy-Metabolism in Depression.* J Neural Transm, 1988. **74**(1): p. 55-59.
134. Lindon, J.C., E. Holmes, and J.K. Nicholson, *Pattern recognition methods and applications in biomedical magnetic resonance.* Progress in Nuclear Magnetic Resonance Spectroscopy, 2001. **39**(1): p. 1-40.
135. Geladi, P. and B.R. Kowalski, *Partial Least-Squares Regression: A Tutorial.* Analytica Chimica Acta, 1986. **185**: p. 1-17.
136. Wold, S., K. Esbensen, and P. Geladi, *Principal component analysis.* Chemometrics and Intelligent Laboratory Systems, 1987. **2**: p. 37-52.
137. Holmes, E., et al., *Chemometric models for toxicity classification based on NMR spectra of biofluids.* Chemical Research in Toxicology, 2000. **13**(6): p. 471-478.
138. Lan, W.X., H. Zhu, and M.L. Liu, *Separating human serums of health and hyperlipidaemia subjects using diffusion-weighted nuclear magnetic resonance spectroscopy.* Chinese Journal of Analytical Chemistry, 2008. **36**(7): p. 935-940.
139. Serkova, N.J., et al., *Early detection of graft failure using the blood metabolic profile of a liver recipient.* Transplantation, 2007. **83**(4): p. 517-521.
140. Chen, H.W., et al., *Combining desorption electrospray ionization mass spectrometry and nuclear magnetic resonance for differential metabolomics without sample preparation.* Rapid Communications in Mass Spectrometry, 2006. **20**(10): p. 1577-1584.
141. Yang, J., et al., *Diagnosis of liver cancer using HPLC-based metabonomics avoiding false-positive result from hepatitis and hepatocirrhosis diseases.* Journal of Chromatography B-Analytical Technologies in the Biomedical and Life Sciences, 2004. **813**(1-2): p. 59-65.
142. Plumb, R.S., et al., *Metabonomics: the use of electrospray mass spectrometry coupled to reversed-phase liquid chromatography shows potential for the screening of rat urine in drug development.* Rapid Communications in Mass Spectrometry, 2002. **16**(20): p. 1991-1996.
143. Robertson, D.G., et al., *Metabonomics: Evaluation of nuclear magnetic resonance (NMR) and pattern recognition technology for rapid in vivo screening of liver and kidney toxicants.* Toxicological Sciences, 2000. **57**(2): p. 326-337.
144. Kim, S.W., et al., *Taxonomic discrimination of cyanobacteria by metabolic fingerprinting using proton nuclear magnetic resonance spectra and multivariate statistical analysis.* Journal of Plant Biology, 2006. **49**(4): p. 271-275.

145. Rasmussen, B., et al., *Multivariate analysis of integrated and full-resolution H-1-NMR spectral data from complex pharmaceutical preparations: St. John's wort.* Planta Medica, 2006. **72**(6): p. 556-563.
146. Sammon Jr, J.W., *A nonlinear mapping for data structure analysis.* IEEE Transactions on Computers, 1969. **C-18**: p. 401-409.
147. Gavaghan, C.L., I.D. Wilson, and J.K. Nicholson, *Physiological variation in metabolic phenotyping and functional genomic studies: use of orthogonal signal correction and PLS-DA.* Febs Letters, 2002. **530**(1-3): p. 191-196.
148. Son, H.S., et al., *Metabolomic Studies on Geographical Grapes and Their Wines Using H-1 NMR Analysis Coupled with Multivariate Statistics.* Journal of Agricultural and Food Chemistry, 2009. **57**(4): p. 1481-1490.
149. Son, H.S., et al., *H-1 NMR-Based Metabolomic Approach for Understanding the Fermentation Behaviors of Wine Yeast Strains.* Analytical Chemistry, 2009. **81**(3): p. 1137-1145.
150. Thi, T.H.D., et al., *Effect of benzothiadiazole on the metabolome of Arabidopsis thaliana.* Plant Physiology and Biochemistry, 2009. **47**(2): p. 146-152.
151. Ekman, D.R., et al., *Profiling lipid metabolites yields unique information on sex- and time-dependent responses of fathead minnows (Pimephales promelas) exposed to 17 alpha-ethynylestradiol.* Metabolomics, 2009. **5**(1): p. 22-32.
152. Trygg, J., *O2-PLS for qualitative and quantitative analysis in multivariate calibration.* Journal of Chemometrics, 2002. **16**(6): p. 283-293.
153. Trygg, J. and S. Wold, *Orthogonal projections to latent structures (O-PLS).* Journal of Chemometrics, 2002. **16**(3): p. 119-128.
154. Trygg, J. and S. Wold, *O2-PLS, a two-block (X-Y) latent variable regression (LVR) method with an integral OSC filter.* Journal of Chemometrics, 2003. **17**(1): p. 53-64.
155. Bylesjo, M., et al., *Orthogonal projections to latent structures as a strategy for microarray data normalization.* BMC Bioinformatics, 2007. **8**.
156. Bylesjo, M., et al., *OPLS discriminant analysis: combining the strengths of PLS-DA and SIMCA classification.* Journal of Chemometrics, 2006. **20**(8-10): p. 341-351.
157. Bylesjo, M., et al., *K-OPLS package: Kernel-based orthogonal projections to latent structures for prediction and interpretation in feature space.* BMC Bioinformatics, 2008. **9**.
158. Kang, J., et al., *Application of a H-1 Nuclear Magnetic Resonance (NMR) Metabolomics Approach Combined with Orthogonal Projections to Latent Structure-Discriminant Analysis as an Efficient Tool for Discriminating between Korean and Chinese Herbal Medicines.* Journal of Agricultural and Food Chemistry, 2008. **56**(24): p. 11589-11595.
159. Wiklund, S., et al., *Visualization of GC/TOF-MS-based metabolomics data for identification of biochemically interesting compounds using OPLS class models.* Analytical Chemistry, 2008. **80**(1): p. 115-122.
160. Bruce, S.J., et al., *Evaluation of a protocol for metabolic profiling studies on human blood plasma by combined ultra-performance liquid chromatography/mass spectrometry: From extraction to data analysis.* Analytical Biochemistry, 2008. **372**(2): p. 237-249.
161. Wold, S., *Pattern-recognition by means of disjoint principal components models.* Pattern Recognition, 1976. **8**(3): p. 127-139.
162. Trygg, J., E. Holmes, and T. Lundstedt, *Chemometrics in metabonomics.* Journal of Proteome Research, 2007. **6**(2): p. 469-479.
163. Dumas, M.E., et al., *Homeostatic signature of anabolic steroids in cattle using H-1-C-13 HMBC NMR metabonomics.* Journal of Proteome Research, 2005. **4**(5): p. 1493-1502.
164. Odunsi, K., et al., *Detection of epithelial ovarian cancer using H-1-NMR-based metabonomics.* International Journal of Cancer, 2005. **113**(5): p. 782-788.
165. McKee, C.L.G., I.D. Wilson, and J.K. Nicholson, *Metabolic phenotyping of nude and normal (Alpk : ApfCD, C57BL10J) mice.* Journal of Proteome Research, 2006. **5**(2): p. 378-384.
166. Vapnik, V., *Estimation of Dependencies Based on Empirical Data*. 1982, New York: Springer Verlag.

167. Boser, B., I. Guyon, and V. Vapnik. in *Proceedings of the 5th Annual ACM Workshop of Computational Learning Theory*. 1992.
168. Cortes, C. and V. Vapnik, *Support-vector networks.* Mach Learn, 1995. **20**(3): p. 273-297.
169. Bennett, K.P. and C. Campbell, *Support Vector Machines: Hype or Hallelujah?* SIGKDD Explorations, 2000. **2**(2): p. 1-13.
170. Yao, X.J., et al., *Comparative study of QSAR/QSPR correlations using support vector machines, radial basis function neural networks, and multiple linear regression.* Journal of Chemical Information and Computer Sciences, 2004. **44**(4): p. 1257-1266.
171. Chen, H.F., et al., *Insight into the bioactivity and metabolism of human glucagon receptor antagonists from 3D-QSAR analyses.* QSAR & Combinatorial Science, 2004. **23**(8): p. 603-620.
172. Mahadevan, S., et al., *Analysis of metabolomic data using support vector machines.* Analytical Chemistry, 2008. **80**(19): p. 7562-7570.
173. Kuhn, S., et al., *Building blocks for automated elucidation of metabolites: Machine learning methods for NMR prediction.* BMC Bioinformatics, 2008. **9**.
174. Bullinger, D., et al., *Bioinformatical evaluation of modified nucleosides as biomedical markers in diagnosis of breast cancer.* Analytica Chimica Acta, 2008. **618**(1): p. 29-34.
175. Kouskoumvekaki, I., et al., *Identification of biomarkers for genotyping Aspergilli using nonlinear methods for clustering and classification.* BMC Bioinformatics, 2008. **9**.
176. Frickenschmidt, A., et al., *Metabonomics in cancer diagnosis: mass spectrometry-based profiling of urinary nucleosides from breast cancer patients.* Biomarkers, 2008. **13**(4): p. 435-449.
177. Shakhnarovich, G., T. Darrell, and P. Indyk, *Nearest-Neighbor Methods in Learning and Vision: Theory and Practice*. 2006: MIT Press.
178. Golbraikh, A. and A. Tropsha, *Beware of q 2 !* J Mol Graph Model, 2002. **20**(4): p. 269-276.
179. Itskowitz, P. and A. Tropsha, *k Nearest neighbors QSAR modeling as a variational problem: Theory and applications.* Journal of Chemical Information and Modeling, 2005. **45**(3): p. 777-785.
180. Tominaga, Y., *Comparative study of class data analysis with PCA-LDA, SIMCA, PLS, ANNs, and k-NN.* Chemometrics and Intelligent Laboratory Systems, 1999. **49**(1): p. 105-115.
181. Bao, Y.G., N. Ishii, and X.Y. Du, *Combining multiple k-nearest neighbor classifiers using different distance functions.* Lecture Notes in Computer Science, 2004. **3177**: p. 634-641.
182. Pechenizkiy, M., *The impact of feature extraction on the performance of a classifier: kNN, Na¡ve Bayes and C4.5.* Lecture Notes in Artificial Intelligence, 2005. **3501**: p. 268-279.
183. Beckonert, O., et al. *NMR-based metabonomic toxicity classification: hierarchical cluster analysis and k-nearest-neighbour approaches*. 2003.
184. Breiman, L., Friedman, J., Stone, C.J., Olshen, R.A., *Classification and Regression Trees*. 1984: Chapman & Hall.
185. Farhi, E. and S. Gutmann, *Quantum computation and decision trees.* Physical Review A, 1998. **58**(2): p. 915-928.
186. Brodley, C.E. and P.E. Utgoff, *Multivariate Decision Trees.* Machine Learning, 1995. **19**(1): p. 45-77.
187. Adam, B.L., et al., *Serum protein fingerprinting coupled with a pattern-matching algorithm distinguishes prostate cancer from benign prostate hyperplasia and healthy men.* Cancer Research, 2002. **62**(13): p. 3609-3614.
188. Qu, Y.S., et al. *Boosted decision tree analysis of surface-enhanced laser desorption/ionization mass spectral serum profiles discriminates prostate cancer from noncancer patients*. 2002.
189. Breiman, L., *"Random Forests".* Machine Learning, 2001. **45**: p. 5-32.
190. Breiman, L. and A. Cutler, *Random Forests Manual v4.0*. 2003, UC Berkeley.
191. de Edelenyi, F.S., et al., *Prediction of the metabolic syndrome status based on dietary and genetic parameters, using Random Forest.* Genes and Nutrition, 2008. **3**(3-4): p. 173-176.

192. Jacoby, E., J. Davies, and M.J.J. Blommers, *Design of small molecule libraries for NMR screening and other applications in drug discovery.* Current Topics in Medicinal Chemistry, 2003. **3**(1): p. 11-23.
193. Wider, G., *Structure determination of biological macromolecules in solution using nuclear magnetic resonance spectroscopy.* Biotechniques, 2000. **29**(6): p. 1278-+.
194. Moore, J.M., *NMR techniques for characterization of ligand binding: Utility for lead generation and optimization in drug discovery.* Biopolymers, 1999. **51**(3): p. 221-243.
195. Srivastava, S. and G. Govil, *Application of NMR to the study of cells and body fluids.* Current Organic Chemistry, 2001. **5**(10): p. 1039-1057.
196. Simon, R., et al., *Pitfalls in the use of DNA microarray data for diagnostic and prognostic classification.* Journal of the National Cancer Institute, 2003. **95**(1): p. 14-18.
197. Ransohoff, D.F., *Opinion - Bias as a threat to the validity of cancer molecular-marker research.* Nature Reviews Cancer, 2005. **5**(2): p. 142-149.
198. Baggerly, K.A., et al., *Signal in noise: Evaluating reported reproducibility of serum proteomic tests for ovarian cancer.* Journal of the National Cancer Institute, 2005. **97**(4): p. 307-309.
199. Ambroise, C. and G.J. McLachlan, *Selection bias in gene extraction on the basis of microarray gene-expression data.* Proceedings of the National Academy of Sciences of the United States of America, 2002. **99**(10): p. 6562-6566.
200. Teahan, O., et al., *Impact of analytical bias in metabonomic studies of human blood serum and plasma.* Analytical Chemistry, 2006. **78**(13): p. 4307-4318.
201. Cavill, R., et al., *Genetic algorithms for simultaneous variable and sample selection in metabonomics.* Bioinformatics, 2009. **25**(1): p. 112-118.
202. Keun, H.C., et al. *Improved analysis of multivariate data by variable stability scaling: application to NMR-based metabolic profiling*. 2003.
203. Bijlsma, S., et al., *Large-scale human metabolomics studies: A strategy for data (pre-) processing and validation.* Analytical Chemistry, 2006. **78**(2): p. 567-574.
204. Webb-Robertson, B.J.M., et al., *A study of spectral integration and normalization in NMR-based metabonomic analyses.* Journal of Pharmaceutical and Biomedical Analysis, 2005. **39**(3-4): p. 830-836.
205. Craig, A., et al., *Scaling and normalization effects in NMR spectroscopic metabonomic data sets.* Analytical Chemistry, 2006. **78**(7): p. 2262-2267.
206. Lindon, J.C., et al., *Summary recommendations for standardization and reporting of metabolic analyses.* Nature Biotechnology, 2005. **23**(7): p. 833-838.
207. Hardy, N.W. and C.F. Taylor, *A roadmap for the establishment of standard data exchange structures for metabolomics.* Metabolomics, 2007. **3**(3): p. 243-248.
208. Griffin, J.L., et al., *Standard reporting requirements for biological samples in metabolomics experiments: mammalian/in vivo experiments.* Metabolomics, 2007. **3**(3): p. 179-188.
209. Sumner, L.W., et al., *Proposed minimum reporting standards for chemical analysis.* Metabolomics, 2007. **3**(3): p. 211-221.
210. van der Werf, M.J., et al., *Standard reporting requirements for biological samples in metabolomics experiments: microbial and in vitro biology experiments.* Metabolomics, 2007. **3**(3): p. 189-194.
211. Kaddurah-Daouk, R. and K.R.R. Krishnan, *Metabolomics: A Global Biochemical Approach to the Study of Central Nervous System Diseases.* Neuropsychopharmacology, 2009. **34**(1): p. 173-186.
212. Weiden, P.J. and P.F. Buckley. *Reducing the burden of side effects during long-term antipsychotic therapy: The role of "Switching" medications*. 2007.
213. Tranulis, C., et al., *Benefits and risks of antipsychotic polypharmacy - An evidence-based review of the literature.* Drug Safety, 2008. **31**(1): p. 7-20.
214. Insel, T.R., *Devising prevention and treatment strategies for the nation's diverse populations with mental illness - Commentary.* Psychiatric Services, 2007. **58**(3): p. 395-395.

215. Lieberman, J.A., et al., *Effectiveness of antipsychotic drugs in patients with chronic schizophrenia.* New England Journal of Medicine, 2005. **353**(12): p. 1209-1223.
216. Kaddurah-Daouk, R., B.S. Kristal, and R.M. Weinshilboum, *Metabolomics: A global biochemical approach to drug response and disease.* Annual Review of Pharmacology and Toxicology, 2008. **48**: p. 653-683.
217. Lindon, J.C., E. Holmes, and J.K. Nicholson, *Metabonomics in pharmaceutical R & D.* FEBS Journal, 2007. **274**(5): p. 1140-1151.
218. Harrigan, G. and R. Goodacre, *Metabolic Profiling: Its Role in Biomarker Discovery and Gene Function Analysis*. 2003, Boston: Kluwer Academic.
219. Kapeller, P., et al., *Preliminary evidence for neuronal damage in cortical grey matter and normal appearing white matter in short duration relapsing-remitting multiple sclerosis: a quantitative MR spectroscopic imaging study.* Journal of Neurology, 2001. **248**(2): p. 131-138.
220. Karrenbauer, V.D., et al., *Plasma cerebrosterol and magnetic resonance imaging measures in multiple sclerosis.* Clinical Neurology and Neurosurgery, 2006. **108**(5): p. 456-460.
221. Frisoni, G.B. and M. Filippi, *Multiple sclerosis and Alzheimer disease through the looking glass of MR imaging.* American Journal of Neuroradiology, 2005. **26**(10): p. 2488-2491.
222. Kleiner-Fisman, G., C. Bergeron, and A.E. Lang, *Presentation of Creutzfeldt-Jakob disease as acute corticobasal degeneration syndrome.* Movement Disorders, 2004. **19**(8): p. 948-949.
223. Jenkins, B.G., et al., *Evidence for impairment of energy-metabolism in-vivo in Huntingtons-disease using localized H-1-NMR spectroscopy.* Neurology, 1993. **43**(12): p. 2689-2695.
224. Brouwer, O.F., et al., *Follow-up magnetic-resonance-imaging in Hallervorden-Spatz disease.* Clinical Neurology and Neurosurgery, 1992. **94**: p. S57-S60.
225. Kang, P.B., J.V. Hunter, and E.M. Kaye, *Lactic acid elevation in extramitochondrial childhood neurodegenerative diseases.* Journal of Child Neurology, 2001. **16**(9): p. 657-660.
226. Khiat, A., et al., *Brain metabolic alterations in Cushing's syndrome as monitored by proton magnetic resonance spectroscopy.* Nmr in Biomedicine, 1999. **12**(6): p. 357-363.
227. Gallelli, K.A., et al., *N-acetylaspartate levels in bipolar offspring with and at high-risk for bipolar disorder.* Bipolar Disorders, 2005. **7**(6): p. 589-597.
228. Choi, I.Y., et al., *In vivo NMR studies of neurodegenerative diseases in transgenic and rodent models.* Neurochemical Research, 2003. **28**(7): p. 987-1001.
229. Rudkin, T.M. and D.L. Arnold, *Proton magnetic resonance spectroscopy for the diagnosis and management of cerebral disorders.* Archives of Neurology, 1999. **56**(8): p. 919-926.
230. Li, L.M., et al., *Lateralization of temporal lobe epilepsy (TLE) and discrimination of TLE from extra-TLE using pattern analysis of magnetic resonance spectroscopic and volumetric data.* Epilepsia, 2000. **41**(7): p. 832-842.
231. Kalra, S., D.L. Arnold, and N.R. Cashman, *Biological markers in the diagnosis and treatment of ALS.* Journal of the Neurological Sciences, 1999. **165**: p. S27-S32.
232. Matthews, P.M., et al., *Assessment of lesion pathology in multiple sclerosis using quantitative MRI morphometry and magnetic resonance spectroscopy.* Brain, 1996. **119**: p. 715-722.
233. Seppi, K. and M.F. Schocke, *An update on conventional and advanced magnetic resonance imaging techniques in the differential diagnosis of neurodegenerative parkinsonism.* Current Opinion in Neurology, 2005. **18**(4): p. 370-375.
234. Kasparova, S., et al., *Effect of coenzyme Q(10) and vitamin E on brain energy metabolism in the animal model of Huntington's disease.* Neurochemistry International, 2006. **48**(2): p. 93-99.
235. Fernandez, A., et al., *Proton magnetic resonance spectroscopy and magnetoencephalographic estimation of delta dipole density: A combination of techniques that may contribute to the diagnosis of Alzheimer's disease.* Dementia and Geriatric Cognitive Disorders, 2005. **20**(2-3): p. 169-177.
236. Pfefferbaum, A., et al., *In vivo brain concentrations of N-acetyl compounds, creatine, and choline in Alzheimer disease.* Archives of General Psychiatry, 1999. **56**(2): p. 185-192.

237. Preul, M.C., et al., *Accurate, noninvasive diagnosis of human brain tumors by using proton magnetic resonance spectroscopy.* Nature Medicine, 1996. **2**(3): p. 323-325.
238. Maurer, K., S. Volk, and H. Gerbaldo, *Auguste D and Alzheimer's disease.* Lancet, 1997. **349**(9064): p. 1546-9.
239. Bianchetti, A. and M. Trabucch, *Clinical aspects of Alzheimer's disease.* Aging (Milano), 2001. **13**(3): p. 221-30.
240. Drachman, D.A., *If we live long enough, will we all be demented?* Neurology, 1994. **44**: p. 1563-1565.
241. Hebert, L.E., et al., *Age specific incidance of Alzheimer's disease in a community population.* Journal of the American Medical Association, 1995. **273**: p. 1354-1359.
242. Rozzini, R., et al., *Dementia is a major predictor of death among the Italian elderly.* Neurology, 2000. **54**(4): p. 1014.
243. Koulu, M. and J. Tuomisto, *Farmakologia ja toksikologia*. 2001, Medicina, Gummerus: Jyväskylä. p. 467-473.
244. Goate, A., et al., *Segregation of a missense mutation in the amyloid precursor protein gene with familial Alzheimer's disease.* Nature, 1991. **349**(6311): p. 704-6.
245. Mattson, M.P., et al., *Presenilins, the endoplasmic reticulum, and neuronal apoptosis in Alzheimer's disease.* Journal of Neurochemistry, 1998. **70**(1): p. 1-14.
246. Strittmatter, W.J. and A.D. Roses, *Apolipoprotein E and Alzheimer's disease.* Annual Review of Neuroscience, 1996. **19**: p. 53-77.
247. De La Torre, J.C., *Alzheimer's disease: How does it start?* Journal of Alzheimer's Disease, 2002. **4**(6): p. 497-512.
248. Geldmacher, D.S. and P.J. Whitehouse, *Evaluation of dementia.* New England Journal of Medicine, 1996. **335**(5): p. 330-6.
249. Rossor, M., *Alzheimer's disease.* British Medical Journal, 1993. **307**(6907): p. 779-82.
250. Lyketsos, C.G., et al., *Mental and behavioral disturbances in dementia: findings from the Cache County Study on Memory in Aging.* The American Journal of Psychiatry, 2000. **157**(5): p. 708-14.
251. Binetti, G., et al., *Delusions in Alzheimer's disease and multi-infarct dementia.* Acta Neurologica Scandinavica, 1993. **88**(1): p. 5-9.
252. Trabucchi, M. and A. Bianchetti, *Delusions.* International Psychogeriatrics, 1996. **8 Suppl 3**: p. 383-5.
253. Cummings, J.L., *Changes in neuropsychiatric symptoms as outcome measures in clinical trials with cholinergic therapies for Alzheimer disease.* Alzheimer Disease and Associated Disorders, 1997. **11 Suppl 4**: p. 1-9.
254. Teri, L., et al., *Cognitive decline in Alzheimer's disease: a longitudinal investigation of risk factors for accelerated decline.* Journals of Gerontology Series A: Biological Sciences and Medical Sciences, 1995. **50A**(1): p. 49-55.
255. Marra, C., M.C. Silveri, and G. Gainotti, *Predictors of cognitive decline in the early stage of probable Alzheimer's disease.* Dementia and Geriatric Cognitive Disorders, 2000. **11**(4): p. 212-8.
256. Strauss, M.E., M.M. Lee, and J.M. DiFilippo, *Premorbid personality and behavioral symptoms in Alzheimer disease. Some cautions.* Archives of Neurology, 1997. **54**(3): p. 257-9.
257. Williams, A., et al., *Aggregate-prone proteins are cleared from the cytosol by autophagy: Therapeutic implications*, in *Current Topics in Developmental Biology, Vol 76*. 2006. p. 89-101.
258. Selkoe, D.J., *Soluble oligomers of the amyloid beta-protein impair synaptic plasticity and behavior.* Behavioural Brain Research, 2008. **192**(1): p. 106-113.
259. Tapiola, T., et al., *Cerebrospinal Fluid beta-Amyloid 42 and Tau Proteins as Biomarkers of Alzheimer-Type Pathologic Changes in the Brain.* Archives of Neurology, 2009. **66**(3): p. 382-389.

260. Hansson, O., et al., *Association between CSF biomarkers and incipient Alzheimer's disease in patients with mild cognitive impairment: a follow-up study.* Lancet Neurology, 2006. **5**(3): p. 228-234.
261. Herukka, S.K., et al., *CSF A beta 42, Tau and phosphorylated Tau, APOE epsilon 4 allele and MCI type in progressive MCI.* Neurobiology of Aging, 2007. **28**(4): p. 507-514.
262. Visser, P.J., *Use of biomarkers to select the target population for clinical trials in subjects with mild cognitive impairment.* Journal of Nutrition Health & Aging, 2009. **13**(4): p. 344-345.
263. Dubois, B., et al., *Research criteria for the diagnosis of Alzheimer"s disease: revising the NINCDS-ADRDA criteria.* Lancet Neurology, 2007. **6**(8): p. 734-746.
264. Andreasen, N., et al., *Sensitivity, specificity, and stability of CSF-tau in AD in a community-based patient sample.* Neurology, 1999. **53**(7): p. 1488-1494.
265. Bouwman, F.H., et al., *Longitudinal changes of CSF biomarkers in memory clinic patients.* Neurology, 2007. **69**(10): p. 1006-1011.
266. Blennow, K., et al., *Longitudinal stability of CSF biomarkers in Alzheimer's disease.* Neuroscience Letters, 2007. **419**(1): p. 18-22.
267. Motter, R., et al., *Reduction of beta-amyloid peptide(42), in the cerebrospinal-fluid of patients with Alzheimers disease.* Annals of Neurology, 1995. **38**(4): p. 643-648.
268. Vandermeeren, M., et al., *Detection of tau proteins in normal and Alzheimers-disease cerebrospinal-fluid with a sensitive sandwich enzyme-linked-immunosorbent-assay.* Journal of Neurochemistry, 1993. **61**(5): p. 1828-1834.
269. Hu, Y.Y., et al., *Elevated levels of phosphorylated neurofilament proteins in cerebrospinal fluid of Alzheimer disease patients.* Neuroscience Letters, 2002. **320**(3): p. 156-160.
270. Ishiguro, K., et al., *Phosphorylated tau in human cerebrospinal fluid is a diagnostic marker for Alzheimer's disease.* Neuroscience Letters, 1999. **270**(2): p. 91-94.
271. Buerger, K., et al., *Differential diagnosis of Alzheimer disease with cerebrospinal fluid levels of tau protein phosphorylated at threonine 231.* Archives of Neurology, 2002. **59**(8): p. 1267-1272.
272. Mills, J. and P.B. Reiner, *Regulation of amyloid precursor protein cleavage.* Journal of Neurochemistry, 1999. **72**(2): p. 443-60.
273. Tanzi, R.E., et al., *Amyloid beta protein gene: cDNA, mRNA distribution, and genetic linkage near the Alzheimer locus.* Science, 1987. **235**(4791): p. 880-4.
274. Sambamurti, K., et al., *Evidence for intracellular cleavage of the Alzheimer's amyloid precursor in PC12 cells.* Journal of Neuroscience Research, 1992. **33**(2): p. 319-29.
275. Ikezu, T., et al., *Caveolae, plasma membrane microdomains for alpha-secretase-mediated processing of the amyloid precursor protein.* Journal of Biological Chemistry, 1998. **273**(17): p. 10485-95.
276. Hartmann, T., et al., *Distinct sites of intracellular production for Alzheimer's disease A beta40/42 amyloid peptides.* Nature Medicine, 1997. **3**(9): p. 1016-20.
277. Gervais, F.G., et al., *Involvement of caspases in proteolytic cleavage of Alzheimer's amyloid-beta precursor protein and amyloidogenic A beta peptide formation.* Cell, 1999. **97**(3): p. 395-406.
278. Haass, C., et al., *Amyloid beta-peptide is produced by cultured cells during normal metabolism.* Nature, 1992. **359**(6393): p. 322-5.
279. Kuo, Y.M., et al., *Water-soluble Abeta (N-40, N-42) oligomers in normal and Alzheimer disease brains.* Journal of Biological Chemistry, 1996. **271**(8): p. 4077-81.
280. Gowing, E., et al., *Chemical characterization of A beta 17-42 peptide, a component of diffuse amyloid deposits of Alzheimer disease.* Journal of Biological Chemistry, 1994. **269**(15): p. 10987-90.
281. Nitsch, R.M., et al., *Metabotropic glutamate receptor subtype mGluR1alpha stimulates the secretion of the amyloid beta-protein precursor ectodomain.* Journal of Neurochemistry, 1997. **69**(2): p. 704-12.

282. Nitsch, R.M., et al., *Release of Alzheimer amyloid precursor derivatives stimulated by activation of muscarinic acetylcholine receptors.* Science, 1992. **258**(5080): p. 304-7.
283. Gabuzda, D., J. Busciglio, and B.A. Yankner, *Inhibition of beta-amyloid production by activation of protein kinase C.* Journal of Neurochemistry, 1993. **61**(6): p. 2326-9.
284. Neve, R.L. and N.K. Robakis, *Alzheimer's disease: a re-examination of the amyloid hypothesis.* Trends in Neurosciences, 1998. **21**(1): p. 15-9.
285. Goedert, M., *Tau protein and the neurofibrillary pathology of Alzheimer's disease.* Trends in Neurosciences, 1993. **16**(11): p. 460-5.
286. Spillantini, M.G. and M. Goedert, *Tau protein pathology in neurodegenerative diseases.* Trends in Neurosciences, 1998. **21**(10): p. 428-33.
287. Goedert, M., et al., *Multiple isoforms of human microtubule-associated protein tau: sequences and localization in neurofibrillary tangles of Alzheimer's disease.* Neuron, 1989. **3**(4): p. 519-26.
288. Goedert, M., et al., *Tau proteins of Alzheimer paired helical filaments: abnormal phosphorylation of all six brain isoforms.* Neuron, 1992. **8**(1): p. 159-68.
289. Goedert, M., et al., *Phosphorylation of microtubule-associated protein tau by stress- activated protein kinases.* FEBS Letters, 1997. **409**(1): p. 57-62.
290. Goedert, M., et al., *Assembly of microtubule-associated protein tau into Alzheimer-like filaments induced by sulphated glycosaminoglycans.* Nature, 1996. **383**(6600): p. 550-3.
291. *Diagnostic and statistical manual of mental disorders (IV-TR) 4th end - text revised*. 2000, Washington DC: American Psychiatric Association.
292. McKhann, G., et al., *Clinical diagnosis of Alzheimer's disease: report of the NINCDS-ADRDA Work Group under the auspices of Department of Health and Human Services Task Force on Alzheimer's disease.* Neurology, 1984. **34**: p. 939-44.
293. Folstein, M.F., S.E. Folstein, and P.R. McHugh, *"Mini-mental state". A practical method for grading the cognitive state of patients for the clinician.* Journal of Psychiatric Research, 1975. **12**(3): p. 189-98.
294. Blessed, G., B.E. Tomlinson, and M. Roth, *The association between quantitative measures of dementia and of senile change in the cerebral grey matter of elderly subjects.* The British Journal of Psychiatry, 1968. **114**(512): p. 797-811.
295. Di Luca, M., et al., *Differential level of platelet amyloid beta precursor protein isoforms: an early marker for Alzheimer disease.* Archives of Neurology, 1998. **55**(9): p. 1195-200.
296. Colangelo, V., et al., *Gene expression profiling of 12633 genes in Alzheimer hippocampal CA1: transcription and neurotrophic factor down-regulation and up-regulation of apoptotic and pro-inflammatory signaling.* Journal of neuroscience Research, 2002. **70**(3): p. 462-73.
297. Zhao, W.Q., et al., *MAP kinase signaling cascade dysfunction specific to Alzheimer's disease in fibroblasts.* Neurobiology of Disease, 2002. **11**(1): p. 166-83.
298. Klawans, H.L., et al., *A pure Parkinsonian syndrome following acute carbon-monoxide intoxication.* Archives of Neurology, 1982. **39**(5): p. 302-304.
299. Huang, C.C., et al., *Progression after chronic manganese exposure.* Neurology, 1993. **43**(8): p. 1479-1483.
300. Helmuth, L., *Neuroscience - Pesticide causes Parkinson's in rats.* Science, 2000. **290**(5494): p. 1068-1068.
301. Langston, J.W., et al., *Selective nigral toxicity after systematic administration of 1-methyl-4-phenyl-1,2,5,6-tetrahydropyrine (MPTP) in the squirrel-monkey.* Brain Research, 1984. **292**(2): p. 390-394.
302. Chen, Y.C.I., et al., *Detection of dopaminergic neurotransmitter activity using pharmacologic MRI: Correlation with PET, microdialysis, and behavioral data.* Magnetic Resonance in Medicine, 1997. **38**(3): p. 389-398.
303. Smith, D.A., et al., *Use of a clinical MR scanner for imaging the rat-brain.* Brain Research Bulletin, 1993. **31**(1-2): p. 115-120.

304. Boska, M.D., et al., *Quantitative H-1 magnetic resonance spectroscopic imaging determines therapeutic immunization efficacy in an animal model of Parkinson's disease.* Journal of Neuroscience, 2005. **25**(7): p. 1691-1700.
305. Brownell, A.L., et al., *Combined PET/MRS brain studies show dynamic and long-term physiological changes in a primate model of Parkinson disease.* Nature Medicine, 1998. **4**(11): p. 1308-1312.
306. Dautry, C., et al., *Serial 1H-NMR spectroscopy study of metabolic impairment in primates chronically treated with the succinate dehydrogenase inhibitor 3-nitropropionic acid.* Neurobiology of Disease, 1999. **6**(4): p. 259-268.
307. Palfi, S., et al., *Fetal striatal allografts reverse cognitive deficits in a primate model of Huntington disease.* Nature Medicine, 1998. **4**(8): p. 963-966.
308. Mittoux, V., et al., *Restoration of cognitive and motor functions by ciliary neurotrophic factor in a primate model of Huntington's disease.* Human Gene Therapy, 2000. **11**(8): p. 1177-1187.
309. Masliah, E., et al., *Dopaminergic loss and inclusion body formation in alpha-synuclein mice: Implications for neurodegenerative disorders.* Science, 2000. **287**(5456): p. 1265-1269.
310. Richfield, E.K., et al., *Heterogeneous dopamine receptor changes in early and late Huntingtons-disease.* Neuroscience Letters, 1991. **132**(1): p. 121-126.
311. van Dellen, A., et al., *N-acetylaspartate and DARPP-32 levels decrease in the corpus striatum of Huntington's disease mice.* Neuroreport, 2000. **11**(17): p. 3751-3757.
312. Griffin, J.L., C.K. Cemal, and M.A. Pook, *Defining a metabolic phenotype in the brain of a transgenic mouse model of spinocerebellar ataxia 3.* Physiological Genomics, 2004. **16**(3): p. 334-340.
313. Tsang, T.A., et al., *Metabolic characterization of the R6/2 transgenic mouse model of Huntington's disease by high-resolution MAS H-1 NMR spectroscopy.* Journal of Proteome Research, 2006. **5**(3): p. 483-492.
314. Jenkins, B.G., et al., *Nonlinear decrease over time in N-acetyl aspartate levels in the absence of neuronal loss and increases in glutamine and glucose in transgenic Huntington's disease mice.* Journal of Neurochemistry, 2000. **74**(5): p. 2108-2119.
315. Henley, S.M.D., G.P. Bates, and S.J. Tabrizi, *Biomarkers for neurodegenerative diseases.* Current Opinion in Neurology, 2005. **18**(6): p. 698-705.
316. Frey, H.J., et al., *Problems associated with biological markers of Alzheimer's disease.* Neurochem Res, 2005. **30**(12): p. 1501-1510.
317. Winblad, B., et al., *Introduction: Mild cognitive impairment: beyond controversies, towards a consensus.* Journal of Internal Medicine, 2004. **256**(3): p. 181-182.
318. DeCarli, C., *Mild cognitive impairment: prevalence, prognosis, aetiology, and treatment.* Lancet Neurology, 2003. **2**(1): p. 15-21.
319. Cheng, L.L., et al., *Quantification of neurons in Alzheimer and control brains with ex vivo high resolution magic angle spinning proton magnetic resonance spectroscopy and stereology.* Magnetic Resonance Imaging, 2002. **20**(7): p. 527-533.
320. Frederick, B.D., et al., *In vivo proton magnetic resonance spectroscopy of the temporal lobe in Alzheimer's disease.* Progress in Neuro-Psychopharmacology & Biological Psychiatry, 2004. **28**(8): p. 1313-1322.
321. Spillantini, M.G., et al., *alpha-synuclein in Lewy bodies.* Nature, 1997. **388**(6645): p. 839-840.
322. Schlossmacher, M.G., et al., *Parkin localizes to the Lewy bodies of Parkinson disease and dementia with Lewy bodies.* American Journal of Pathology, 2002. **160**(5): p. 1655-1667.
323. Hoang, T.Q., et al., *Quantitative proton-decoupled P-31 MRS and H-1 MRS in the evaluation of Huntington's and Parkinson's diseases.* Neurology, 1998. **50**(4): p. 1033-1040.
324. Bender, A., et al., *Creatine supplementation lowers brain glutamate levels in Huntington's disease.* Journal of Neurology, 2005. **252**(1): p. 36-41.

325. Underwood, B.R., et al., *Huntington disease patients and transgenic mice have similar pro-catabolic serum metabolite profiles.* Brain, 2006. **129**: p. 877-886.
326. Verbessem, P., et al., *Creatine supplementation in Huntington's disease - A placebo-controlled pilot trial.* Neurology, 2003. **61**(7): p. 925-930.
327. Tabrizi, S.J., et al., *Creatine therapy for Huntington's disease: Clinical and MRS findings in a 1-year pilot study.* Neurology, 2003. **61**(1): p. 141-142.
328. Matthews, R.T., et al., *Creatine and cyclocreatine attenuate MPTP neurotoxicity.* Experimental Neurology, 1999. **157**(1): p. 142-149.
329. Tourbah, A., et al., *Localized proton magnetic resonance spectroscopy in relapsing remitting versus secondary progressive multiple sclerosis.* Neurology, 1999. **53**(5): p. 1091-1097.
330. Mader, I., et al., *Serial proton MR spectroscopy of contrast-enhancing multiple sclerosis plaques: Absolute metabolic values over 2 years during a clinical pharmacological study.* American Journal of Neuroradiology, 2000. **21**(7): p. 1220-1227.
331. Arnold, D.L., et al., *Proton magnetic-resonance spectroscopy of human brain invivo in the evaluation of multiple-sclerosis - assessment of the load of disease.* Magnetic Resonance in Medicine, 1990. **14**(1): p. 154-159.
332. Davie, C.A., et al., *H-1 magnetic resonance spectroscopy of chronic cerebral white matter lesions and normal appearing white matter in multiple sclerosis.* Journal of Neurology Neurosurgery and Psychiatry, 1997. **63**(6): p. 736-742.
333. Fu, L., et al., *Imaging axonal damage of normal-appearing white matter in multiple sclerosis.* Brain, 1998. **121**: p. 103-113.
334. Narayana, P.A., et al., *Serial proton magnetic resonance spectroscopic imaging, contrast-enhanced magnetic resonance imaging, and quantitative lesion volumetry in multiple sclerosis.* Annals of Neurology, 1998. **43**(1): p. 56-71.
335. Sitter, B., et al., *Cervical cancer tissue characterized by high-resolution magic angle spinning MR spectroscopy.* Magnetic Resonance Materials in Physics Biology and Medicine, 2004. **16**(4): p. 174-181.
336. Sitter, B., et al., *Comparison of HR MAS MR spectroscopic profiles of breast cancer tissue with clinical parameters.* NMR in Biomedicine, 2006. **19**(1): p. 30-40.
337. Whitehead, T.L. and T. Kieber-Emmons, *Applying in vitro NMR spectroscopy and H-1 NMR metabonomics to breast cancer characterization and detection.* Progress in Nuclear Magnetic Resonance Spectroscopy, 2005. **47**(3-4): p. 165-174.
338. Cheng, L.L., et al., *Evaluating human breast ductal carcinomas with high-resolution magic-angle spinning proton magnetic resonance spectroscopy.* Journal of Magnetic Resonance, 1998. **135**(1): p. 194-202.
339. Bathen, T.F., et al., *MR-determined metabolic phenotype of breast cancer in prediction of lymphatic spread, grade, and hormone status.* Breast Cancer Research and Treatment, 2007. **104**(2): p. 181-189.
340. Phillips, M., et al., *Prediction of breast cancer using volatile biomarkers in the breath.* Breast Cancer Research and Treatment, 2006. **99**(1): p. 19-21.
341. Lyng, H., et al., *Metabolic mapping by use of high-resolution magic angle spinning H-1 MR spectroscopy for assessment of apoptosis in cervical carcinomas.* BMC Cancer, 2007. **7**.
342. Tate, A.R., et al., *Distinction between normal and renal cell carcinoma kidney cortical biopsy samples using pattern recognition of H-1 magic angle spinning (MAS) NMR spectra.* NMR in Biomedicine, 2000. **13**(2): p. 64-71.
343. Righi, V., et al., *Ex vivo HR-MAS magnetic resonance Spectroscopy of normal and malignant human renal tissues.* Anticancer Research, 2007. **27**(5A): p. 3195-3204.
344. Kind, T., et al., *A comprehensive urinary metabolomic approach for identifying kidney cancer.* Analytical Biochemistry, 2007. **363**(2): p. 185-195.
345. Messana, I., et al., *Proton nuclear magnetic resonance spectral profiles of urine in type II diabetic patients.* Clinical Chemistry, 1998. **44**(7): p. 1529-1534.

346. Zuppi, C., et al., *Proton nuclear magnetic resonance spectral profiles of urine from children and adolescents with type 1 diabetes.* Clinical Chemistry, 2002. **48**(4): p. 660-662.
347. Salek, R.M., et al., *A metabolomic comparison of urinary changes in type 2 diabetes in mouse, rat, and human.* Physiological Genomics, 2007. **29**(2): p. 99-108.
348. Otvos, J.D., E.J. Jeyarajah, and D.W. Bennett, *Quantification of plasma-lipoproteins by proton nuclear-magnetic-resonance spectroscopy.* Clinical Chemistry, 1991. **37**(3): p. 377-386.
349. Kuller, L., et al., *Nuclear magnetic resonance spectroscopy of lipoproteins and risk of coronary heart disease in the Cardiovascular Health Study.* Arteriosclerosis Thrombosis and Vascular Biology, 2002. **22**(7): p. 1175-1180.
350. Brindle, J.T., et al., *Application of chemometrics to H-1 NMR spectroscopic data to investigate a relationship between human serum metabolic profiles and hypertension.* Analyst, 2003. **128**(1): p. 32-36.
351. Kirschenlohr, H.L., et al., *Proton NMR analysis of plasma is a weak predictor of coronary artery disease.* Nature Medicine, 2006. **12**(6): p. 705-710.
352. Nicholson, J.K., et al., *Quantitative high-resolution H-1-NMR urinanalysis studies on the biochemical effects of cadmium in the rat.* Molecular Pharmacology, 1989. **36**(3): p. 398-404.
353. Beer, M., et al., *Altered energy metabolism after myocardial infarction assessed by 31 P-MR-spectroscopy in humans.* European Radiology, 2000. **10**(8): p. 1323-8.
354. Wevers, R.A., et al., *Standardized method for high-resolution 1H-NMR of cerebrospinal fluid.* Clinical Chemistry, 1995. **41**: p. 744-751.
355. Petersen, R.C., et al., *Aging, memory, and mild cognitive impairment.* International Psychogeriatrics, 1997. **9**(Suppl. 1): p. 65-69.
356. Roman, G.C., et al., *Vascular dementia: Diagnostic criteria for research studies. report of the NINDS-AIREN International Workshop.* Neurology, 1993. **43**(2): p. 250-60.
357. Neary, D., et al., *Frontotemporal lobar degeneration - A consensus on clinical diagnostic criteria.* Neurology, 1998. **51**(6): p. 1546-1554.
358. McKeith, I.G., et al., *Diagnosis and management of dementia with Lewy bodies - Third report of the DLB consortium.* Neurology, 2005. **65**(12): p. 1863-1872.
359. Qi, Y.J., Z. Bar-Joseph, and J. Klein-Seetharaman, *Evaluation of different biological data and computational classification methods for use in protein interaction prediction.* Proteins-Structure Function and Bioinformatics, 2006. **63**(3): p. 490-500.
360. Dean, R.T., et al., *Biochemistry and pathology of radical-mediated protein oxidation.* Biochemical Journal, 1997. **324**: p. 1-18.
361. Kang, J.H., *Oxidative modification of neurorilament-L by the cytochrome c and hydrogen peroxide system.* Bulletin of the Korean Chemical Society, 2007. **28**(1): p. 77-80.
362. Stamelou, M., et al., *In vivo evidence for cerebral depletion in high-energy phosphates in progressive supranuclear palsy.* Journal of Cerebral Blood Flow and Metabolism, 2009. **29**(4): p. 861-870.
363. Henchcliffe, C., et al. *Multinuclear Magnetic Resonance Spectroscopy for in Vivo Assessment of Mitochondrial Dysfunction in Parkinson's Disease*. 2008.
364. Iwangoff, P., et al., *Glycolytic-enzymes from human autoptic brain cortex - normal aged and demented cases.* Mechanisms of Ageing and Development, 1980. **14**(1-2): p. 203-209.
365. Bubber, P., et al., *Mitochondrial abnormalities in Alzheimer brain: Mechanistic implications.* Annals of Neurology, 2005. **57**(5): p. 695-703.
366. Brooks, W.M., et al., *Gene expression profiles of metabolic enzyme transcripts in Alzheimer's disease.* Brain Research, 2007. **1127**(1): p. 127-135.
367. Baquer, N.Z., et al., *A metabolic and functional overview of brain aging linked to neurological disorders.* Biogerontology, 2009. **10**(4): p. 377-413.
368. Adhihetty, P.J. and M.F. Beal, *Creatine and Its Potential Therapeutic Value for Targeting Cellular Energy Impairment in Neurodegenerative Diseases.* Neuromolecular Medicine, 2008. **10**(4): p. 275-290.

369. Karoly, R., K. Peter, and V. Laszlo, *Neuroprotection in Parkinson's disease and other neurodegenerative disorders: preclinical and clinical findings.* Ideggyogyaszati Szemle-Clinical Neuroscience, 2009. **62**(1-2): p. 25-34.
370. Wiedemann, F.R., et al., *Mitochondrial DNA and respiratory chain function in spinal cords of ALS patients.* Journal of Neurochemistry, 2002. **80**(4): p. 616-625.
371. Ernst, T., et al., *Frontotemporal dementia and early Alzheimer disease: Differentiation with frontal lobe H-1 NTR spectroscopy.* Radiology, 1997. **203**(3): p. 829-836.
372. Sattler, R. and M. Tymianski, *Molecular mechanisms of calcium-dependent excitotoxicity.* Journal of Molecular Medicine-Jmm, 2000. **78**(1): p. 3-13.
373. Marambaud, P., U. Dreses-Werringloer, and V. Vingtdeux, *Calcium signaling in neurodegeneration.* Molecular Neurodegeneration, 2009. **4**: p. 15.
374. Henderson, S.T., *Ketone bodies as a therapeutic for Alzheimer's disease.* Neurotherapeutics, 2008. **5**(3): p. 470-480.
375. Tai, K.K., et al., *Ketogenic diet prevents cardiac arrest-induced cerebral ischemic neurodegeneration.* Journal of Neural Transmission, 2008. **115**(7): p. 1011-1017.
376. Magni, F., et al., *Simultaneous determination of plasma levels of alpha-ketoisocaproic acid and leucine and evaluation of alpha-[1-13C]ketoisocaproic acid and [1-13C]leucine enrichment by gas chromatography-mass spectrometry.* Analytical Biochemistry, 1994. **220**(2): p. 308-314.
377. Ohie, T., et al., *Gas chromatography-mass spectrometry with tert.-butyldimethylsilyl derivation: use of the simplified sample preparations and the automated data system to screen for organic acidemias.* Journal of Chromatography B: Biomedical Sciences and Applications, 2000. **746**(1): p. 63-73.
378. Gibson, G.E., et al. *The alpha-ketoglutarate-dehydrogenase complex - A mediator between mitochondria and oxidative stress in neurodegeneration*. 2005.
379. Walton, H.S. and P.R. Dodd. *Glutamate-glutamine cycling in Alzheimer's disease*. 2007.
380. Sitter, B., et al., *High-resolution magic angle spinning and H-1 magnetic resonance spectroscopy reveal significantly altered neuronal metabolite profiles in CLN1 but not in CLN3.* Journal of Neuroscience Research, 2004. **77**(5): p. 762-769.
381. Zhou, Q.Q., et al., *Activation of c-Jun-N-terminal kinase and decline of mitochondrial pyruvate dehydrogenase activity during brain aging.* Febs Letters, 2009. **583**(7): p. 1132-1140.
382. Park, J.H., et al., *Pyruvate slows disease progression in a G93A SOD1 mutant transgenic mouse model.* Neuroscience Letters, 2007. **413**(3): p. 265-269.
383. Kang, J.H., *Protection by Histidine Dipeptides against Acrolein-induced Neurofilament-L Aggregation.* Bulletin of the Korean Chemical Society, 2008. **29**(9): p. 1732-1736.
384. Bellia, F., et al., *New glycosidic derivatives of histidine-containing dipeptides with antioxidant properties and resistant to carnosinase activity.* European Journal of Medicinal Chemistry, 2008. **43**(2): p. 373-380.
385. Hipkiss, A.R., *Could carnosine or related structures suppress Alzheimer's disease?* Journal of Alzheimers Disease, 2007. **11**(2): p. 229-240.
386. Agren, H. and F. Niklasson, *Creatinine and Creatine in Csf - Indexes of Brain Energy-Metabolism in Depression.* Journal of Neural Transmission, 1988. **74**(1): p. 55-59.
387. Keller, J.N., *Age-related neuropathology, cognitive decline, and Alzheimer's disease.* Ageing Research Reviews, 2006. **5**: p. 1-13.
388. Skoog, I., et al., *Cerebrospinal fluid beta-amyloid 42 is reduced before the onset of sporadic dementia: A population-based study in 85-year-olds.* Dementia and Geriatric Cognitive Disorders, 2003. **15**(3): p. 169-176.
389. Fagan, A.M., et al., *Cerebrospinal fluid tau/beta-amyloid(42) ratio as a prediction of cognitive decline in nondemented older adults.* Archives of Neurology, 2007. **64**(3): p. 343-349.
390. Mariani, E., R. Monastero, and P. Mecocci. *Mild cognitive impairment: A systematic review*. 2007.

391. Holmes, C., et al., *Validity of current clinical criteria for Alzheimer's disease, vascular dementia and dementia with Lewy bodies.* British Journal of Psychiatry, 1999. **174**: p. 45-50.
392. Londos, E., et al., *Neuropathological correlates to clinically defined dementia with Lewy bodies.* International Journal of Geriatric Psychiatry, 2001. **16**(7): p. 667-679.
393. Crystal, H.A., et al., *The relative frequency of "dementia of unknown etiology" increases with age and is nearly 50% in nonagenarians.* Archives of Neurology, 2000. **57**(5): p. 713-719.
394. Xuereb, J.H., et al. *Neuropathological findings in the very old - Results from the first 101 brains of a population-based longitudinal study of dementing disorders*. 2000.
395. Jellinger, K., *Frequency of "Dementia of unknown etiology" increases with age.* Archives of Neurology, 2001. **58**(9): p. 1498-1499.
396. Silver, M.H., et al., *Distinguishing between neurodegenerative disease and disease-free aging: Correlating neuropsychological evaluations and neuropathological studies in centenarians.* Psychosomatic Medicine, 2002. **64**(3): p. 493-501.
397. Haroutunian, V., et al., *Role of the neuropathology of Alzheimer disease in dementia in the oldest-old.* Archives of Neurology, 2008. **65**(9): p. 1211-1217.
398. Lopez, O.L., et al., *Research evaluation and prospective diagnosis of dementia with Lewy bodies.* Archives of Neurology, 2002. **59**: p. 43-46.
399. Kosaka, K., et al., *Diffuse type of Lewy body disease: progressivedementia with abundant cortical Lewy bodies and senile changes of varying degree – A new disease?* Clinical neuropathology, 1984. **3**: p. 185-192.
400. Giannakopoulos, P., et al., *Assessing the cognitive impact of Alzheimer disease pathology and vascular burden in the aging brain: the Geneva experience.* Acta Neuropathologica, 2006. **113**(1): p. 1-12.
401. Carrette, O., et al., *A panel of cerebrospinal fluid potential biomarkers for the diagnosis of Alzheimer's disease.* Proteomics, 2003. **3**(8): p. 1486-1494.
402. Abdi, F., et al., *Detection of biomarkers with a multiplex quantitative proteomic platform in cerebrospinal fluid of patients with neurodegenerative disorders.* Journal of Alzheimer's Disease, 2006. **9**(3): p. 293-348.
403. Finehout, E.J., et al., *Cerebrospinal fluid proteomic biomarkers for Alzheimer's disease.* Annals of Neurology, 2007. **61**(2): p. 120-129.
404. Simonsen, A.H., et al., *Novel panel of cerebrospinal fluid biomarkers for the prediction of progression to Alzheimer dementia in patients with mild cognitive impairment.* Archives of Neurology, 2007. **64**(3): p. 366-370.
405. Simonsen, A.H., et al., *Identification of a novel panel of cerebrospinal fluid biomarkers for Alzheimer's disease.* Neurobiology of Aging, 2007. **22**.
406. Nicoli, F., et al., *Cerebrospinal fluid metabolic profiles in multiple sclerosis and degenerative dementias obtained by high resolution proton magnetic resonance spectroscopy.* Comptes Rendus de l Academie des Sciences. Serie III, 1996. **319**: p. 623-631.
407. Kosunen, O., et al., *Diagnostic accuracy of Alzheimer's disease: a neuropathological study.* Acta Neuropathologica, 1996. **91**(2): p. 185-193.
408. Longa, E.Z., et al., *Reversible middle cerebral artery occlusion without craniectomy in rats.* Stroke, 1989. **20**(1): p. 84-91.
409. Sauer, H. and W.H. Oertel, *Progressive degeneration of nigrostriatal dopamine neurons following intrastriatal terminal lesions with 6-hydroxydopamine: A combined retrograde tracing and immunocytochemical study in the rat.* Neuroscience, 1994. **59**(2): p. 401-415.
410. Brooks, B.R., et al., *El Escorial revisited: Revised criteria for the diagnosis of amyotrophic lateral sclerosis.* Amyotrophic Lateral Sclerosis and Other Motor Neuron Disorders, 2000. **1**(5): p. 293-299.
411. Rowland, L.P. and N.A. Shneider, *Medical progress: Amyotrophic lateral sclerosis.* New England Journal of Medicine, 2001. **344**(22): p. 1688-1700.
412. Forman, M.S., J.Q. Trojanowski, and V.M.Y. Lee, *TDP-43: a novel neurodegenerative proteinopathy.* Current Opinion in Neurobiology, 2007. **17**(5): p. 548-555.

413. Pradat, P.-F. and M. Dib, *Biomarkers in Amyotrophic Lateral Sclerosis.* Molecular Diagnosis & Therapy, 2009. **13**(2): p. 115-125.
414. Traynor, B.J., et al., *Amyotrophic lateral sclerosis mimic syndromes - A population-based study.* Archives of Neurology, 2000. **57**(1): p. 109-113.
415. Pohl, C., et al., *Proton magnetic resonance spectroscopy of the motor cortex in 70 patients with amyotrophic lateral sclerosis.* Archives of Neurology, 2001. **58**(5): p. 729-735.
416. Sarchielli, P., et al., *Magnetic resonance imaging and H-1-magnetic resonance spectroscopy in amyotrophic lateral sclerosis.* Neuroradiology, 2001. **43**(3): p. 189-197.
417. Suhy, J., et al., *Early detection and longitudinal changes in amyotrophic lateral sclerosis by H-1 MRSI.* Neurology, 2002. **58**(5): p. 773-779.
418. Spreux-Varoquaux, O., et al., *Glutamate levels in cerebrospinal fluid in amyotrophic lateral sclerosis: a reappraisal using a new HPLC method with coulometric detection in a large cohort of patients.* Journal of the Neurological Sciences, 2002. **193**(2): p. 73-78.
419. Howland, D.S., et al., *Focal loss of the glutamate transporter EAAT2 in a transgenic rat model of SOD1 mutant-mediated amyotrophic lateral sclerosis (ALS).* Proceedings of the National Academy of Sciences of the United States of America, 2002. **99**(3): p. 1604-1609.
420. Griffin, J.L. and R.M. Salek, *Metabolomic applications to neuroscience: more challenges than chances?* Expert Review of Proteomics, 2007. **4**(4): p. 435-437.
421. Brown, M., et al., *Mass spectrometry tools and metabolite-specific databases for molecular identification in metabolomics.* Analyst, 2009. **134**(7): p. 1322-1332.
422. Schnackenberg, L.K., J. Kaput, and R.D. Beger, *Metabolomics: a tool for personalizing medicine?* Personalized Medicine, 2008. **5**(5): p. 495-504.

Kuopio University Publications C. Natural and Environmental Sciences

C 238. Pinto, Delia M. Ozonolysis of constitutively-emitted and herbivory-induced volatile organic compounds (VOCs) from plants: consequences in multitrophic interactions.
2008. 110 p. Acad. Diss.

C 239. Berberat neé Kurkijärvi, Jatta. Quantitative magnetic resonance imaging of native and repaired articular cartilage: an experimental and clinical approach.
2008. 90 p. Acad. Diss.

C 240. Soininen, Pasi. Quantitative ^{1}H NMR spectroscopy: chemical and biological applicatons.
2008. 128 p. Acad. Diss.

C 241. Klemola, Kaisa. Cytotoxicity and spermatozoa motility inhibition resulting from reactive dyes and dyed fabrics.
2008. 67 p. Acad. Diss.

C 242. Pyykönen, Teija. Environmental factors and reproduction in farmed blue fox (Vulpes lagopus) vixens.
2008. 78 p. Acad. Diss.

C 243. Savolainen, Tuomo. Modulaarinen, adaptiivinen impedanssitomografialaitteisto.
2008. 188 p. Acad. Diss.

C 244. Riekkinen, Ossi. Development and application of ultrasound backscatter methods for the diagnostics of trabecular bone.
2008. 79 p. Acad. Diss.

C 245. Autio, Elena. Loose housing of horses in a cold climate: effects on behaviour, nutrition, growth and cold resistance.
2008. 76 p. Acad. Diss.

C 246. Saramäki, Anna. Regulation of the p21 (CDKNIA) gene at the chromatin level by 1 alfa,25-dihydroxyvitamin D3.
2008. 100 p. Acad. Diss.

C 247. Tiiva, Päivi. Isoprene emission from northern ecosystems under climate change.
2008. 98 p. Acad. Diss.

C 248. Himanen, Sari J. Climate change and genetically modified insecticidal plants: plant-herbivore interactions and secondary chemistry of Bt Cryl Ac-Toxin producing oilseed rape (Brassica napus L.) under elevated CO2 or O3.
2008. 42 p. Acad. Diss.

C 249. Silvennoinen, Hanna. Nitrogen and greenhouse gas dynamics in rivers and estuaries of theBothnian Bay (Northern Baltic Sea).
2008. 98 p. Acad. Diss.

C 250. Degenhardt, Tatjana. An integrated view of PPAR-dependent transcription.
2009. 120 p. Acad. Diss.

C 251. Häikiö, Elina. Clonal differences of aspen (Populus spp.) in responses to elevated ozone and soil nitrogen.
2009. 49 p. Acad. Diss.

C 252. Hassinen, Viivi H. Search for metal-responsive genes in plants: putative roles in metal tolerance of accumulation.
2009. 84 p. Acad. Diss.